LAPPEENRANTA-LAHTI UNIVERSITY OF TECHNOLOGY LUT
LUT School of Energy Systems
LUT Mechanical Engineering

*Satish Bastakoti*

# ANALYZING AND INTERPRETING CONDITION OF THE ROTATING MACHINE SYSTEM BY PROCESSING MEASURED VIBRATION PARAMETERS

Examiner(s): Professor Jussi Sopanen
D. Sc. (Tech.) Emil Kurvinen

## ABSTRACT

Lappeenranta-Lahti University of Technology LUT
LUT School of Energy Systems
LUT Mechanical Engineering

Satish Bastakoti

**Analyzing and interpreting condition of the rotating machine system by processing measured vibration parameters**

Master's thesis

2019

104 pages, 39 figures, 17 tables, and 3 appendices

Examiners: Professor Jussi Sopanen
D. Sc. (Tech.) Emil Kurvinen

Keywords: Machine condition monitoring, residual unbalance detection, rotating machine system, vibration analysis

The condition of the rotating machine deteriorates during its operation due to reasons such as installation defects, wear, and tear, poor lubrication, excessive operational loads, etc. It leads to faults or failure of rotating machine or its components. These developing faults or failures can be detected and identified through analysis of vibration parameters and their interpretation. This helps to know the condition of the rotating machine. It is done to protect the machine and the components, personnel and do predictive maintenance.

This study focuses on finding required vibration parameters to be measured, the appropriate sensors used for measuring, proper mounting locations, data formats and transferring of measurement data for needed processing. It looks at how these processed measurement data are analyzed using different techniques to interpret the condition of the rotating machines. As a case study for the project, the measurements of vibration parameters from an induction motor were processed and analyzed to identify the location and magnitude of single plane residual unbalance. The objective was to use unbalance information to verify the dynamics of the studied motor by comparing the measured and simulated displacement of rotor through its numerical finite element model.

The absolute radial vibration of nonrotating part, absolute or relative, radial or axial displacement vibration, phase reference and rotation speeds of rotating part are required vibration parameters. The accelerometers or velocity sensors are used to measure absolute vibration. The displacement sensors are used to measure the relative displacement of rotating parts. Optical or inductive or eddy current based transducer are used to measure phase reference and rotation speed. The bearing housing is one appropriate location to measure the vibration parameters. Signal analysis techniques in the time and frequency domain are used to interpret the state of the machine. The dynamics of the motor could not be verified with single plane unbalance for all the measured speeds through numerical method.

**ACKNOWLEDGMENTS**

I sincerely thank supervisors Emil Kurvinen and Professor Jussi Sopanen for giving me a great opportunity to work in this project and complete my master's degree. I acknowledge and appreciate all the help and guidance from friends, families, and colleagues especially Tuhin Choudhury. I would like to deliver my sincere gratitude for all the support, guidance and help.

Satish Bastakoti
December 2019
Lappeenranta, Finland

**TABLE OF CONTENTS**

## LIST OF SYMBOLS AND ABBREVIATIONS

| | |
|---|---|
| 0-p | Zero to peak |
| $AR$ | Amplitude Resolution of ADC |
| $B$ | Bandwidth or line spacing |
| $\boldsymbol{C}$ | Damping matrix |
| $D$ | Outer diameter of hollow disc |
| $d$ | Inner diameter of hollow disc |
| $e_{ub}$ | The eccentricity of the unbalance at node n |
| $\boldsymbol{F}$ | Vector of externally applied forces |
| $f$ | Frequency (Hz) |
| $f_0$ | Fundamental frequency |
| $f_1$ | First integer harmonics |
| $f_2$ | Second integer harmonics |
| $f_3$ | Third integer harmonics |
| $F_{ub}$ | Unbalance force |
| $f_{max}$ | Maximum frequency of interest (Hz) |
| $\boldsymbol{G}$ | Gyroscopic matrix |
| $g$ | Acceleration due to gravity |
| $h$ | Length of hollow disc |
| $I_p$ | Polar mass moment of inertia of hallow disc |
| $\boldsymbol{K}$ | Stiffness matrix |
| $M$ | Mass of hollow disc |
| $\boldsymbol{M}$ | Mass matrix |
| $N$ | Number of discrete data points |
| $m_{ub}$ | unbalance mass |
| $n$ | Number of bits |
| $N_{LOR}$ | Number of lines of resolution (LOR) |
| p-p | Peak to peak |
| $\boldsymbol{q}$ | vector of nodal coordinates |
| $\boldsymbol{Q}_1$ | Unbalance force vectors related to the constant rotational velocity |

| | |
|---|---|
| $\boldsymbol{Q}_2$ | Unbalance force vectors related to variable rotational speed |
| $\boldsymbol{q}_n^c$ | Unbalance vector of n$^{th}$ node related to constant speed |
| $\boldsymbol{q}_n^{nc}$ | Unbalance vector of n$^{th}$ node related to non-constant speed |
| $R$ | Range of analog measurement |
| $T$ | Minimum record length (s) |
| $Ub(r)$ | Single plane speed dependent unbalance (kg·m) |
| $v_i$ | Vibration amplitude of $i^{th}$ data point |
| $\bar{v}$ | Mean of vibration data points |
| V | Volt |
| $V_{CF}$ | Crest Factor of vibration signal |
| $V_{kur}$ | Kurtosis of vibration |
| $V_{RMS}$ | Root mean square vibration amplitude |
| $X_0$ | Maximum displacement |
| $x(t)$ | Displacement at time t |
| $\dot{x}(t)$ | Velocity at time t |
| $\ddot{x}(t)$ | Acceleration at time t |
| | |
| $\alpha$ | Phase angle |
| $\rho$ | Equivalent density of hollow disc |
| $\sigma$ | Standard deviation of vibration data points |
| $\Omega$ | Rotation speed |
| $\omega$ | Angular velocity (rad/s) |
| | |
| a.c. | Alternating current |
| ADC | Analog to Digital Converter |
| AMBs | Active Magnetic Bearings |
| BW | Backward Whirl |
| CF | Crest Factor |
| d.c. | Direct current |
| DE | Drive end |
| dof | degrees of freedom |
| Ether CAT | Ethernet for Control Automation Technology |

| | |
|---|---|
| FE | Finite Element |
| FFT | Fast Fourier Transform |
| FW | Forward Whirl |
| LOR | Number of lines of resolution |
| MATLAB | Matrix Laboratory |
| MIMOSA | Machinery Information Management Open System Alliance |
| NDE | Nondrive end |
| RMS | Root Mean Square |
| RoBeDyn | Rotor-Bearing Dynamics Toolbox for MATLAB |
| RPM | Rotation per minute |
| 1X | Once per revolution excitation |
| 2X | Twice per revolution excitation |
| 3D | Three Dimensional |

# 1 INTRODUCTION

The machine is defined as a mechanical system designed to perform a specific task to transform motion, force or energy. The machine system is the mechanical system having subsystems that are made of components that support the action and work of the machine itself. (SFS-ISO 13372 2013, p. 3.) The rotating machine is the machine that rotates which can be either driving or driven. Both driving and the driven system can be mechanical or electrical machines. The driving and driven machines as a system are considered as the rotating machine system. A driving system such as an electric motor is coupled with a driven system such as a rotor to achieve the function of the rotating machine system. The driving and the driven system and their components in the subsystem level depend on the design and function of the machine system itself. Any rotating machine has nonrotating elements and rotating elements. In electric motors, the stator is a fixed element while the rotor is a rotating element. Figure 1 shows the typical components of a rotating machine system.

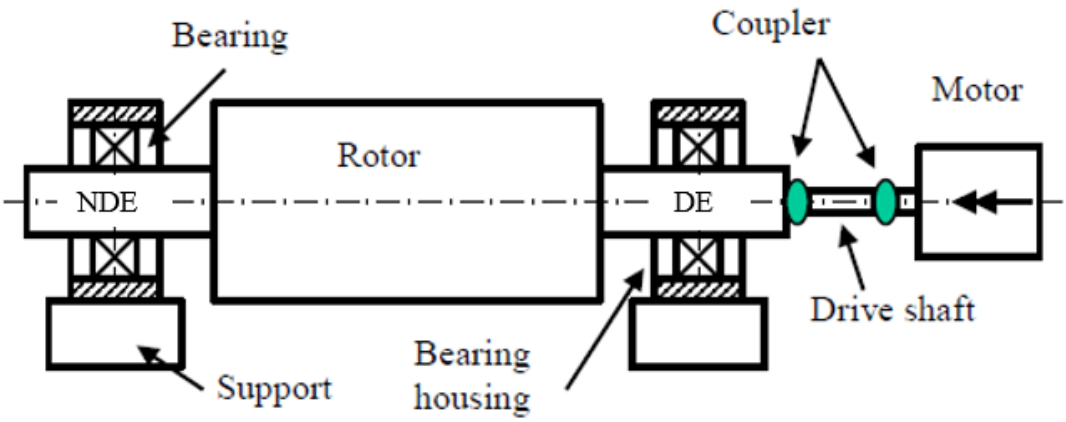


**Figure 1.** Components of a rotating machine system with driving and driven machine. The side of the rotor which is connected to the motor is called drive end (DE) and the other end is called non-drive end (NDE). (Mod. Sopanen 2004, p. 15).

In Figure 1, the rotating machine system consists of the driving system which is a motor and the driven system which is rotor mounted on bearing support. The motor provides the required energy and the rotor performs the specifically designed task. Rotating machines are used in different industries for various industrial applications. They are used for many applications such as manufacturing, power generation, pumping, blowing, etc. Electric

motor driven system uses between 43% and 46% of global electricity, which is the largest source of electricity use. The industrial sector uses 64% of total global energy consumed by the electric motor-driven systems. (Waide & Brunner 2011, p. 11.) During its use, due to many reasons such as installation defects, wear and tear, vibrations, poor lubrication, excessive operational loads, etc., the condition of the machine system deteriorates. The condition of the machine system refers to the state of components or subsystem that indicates any faults or failure. Any failure or faults in component or subsystem deteriorate the state of the machine and the component involved. The condition of the machine is normal if there are no faults and failure at the component or system level. (SFS-ISO 13372 2012, p. 1-2.) The state of the machine can be defined in terms of the deterioration of components due to faults in the machine. The level of deterioration due to faults can be estimated in terms of the percentage of life used. The machines or components has 0% life used when it is new, and 100% life used when it is in a failed condition. The axis of the percentage of life used is also called the severity axis for a given component or machine that determines its state. (SFS-ISO 13381-1 2015, p. 13.)

The bearing failure accounts for 51% of electrical motor failures. One of the reasons why bearing fails prematurely in electrical motors is always due to excessive vibration. (ABB 2015, p. 3-23.) Vibration in structures is due to time varying excitation forces. The amplitude of vibration on structural location due to harmonic excitation can be determined when its amplitude, frequency, and spatial distribution are known. Every structure has an infinite number of natural frequencies and respective mode shapes that show how the structure vibrates at the specific natural frequency. When the excitation force's frequency is equal to any one of the natural frequencies of the structure, the amplitude of vibration may get large even with a low amplitude of excitation forces due to resonance. (Roivainen 2009, p. 26.)

Approximately about 90% of vibration in rotating machines is excitation due to unbalance or misalignment in rotating components. Other approximately 10% of vibration in rotating machines are due to many reasons such as mechanical looseness, bent rotor, eccentric gears, bad drive chains, electromagnetic forces, rubbing, etc. (McMillan 2004, p. 12.) In other words, vibration due to unbalance or misalignment in the rotor is transmitted to the bearings that causes bearing failures in the rotating machine system. Thus, measuring and analyzing vibration has proven to be a good measure to assess machine condition and then do the

required maintenance before it fails (Goyal & Pabla 2015, p. 585). The vibration of a rotating machine system is measured for many purposes. A single vibration measurement is generally done for experimental modal analysis to verify the modeled dynamics of the simulation model or to check conformity with applicable standards that limits vibration in the specific machines. While continuous and periodic measurements of vibration are done to monitor the condition of the machine system for predictive maintenance and use the acquired information for product development. The information regarding the condition of the rotating machine system can be analyzed and interpreted through vibration signal processing techniques.

In order to analyze and interpret the condition of the machine system, it is important to measure all the required parameters needed from the rotating machine system. These measured parameters are then analyzed to interpret the condition of the machine system. Continuous or periodic measurement, analysis, and interpretation will show the instantaneous or the relative changes in the condition of the machine system. Monitoring the condition of rotating machine system through measurement and analysis of the machine system's vibration is called vibration condition monitoring. It is done to protect the machine system, improve the safety of personnel, identify problems, avoid machine failure, extend equipment life, improve maintenance procedure, etc. It involves measurement and analysis of vibration signals for tracking changes in the vibration behavior of the machine. Vibration behavior of rotating machine can change over time due to many reasons such as wear or damage of bearing, changes in balance, gear or coupling defects, rotor alignment, cracks in components, rubbing of parts, mechanical looseness, etc. Change in vibration behavior indicates a change in the machine system's condition and why it is changing is understood through signal analysis and its interpretation. (SFS-ISO 13373-1 2002, p. v.)

According to an online survey conducted in 2004 from industries around the world, 17.29% of companies use maintenance based on vibration condition monitoring and analysis. About 95.54% of the company surveyed agreed that the motivation behind using a condition monitoring system was to reduce the number of unscheduled machine breakdowns. About 30.77% of the companies provide information from condition-based monitoring in the form of charts and 25.06% provide in the form of alarms. (Higgs et al. 2004, p. 11-15.)

## 1.1 Research background

The work of this master's thesis is a part of the research project conducted in LUT University's Laboratory of machine dynamics for developing a mathematical model-based vibration analyzer and interpreter for identifying the state of the rotating machine. The aim of the project is to commercialize a software solution that can automatically analyze and interpret the machine's condition by processing the measured vibration signal through its mathematical model. The work of this thesis was to find all the necessary information and processes regarding the monitoring of rotating machine's condition from sensors to signal analysis and its interpretations. This information and processes are then implemented in the case study to identify the magnitude and location of a single plane residual unbalance of the 3 phase 11 kW induction motor through its mathematical model. The measured vibration is then compared with the response obtained from the simulation of the mathematical model. The work is relevant to the project for implementing the process and information for complementing the mathematical model which is physics-based software solution that works for different types of rotating machines. Since the software is based on the mathematical model, the case study will help in the verification of the modeled machine dynamics of the 3 phase 11 kW induction motor.

## 1.2 Research questions

The research problem is to find out how vibration and other signals measured from rotating machines can be processed to analyze and interpret the state of the machine or its components. The goal of the thesis work is to find answers to the research questions and solve the research problem. The research questions are, what to measure, why to measure, how to measure and where to measure required parameters from rotating machines to analyze and interpret the condition of the machine and or its components? What is the data format of these measurements and how these are transferred to make required analysis? What are the different signal analysis techniques and how to interpret the results from these analyses? How these measured parameters and processed results can be used to verify the mathematical model of the specific rotating machine used in the industry?

## 1.3 Research methods

In this study, the main research methods are a literature review and quantitative research. The case study of the standard 3 phase 11 kW induction motor was done by means of a

quantitative and simulation research method. While the rest of the work was done by means of a literature review.

## 1.4 Delimitation

From the perspective of the project's aim of developing a model-based software solution, two things that matter the most are the measurement data and the machine dynamics-based machine system's mathematical model. How it is being measured in old and new machines, what are measuring arrangements and how vibration parameters are defined, do not matter from the software's perspective. But these matter from the perspective of the business model and how the offering will be implemented. Thus, it is important to know how vibration is being measured and how these measurements are being analyzed from the perspective of industry practices and relevant standards. Thus, the work focuses from the perspective of industry practices on how vibration is being measured and the state of the machine being analyzed. The study is limited to the rotating machine or non-reciprocating machine and excludes reciprocating machine such as internal combustion engine. It is because the project is not aiming to develop the software solution for such engine.

The study does not include measurement and analysis of torsional and axial vibration of the rotating machine because these are not typically monitored in industrial rotating machine. It does not include the processing of historical measurements from the machines. The work only deals with the vibration processing of present measurements to analyze the present condition of the machine. The study only deals with vibration produced by the machine and not from any other sources other than the machine itself. The process of measurement described in the thesis is based on state of the art of sensors and these may not be valid if it changes in the future. The signal analysis techniques are limited in time domain and frequency domain only. The time domain analysis is limited to plotting and statistical functions and frequency domain analysis is limited to Fast Fourier Transformation (FFT) only.

The mathematical model was based on Rotor-Bearing Dynamics (RoBeDyn) toolbox for Matrix Laboratory (MATLAB) software. The RoBeDyn template was edited to make the finite element (FE) model of the rotor in the MATLAB 2018b version. The design dimensions without manufacturing tolerances of the rotor were used to model it in RoBeDyn.

It is based on three-dimensional (3D) Timoshenko beam elements. The effect of the temperature in both measurements and the FE model is not considered in this work.

## 1.5 Structure of the thesis

The overall workflow process of the master's thesis work is presented in Figure 2.

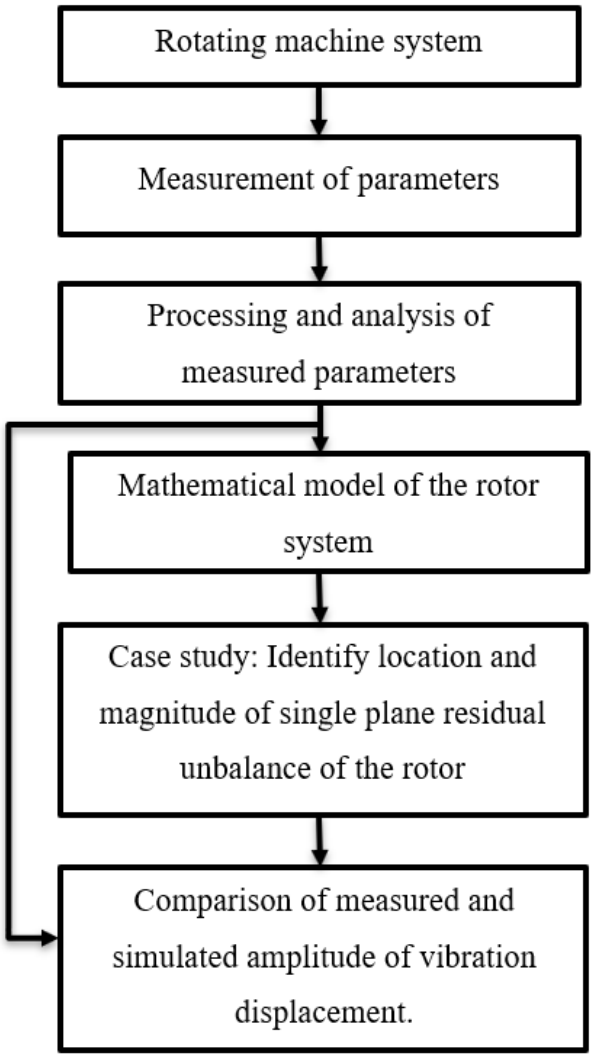


**Figure 2.** The overall workflow of the master's thesis work.

Each chapter of this thesis reflects the workflow process as shown in Figure 2. The rotating machine system and the need for condition monitoring and analysis have been explained in chapter 1. Chapter 2 explains all the parameters that are required to be measured from the rotating machine system in order to assess the condition of the machine and its components. The chapter also explains what sensors to use for measurement, where to measure, how to measure and when to measure. Chapter 3 explains what is done to the measured data and

how these are used to assess the condition of the machine system. Chapter 4 explains how mathematical model is made and how it is used to find the displacement of rotors at specific locations. Chapter 5 describes the case study and how the magnitude and location of a single plane residual unbalance was searched from the rotor's FE model by using the measured data from the standard 3 phase 11 kW induction motor. The results and analysis of the measurements are pretested in chapter 6. Chapter 7 presents a discussion on results and analysis. The conclusion of the thesis work is presented in chapter 8.

# 2 SENSORS AND MEASUREMENT PARAMETERS FOR ANALYSIS

The standard SFS-ISO 13373-1 provides guidelines for measuring vibrations from rotating machine system in order to monitor its condition. The objectives are to support rotating machine industry for implementing and performing vibration measurements in similar manner as in the guidelines. It covers vibration condition monitoring of both driven and driving system that can be mechanical or electrical machine. (SFS-ISO 13373-1 2002.) The measurements required for vibration signal analysis to interpret the state of the machine system are the vibration of rotating and non-rotating components, phase of the vibration signals and rotation speed of the machine (SFS-ISO 13373-1 2002, p. 15). However, the temperature can also be measured at the bearing and the housing to monitor the state of the bearing. The temperature of the bearing should not exceed the designed working limit. The rise in temperature of bearing can provide information about the state of the bearing such as degradation of grease or bearing. (Zhou, Habetler & Harley 2007, p. 4.) According to a study done by Kantoríková & Fabian (Kantoríková & Fabian 2019), while operating a rolling bearing at higher temperatures than the maximum operating temperature, the decrease in the strength and lifetime of bearing was observed.

The temperature of the rotor system is also being measured and monitored to predict the thermal effects in rotating machines through simulation of the mathematical rotor model. Thermal effects deform the rotor which is referred to as thermal bow. This adds to the unbalance in the rotor geometry and leads to increased vibration of the system. (Gu & Chu 2014, p. 4030.)

The vibration of any parts of rotating machine can be measured in terms of three parameters with appropriate sensors at different operating conditions and speeds. These are displacement, velocity, and acceleration vibration. (Scheffer & Girdhar 2004, p. 13-21.) The sensors that are needed to measure the required vibration parameters are explained in the following subchapters.

## 2.1 Vibration displacement sensor

Vibration measured in terms of displacement is called vibration displacement. A vibrating body travels from one extreme to another and this total distance traveled is called p-p (peak to peak) vibration displacement. It can also be referred only as 0-p (zero to peak) which is half of the p-p vibration displacement. The displacement vibration is measured in micrometer (μm). The displacement vibration of a vibrating body at any time can be calculated as, (Scheffer & Girdhar 2004, p. 14-19.)

$$x(t) = X_0 \bullet \sin(\omega t), \tag{1}$$

where, $x(t)$ is displacement at time *t*, $X_0$ is maximum displacement or 0-p and $\omega$ is the angular velocity in rad/s. The angular velocity $\omega$ can be calculated as, (Scheffer & Girdhar 2004, p. 14.)

$$\omega = 2\pi f, \tag{2}$$

where, $f$ is the frequency in Hz. Vibration sensor such as velocity and acceleration sensor can be attached with the body being measured, to get the vibration displacement after mathematical integration. But these sensors are not technically displacement sensors but can measure displacement vibration of non-rotating components where it is physically attached. (Scheffer & Girdhar 2004, p. 14.)

The sensors that measure vibration displacement of a component are called displacement transducers also known as proximity probe transducers. Proximity transducer is the non-contacting sensor that measures vibration displacement of a body without being in physical contact with the body being measured. These sensors are used to measure displacement vibration of the component where it is not possible to physically attach the sensor such as on rotating rotor. It can measure both vibration displacement and position of rotating rotor relative to the stationary bearing or machine housing. It provides an a.c. (alternating current) component for vibration displacement and d.c. (direct current) component for the position of the rotor. (SFS-ISO 13373-1 2002, p. 19-20.)

The most commonly used proximity transducers are based on the eddy current principle. It consists of a coil that generates a magnetic field that is emitted from a probe tip. Eddy current is generated, when electro-conductive material such as steel rotor is introduced into the magnetic field emitted by the probe. The oscillator/demodulator component in a sensor demodulates the signal due to eddy current and provides d.c. component which is proportional to the gap between the probe and the rotor and the a.c. component which is directly proportional to the vibration. (Scheffer & Girdhar 2004, p. 35.) The output of the proximity sensors is influenced by variation in ambient temperature. When using proximity transducers, it is important to make sure that the area of the probe tip is clear for the conducting material and must be recalibrated for rotor made of different materials. (SFS-ISO 13373-1 2002, p. 19-20.)

Beside proximity sensors, there are other types of sensors that measure displacement based on the change in inductance, capacitance, magnetic flux, and light intensity. When the ferromagnetic material approaches the inductor coil, its inductance changes. This change in inductance is used to measure displacement by inductive sensors. Similarly, capacitive based displacement sensors measure displacement when capacitance changes. Displacement sensors that are based on the measurement of flux density between air gaps are called magnetic displacement sensors. Optical displacement sensors measure displacement based on measurement of reflected light intensity from a vibrating object. Depending upon available space and mounting requirements, eddy current based displacement sensors can be of probe or transverse flux type. Displacement sensors where eddy current sensor coil is placed on the printed circuit board and placed around the rotor are called transverse flux sensors. Transverse flux sensors can also be based on the measurement of capacitance. (Maslen & Schweitzer 2009, p. 101-105.)

## 2.2 Vibration velocity sensor

Vibration measured in terms of velocity is called vibration velocity. The maximum velocity of vibration is called a vibration velocity peak. It is measured as mm/s. The velocity vibration of a body at any time can be calculated by differentiating equation (1) with respect to time. (Scheffer & Girdhar 2004, p. 15.)

$$\dot{x}(t) = X_0 \bullet \omega \bullet \cos(\omega t) \tag{3}$$

In equation (3), $\dot{x}(t)$ is the velocity at time $t$, $X_0$ is maximum displacement or 0-p and $\omega$ is the angular velocity in rad/s. The velocity $\dot{x}(t)$ is out of phase with displacement $x(t)$ by 90º. (Scheffer & Girdhar 2004, p. 15.)

The velocity sensor measures the vibration velocity of a component by being in physical contact with the body being measured. Generally, these transducers are mounted on the non-rotating part of the machine. (SFS-ISO 13373-1 2002, p. 18.) The vibration velocity of a non-rotating part can also be measured with piezoelectric or strain gauge accelerometers with built-in electronic integrators. It integrates the measured acceleration to provide a voltage proportional to the vibration velocity of the body. (Cheatle 2006, p. 99-100.) But common velocity transducer which measures velocity vibration only is based on the principle of motion of magnet in coil or coil in magnet as shown in Figure 3 (Scheffer & Girdhar 2004, p. 30).

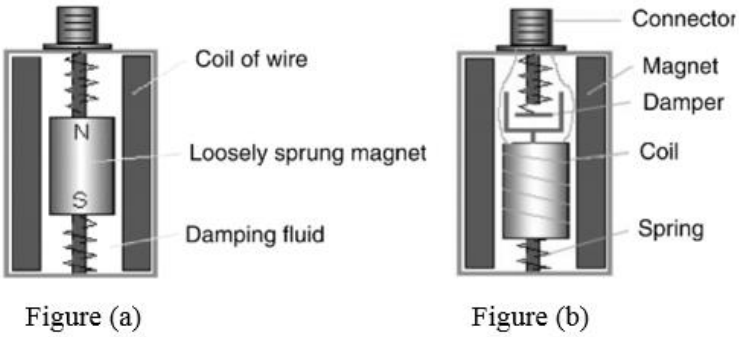


**Figure 3.** Two basic types of velocity transducers, magnet-in-coil shown in Figure (a) and coil-in-magnet shown in Figure (b) (Scheffer & Girdhar 2004, p. 30).

The vibration of the body being measured creates the relative motion between the magnet and the coil in its sensitive axis. The sensitive axis is an axis where a magnet can move, and vibration velocity will be measured in the same axis. These both sensors shown in Figure 3 measures vibration velocity in vertical direction. Due to the relative motion, voltage signal correlating with the vibration is induced. These induced voltages are processed to get the vibration of the body in the sensitive axis. These sensors are self-generating and do not require external devices to produce a voltage signal. It is sensitive to vibration in axis other than sensitive axis and that can damage the sensor. Vibration sensors are manufactured

differently for vertical and horizontal mounting machines considering gravity force. (Scheffer & Girdhar 2004, p. 30.)

Velocity transducers have built-in resonant natural frequency and thus vibration velocity measured is accurate above its natural frequency. If the velocity measurement below to that of its natural frequency is required, it must be calibrated for the purpose. Due to internal moving parts in these sensors, they are sensitive to mechanical damage and wear when using in the range above the operating range. It is also sensitive to ambient magnetic fields and interference. Velocity sensors with two coils require less magnetic shielding than with one coil. (SFS-ISO 13373-1 2002, p. 19.)

## 2.3 Vibration acceleration sensor

Vibration measured in terms of acceleration is called vibration acceleration. The acceleration vibration of a vibrating body at any time can be calculated by differentiating equation (3) with respect to time. It is measured in m/s$^2$. (Scheffer & Girdhar 2004, p. 15.)

$$\ddot{x}(t) = -X_0 \cdot \omega^2 \cdot \sin(\omega t) \tag{4}$$

In equation (4), $\ddot{x}(t)$ is the acceleration at time *t*, $X_0$ is maximum displacement or 0-p and $\omega$ is the angular velocity in rad/s. The acceleration $\ddot{x}(t)$ is out of phase with velocity $\dot{x}(t)$ by 90º.

The sensor that measure vibration acceleration are called accelerometers. It is a seismic device whose output is proportional to the absolute vibratory acceleration of the machine element being monitored. Typically, accelerometers are mounted on the non-rotating part of the machine. (SFS-ISO 13373-1 2002, p. 17.)

The piezoelectric acceleration sensors are typically used in rotating machines to measure the acceleration vibration of its parts that are not rotating. Inside these sensors, mass is spring-loaded against a piezoelectric crystal. When the sensor is accelerated, the mass exerts varying magnitude of force on the crystal. The crystal then produces charge that is proportional to the magnitude of force due to acceleration. The produced charge is converted by charge amplifier into mV/g (millivolts per acceleration due to gravity). This output

voltage is proportional to the acceleration measured. Depending upon the location of the charge amplifier, piezoelectric acceleration sensors are of two types. They are current or voltage mode type and charge mode type. There is an internal amplifier in constant current or voltage mode type accelerometers. The constant current or regulated voltage is used as power source to these types of accelerometers. There is no internal charge amplifier in charge mode type accelerometers. Thus, it requires external charge amplifier. (Scheffer & Girdhar 2004, p. 32-33.) Figure 4 shows the accelerometer sensor with a built-in temperature sensor (Valmet 2015.)


**Figure 4.** Piezoelectric accelerometer with a built-in temperature sensor (Valmet 2015).

2.4 Phase reference and rotation speed sensor

Phase angle measures the angular or time difference of one sinusoidal wave to another or vibration signal to a fixed reference. It is an important parameter when evaluating signals. Phase lag is commonly used for analyzing the state of the rotating machine system. Phase lag gives information about the time difference between the reference point on the rotor and the maximum of zero crossings of the vibration signal. (SFS-ISO 13373-1 2002, p. 15.)

Typical instruments that measure the rotation speed and phase of the signals are optical sensors, dual-channel analyzers, photocells, and Keyphasor. In the optical sensor, stroboscope flashes high-density light at certain frequencies for observing phase difference. It requires reference marks such as keyway or notch or angular scale marking from 0 to 360 degrees on the rotor. The stroboscope is triggered by a 1X (Once per revolution) vibration signal which makes a reference mark to be stationery at some position. It is an approximation method. Dual-channel analyzers can take two simultaneous inputs from accelerometers at two different locations. It helps to analyze the phase from two vibration signals collected. It

does not require any reference mark in the machine. It can provide a phase difference accurately at any frequency. Photocell or photodetector requires a reflective surface such as tape on the rotor to reflect the light. Each time the light is reflected, it produces pulse to indicate when one full rotation was complete. The location of the reflective tape is treated as a reference point and as zero degrees. Based on this reference point, the phase of signal is expressed as its relative. These photocells can also measure the rotation speed of the rotor. Photocell need to be installed within proximity of the rotor. The reflectivity of the target area is important for photocells to get the reflection of light from the target area. Keyphasor which are also called electromagnetic or non-contact pickups uses keyway or notch on the rotor as reference point such that each time the keyway passes during rotation, it generates output voltage pulse. This output voltage pulse is compared to the measured vibration signal to find when the maximum vibration amplitude occurred. The time at which maximum vibration occurred and the corresponding voltage level from Keyphasor helps to determine the phase difference. The photocell and Keyphasor cannot find the phase difference without analyzing vibration signal. However, these sensors help in finding accurate phase difference and rotation speed. (Scheffer & Girdhar 2004, p. 47-51.)

## 2.5 Measuring parameters

In order to analyze and interpret the condition of the rotating machine system, it is important to measure all the required parameters needed from the rotating machine system. However, what parameters are required to be measured and analyzed to interpret the condition of the machine system depends on what faults or failure in the machine or components are being monitored. (SFS-ISO 13373-1 2002, p. 1-7.)

In total, there are five unique parameters that are needed to be measured from any rotating machine for the purpose of condition analysis and interpretation. Three of these are vibration parameters and one is phase reference and the other is rotation speed of the rotor system respectively. Phase reference and rotation speed are measured by just one sensor. These five unique parameters can be divided into two measurement categories based on the machine part where the measurement is being made. These unique parameters are categorized in Table 1 based on machine element where the measurement is being made such as the rotating part or non-rotating part. (SFS-ISO 13373-1 2002, p. 31-36.)

*Table 1. Parameters that are needed to be measured from the rotating machine system for vibration analysis and interpretation (SFS-ISO 13373-1 2002, p. 31-36).*

| Measurements | Measurement on non-rotating part | Measurements on rotating part | Remarks |
|---|---|---|---|
| 1. | Absolute radial vibration of non-rotating parts. | - | Required for all types of the machine at each bearing housing. |
| 2. | - | Relative or absolute radial vibration displacement of the rotor. | Either one of these depending upon evaluation criteria at each bearing housing. |
| 3. | - | Relative or absolute axial vibration displacement of the rotor. | Requires generally to the machine with fluid film bearing. |
| 4. | - | Phase reference and rotation speed of the rotor. | Required to all types of machines. |

Thus, depending upon the machine types and condition of machine being interpreted through vibration analysis, a total of five parameters are required to be measured for machine with fluid film bearing as shown in Table 1. For other machines, it is not recommended to measure axial vibration displacement of rotor and thus only require four measurement parameters. (SFS-ISO 13373-1 2002, p. 31-36.)

Depending upon what sensor measures and how it measures, the vibration measurement can be absolute or relative. For instance, an accelerometer attached to a vibrating component measures only the acceleration vibration of the body that is being measured. Thus, it measures only the vibration of the component and is the absolute vibration of the body. In a similar way, velocity sensors measure the absolute velocity vibration of the body being measured. However, due to the design of the displacement sensors such as proximity probe and how these are used to measure the displacement of the rotor in the industry for condition monitoring, it is also called relative displacement sensors. It measures vibration

displacement of the first body by being mounted on the second body that is vibrating itself. In other words, these sensors measure the displacement of the first body by not being in physical contact with the body being measured. (SFS-ISO 13373-1 2002, p. 11-12.)

## 2.6 Measurement on non-rotating part

Vibration measurement of the non-rotating part such as bearing housing is done mainly for three reasons. One is to measure vibration for acceptance testing, another is to analyze and interpret the condition of the component and third is to assist in measuring absolute radial vibration of the rotor. (SFS-ISO 13373-1 2002, p. 8-12.) How vibration is measured from non-rotating part of the machine system is explained in the following subchapter.

### 2.6.1 Absolute radial vibration of non-rotating part

Seismic transducers such as velocity transducer or accelerometer are used to measure the absolute vibration of non-rotating part such as bearing housing. Either velocity transducer or accelerometer can be used for the measurement of absolute radial vibration of nonrotating part. Absolute vibration velocity is measured in mm/s and absolute vibration acceleration is measured in $m/s^2$. (SFS-ISO 20816-1 2017, p. 7-8.) For both vertically and horizontally mounted machines, either two velocity sensors or two accelerometers are mounted in bearing housing to measure vibration in two radial directions in the same transverse plane. Figure 5 shows the location of two similar seismic transducers for measuring the absolute radial vibration of horizontal machine at bearing housing. (SFS-ISO 13373-1 2002, p. 8-9.)

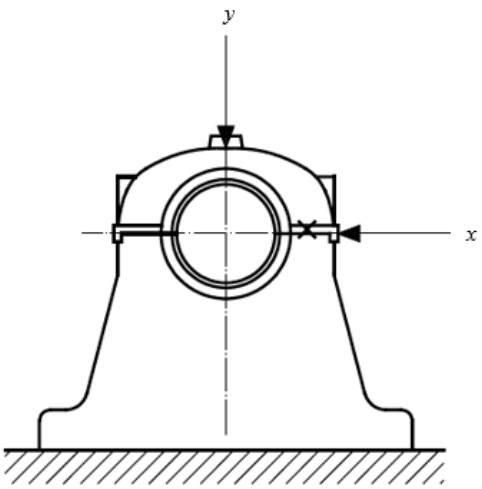


**Figure 5.** Measurement location of absolute radial vibration at bearing housing in the radial *x*-axis and *y*-axis in the same transverse plane (Mod. SFS-ISO 13373-1 2002, p. 9).

2.7 Measurement on the rotating part

From the rotating part of the machine, it is necessary to measure relative or absolute radial vibration displacement of the rotor. Except in rotating machine system such as small industrial steam turbines, medium and small pumps, and medium and small motors with rolling element bearing, it is not required to measure radial vibration displacement of rotors. (SFS-ISO 13373-1 2002, p. 31-36.) The reason for not measuring on these machines is due to its design, bearing types being used and stiffness of bearings. If the stiffness of anti-friction or rolling element bearing is higher than that of bearing housing, the housing vibration follows the rotor motion and thus housing vibration is enough to indicate the rotor vibration. In such case, only measuring absolute radial vibration of bearing housing is enough. In the machine with sleeve bearing, the rotor is not as firmly supported as in the case of the antifriction bearing. In such case, the bearing housing does not follow the vibration of the rotor and thus the absolute or relative radial vibration of the rotor is required to be measured. (Rajendra et.al. 2018, p. 48.)

According to SFS-ISO 20816-1:2017, which parameter to select in order to measure the vibration of the rotor on machine that requires it, depends on the reasoning behind the measurement. This reasoning behind the measurement is called evaluation criteria. Evaluation criteria itself depends on many factors such as bearing type, clearance, diameter, type of machine, rotor mass, stiffness, rotational speed, etc. (SFS-ISO 20816-1 2017, p. 16-17.) For instance, absolute rotor displacement vibration is required to be measured from machine having flexible rotors or having a soft rotor support structure or for machine that operate near the rotor natural frequency (SFS-ISO 13373-1 2002, p. 12). From the perspective of evaluation criteria, which parameter to select for measuring the vibration of the rotor is presented as list below (SFS-ISO 20816-1 2017, p. 16-17).

A. Change in rotor vibration

If the reason behind measurement is to monitor and interpret why rotor vibration is changing, then which parameter to select for measuring rotor vibration depends on two conditions. These two conditions are as follows. (SFS-ISO 20816-1 2017, p. 16-17.)

1. If the absolute displacement vibration of the structure or part where the relative displacement sensor is being mounted is less than 20% of relative rotor vibration

displacement, then relative or absolute radial vibration displacement of the rotor can be used to measure the rotor vibration (SFS-ISO 20816-1 2017, p. 16).

2. But if the absolute displacement vibration of the structure or part where the displacement sensor is being mounted to measure the radial vibration displacement of the rotor is equal to or more than 20% of relative rotor vibration displacement, then the absolute radial vibration displacement of the rotor must also be measured. And if the absolute vibration is found to be larger than relative vibration, then absolute vibration displacement of the rotor must be used to measure rotor vibration. (SFS-ISO 20816-1 2017, p. 16.)

B. Dynamic load on bearing

If the reason behind rotor displacement measurement is to interpret dynamic load on the bearing, then relative rotor displacement vibration must be used to measure the rotor vibration (SFS-ISO 20816-1 2017, p. 16).

C. Rotor/stator clearance

If the reason behind rotor displacement measurement is to interpret the clearance between the stator and the rotor then which parameter to select for measuring rotor vibration depends on two conditions. These two conditions are listed below.

1. If the radial displacement vibration of the structure or part where the displacement sensor is being mounted to measure the radial vibration displacement of the rotor is less than 20% of relative rotor vibration displacement, then relative radial vibration displacement of the rotor can be used to measure rotor vibration to monitor the clearance. (SFS-ISO 20816-1 2017, p. 16.)
2. But if the absolute displacement vibration of the structure or part where the displacement sensor is being mounted to measure the radial vibration displacement of the rotor is equal to or more than 20% of relative rotor vibration displacement then, the relative may still be used as a measurement of clearance. But special arrangement for measurement is required, when absolute displacement vibration of structure or part being measured does not represent the vibration of the stator. (SFS-ISO 20816-1 2017, p. 16.)

The key point about measuring the clearance between rotor and stator is selecting the appropriate location to measure the relative radial vibration of the rotor and the absolute radial vibration of the stator. If the absolute radial vibration of the stator is measured in such a place which do not portray the reality in terms of vibration of the stator, then conditions do not apply. Meaning appropriate locations must be identified to measure the absolute radial vibration of the stator. (SFS-ISO 20816-1 2017, p. 16.)

### 2.7.1 Relative radial vibration displacement of the rotor

Relative radial vibration displacement of the rotor can be measured with two non-contacting displacement sensors which are mounted in an appropriate location on non-rotating parts of the machine such as bearing housing. Only one single transducer can also be used when it provides enough information regarding the rotor relative vibration of the machine but that will limit some signal analysis techniques. These two sensors can be placed at any angular position but must be in the same transverse plane and perpendicular to the rotor centerline in the bearing or close to bearing housing as possible. (SFS-ISO 13373-1 2002, p. 11.) These displacement sensors or proximity probe are mounted away from the bearing centerline towards the center of the rotor. The axial distance between the bearing centerline and the location of the sensor must be within 25 mm. (Scheffer & Girdhar 2004, p. 39.) It is common in the industry to mount these sensors either in two radial *x*-axis and *y*-axis or in radial ±45º from radial *y*-axis in the same transverse plane as shown in Figure 6 (SFS-ISO 13373-1 2002, p. 11).

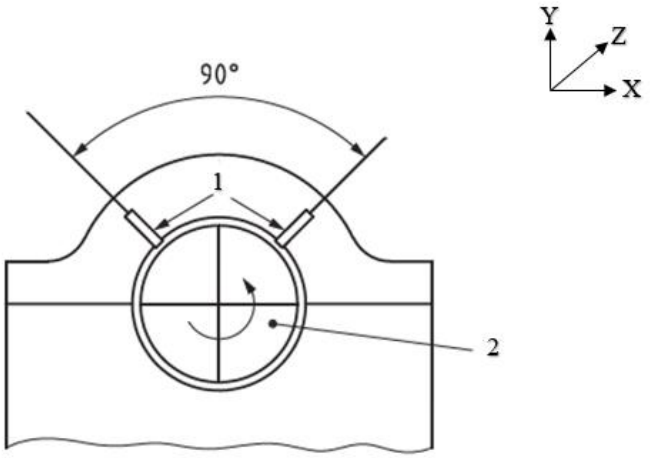


**Figure 6.** The mounting position of proximity probes for measuring relative radial vibration of the rotor at the bearing housing. The parts indicated by number 1 are two proximity probes and part indicated by number 2 is the rotor. (Mod. SFS-ISO 20816-1 2017, p. 13.)

### 2.7.2 Absolute radial vibration displacement of the rotor

Absolute radial vibration displacement of the rotor can be measured by two non-contacting transducers and two seismic transducers. The common method of mounting these sensors in bearing housing for measuring absolute radial vibration of the rotor is shown in Figure 7. (SFS-ISO 20816-1 2017, p. 13-14.)

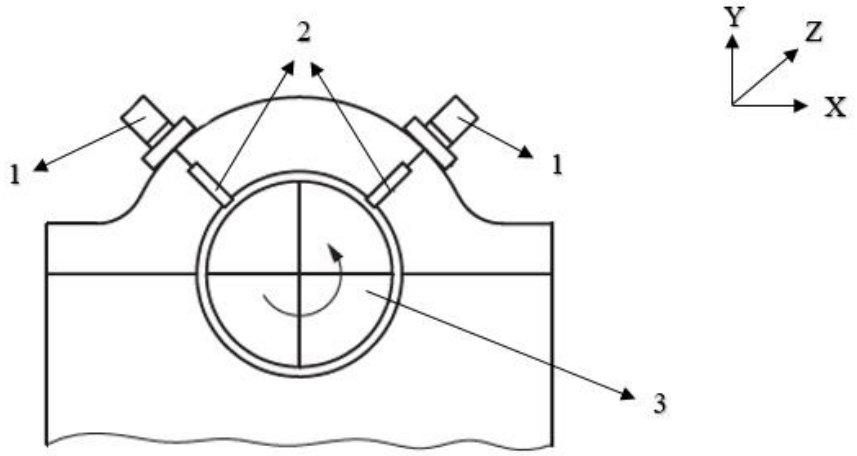


**Figure 7.** Mounting location for seismic and non-contacting transducer for measuring absolute radial vibration displacement of the rotor at bearing housing. The part indicated by number 1 are seismic transducers and part indicated by number 2 are non-contacting transducers. (Mod. SFS-ISO 20816-1 2017, p. 13-14.)

As shown in Figure 7, the non-contacting and seismic transducers are mounted as either in two radial *x*-axis and *y*-axis or in radial ±45° from the radial *y*-axis, in the same transverse plane. The seismic transducer is mounted close to a non-contacting transducer such that these transducers undergo same absolute vibration as that of non-contacting sensors in the direction of measurement. Thus, the sensitive axis of both sensors must be parallel to each other. (SFS-ISO 20816-1 2017, p. 13-14.)

Whichever seismic transducer, velocity or accelerometer is used, it can be integrated to get the absolute displacement vibration of the bearing housing at the location of its mounting. And when the absolute vibration displacement of the seismic transducer is vectorially added to displacement measured by the non-contracting transducer at the same time reference, the absolute vibration displacement of the rotor is obtained. The same time reference means that

they are measured at the same time. For that reason, the same time reference must be used for measuring the output of both sensors. (SFS-ISO 20816-1 2017, p. 13-14.)

Absolute radial vibration displacement of the rotor can also be measured with the use of seismic transducer and rotor rider. Since this method has limited rotor rotational range for measurement, it is not being used for machine that operates at a higher rotational speed. (SFS-ISO 13373-1 2002, p. 12.)

### 2.7.3 Phase reference and rotation speed of the rotor

Acceleration, velocity and displacement vibration are vector quantities and thus when comparing two vibration parameters, it is necessary to compare the phase angle between them (SFS-ISO 20816-1 2017, p. 8). Phase angle measures the angular or time difference of one sinusoidal signal to another or vibration signal to a fixed reference. For phase reference and rotation speed, optical or inductive or eddy current based transducer is used which generates a signal when it passes a phase reference point on the rotor. The phase reference point on the rotor is also called a trigger location. It can be any arbitrary location but the keyway in the rotor is recommended as a reference point. Similar transducers must be used for measuring the phase difference between two locations to avoid instrumentation error. If different transducers are used, then it is necessary to make compensation adjustments for the differences. (SFS-ISO 13373-1 2002, p. 15.)

## 2.8 Machine operational state for measurement

The measurement from the rotating machine must be taken in different operating modes of the machines which it will or has been used for. Different operating modes refers to machine loading condition and the rotation speed of the machine. For new machines, vibration measurements are taken after a wear-in period of a few days or weeks after its operation. (SFS-ISO 13373-1 2002, p. 21-22.)

The vibration of the rotating machine is measured during run-up and coast-down and during steady state operation. Run-up vibration is vibration during a startup operation of the rotating machine and coast-down vibration is vibration when the machine is being shut down. Steady-state operation refers to operation at a constant speed of rotating machine which is done by bringing the rotation speed of the rotor at a desired constant speed. The vibration

measurements are taken after the initial vibration due to run-up has subsidized. In rotating machines that are attached with electrical motor, a steady state is achieved by supplying constant amplitude excitation voltage in the field of the motor. (Vance 1988, p. 374.)

## 2.9 Selection of appropriate sensors

The selection of appropriate sensors for vibration measurements is an important aspect of monitoring state of the rotating machine. What sensors to select for measuring the vibration of the rotating machine depends on machine type, its components, its design, rotor material and its surface finish, data acquisition devices, rotating speed, etc. But from the perspective of the sensor itself, the most important aspects that need to be considered are the sensor's magnitude and frequency range of the measurements. (SFS-ISO 13373-1 2002, p. 14-20.)

The magnitude range of the sensor refers to the range of vibration amplitude a sensor can measure. Vibration sensors selected must be able to measure the lowest to highest anticipated vibration amplitude in the rotating machine. Frequency range refers not only to the frequency at which the rotor is rotating but rather at what frequency the component such as housing and rotor could vibrate. Depending upon what is being monitored, the frequency range must be able to measure vibration and harmonics of components such as bearings, gears, vanes, etc. (SFS-ISO 13373-1 2002, p. 14.)

For the machines rotating under 10 Hz or 600 RPM, the vibration acceleration amplitude is very small and vibration velocity amplitude is modest. But there is a large vibration in terms of displacement. Thus, displacement sensors are used to measure vibration when machines are rotating below 10 Hz. (Scheffer & Girdhar 2004, p. 39.) According to sensor selection guidelines from SFS-ISO 13373-1, appropriate sensors for vibration measurements are selected based on the anticipated magnitude and frequency range as shown in Figure 8.

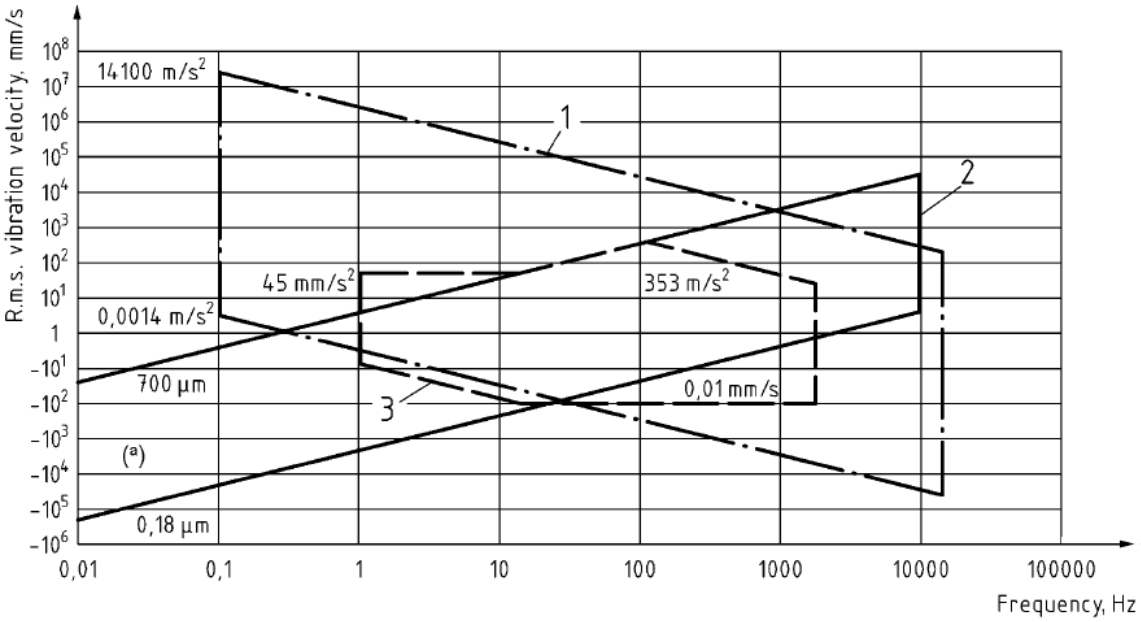


**Figure 8.** Selection of sensor based on anticipated vibration amplitude and frequency range in rotating machine (SFS-ISO 13373-1 2002, p. 17).

In Figure 8, the range of vibration magnitude and frequency enclosed by plane 1 refers to the piezo-electric accelerometer, plane 2 refers to eddy current proximity probe for displacement measurement and plane 3 refers to electro-mechanical velocity transducers. The symbol (a) refers to d.c. component of proximity probe that measures the position of the rotor. According to Figure 8, such a sensor must be selected for vibration measurement that has enclosed the expected frequency and magnitude range of the specific machine within the plane of the respective sensor. (SFS-ISO 13373-1 2002, p. 17.)

Other factors to be considered when selecting sensors are its measurement accuracy, linear range, sampling frequency, the resonant frequency of the sensor, mounting possibility, sensitivity based on the ambient condition of machine such as temperature, magnetic and electric fields, dust, insulation faults, etc. (SFS-ISO 13373-1 2002, p. 14-21).

## 2.10 Sensor attachment

Vibration measurement critically depends on how accurately the vibration of the machine component is being transferred to the transducer that is measuring vibration. The preferred method for attaching transducers is by a rigid mechanical fastening. It is achieved by drilling tapped holes in the transducer and machine and joining them together with threaded stud.

Stud mounting is the best way to attach transducers which can transfer high-frequency signals with little or no signal loss. It is also recommended to apply a light coat of silicone grease or equivalent to all the mating surfaces to further improve vibration transmission from the machine component to the transducer. When it is not possible to stud mount the transducers, cement is an option for the purpose. But however, the stiffness of the cement must be high when cured. Adhesives should not be used because they do not transmit vibration signals accurately. Another method of attaching the transducers is by means of a permanent magnet. The flatness of the mounting surface is critical when attaching transducers with the permanent magnet. Magnetic and cement attachment is limited by frequency, temperature, and amplitude for measuring vibration. In some cases, the transducers can be mounted on a bracket which then can be attached to the machine. Depending upon how the transducer is attached, the mounted resonance frequency of the transducer is reduced. There is no reduction in resonance frequency when attaching a sensor with a rigid stud mount. But for all other mounting methods, the resonance frequency of the sensor is reduced. (SFS-ISO 13373-1 2002, p. 20-21.)

# 3 SIGNAL PROCESSING AND ANALYSIS OF VIBRATION DATA

After measuring required parameters from rotating machines as explained in chapter 2, it is necessary to process these measured signals into measurement parameters. Measured signal is in terms of parameters depending upon sensors such as capacitance, voltage etc. and these are converted into vibration parameters such as displacement. These vibration parameters are further processed to remove non-related signals such as noise and formatted in the form required for analysis. Figure 9 shows the process of how measurements from transducers are processed to do required signal analysis. (Mohanty 2015, p. 49-52.)

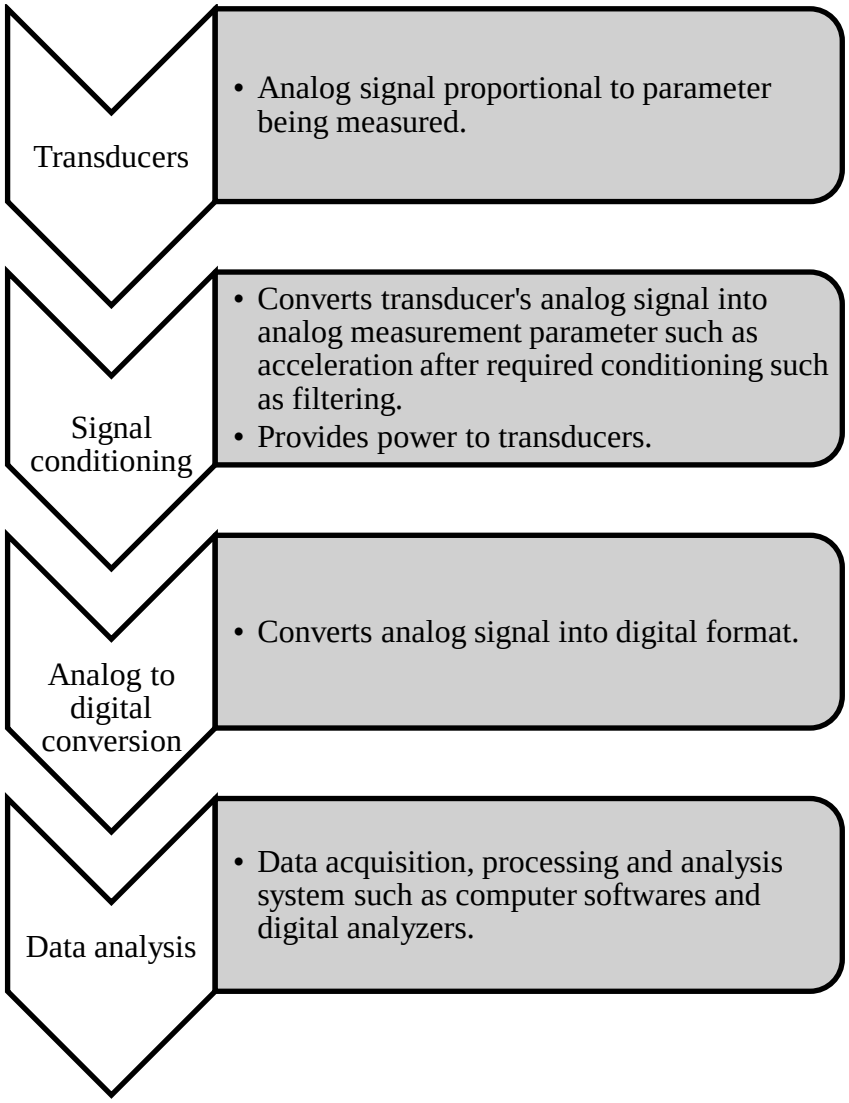


**Figure 9.** The process from measurement to signal analysis (Mohanty 2015, p. 49-52).

All the four processes shown in Figure 9 can be integrated in one single instrument or multiple instruments. For instance, dynamic signal analyzer is one such instrument which does measurement, signal conditioning, Analog to digital conversion (ADC) and data analysis all by itself. (PHOTON+ Dynamic signal analyzer 2016).

## 3.1 Signal conditioning system

The output signal of sensors depends on what is the principle behind the sensing technology and what internal signal condition processes it does. For instance, typical piezoelectric charge accelerometer gives only the charge in piezoelectric material as output. This proportional charge output provides the acceleration vibration after required signal conditioning. (Piezoelectric Charge Accelerometer Types 4371 and 4371-V 2018.)

The measured signal of the transducer is continuous in time and thus is analog in nature. These signals from transducers need additional processing such as signal amplification, noise reduction, filtering, linearization, integration, differentiation, etc. These conditioning processes can be done by the help of analog standalone signal conditioners or dedicated digital signal processing software after converting analog signals to digital by ADC. The signal conditioning system also provides the required power to the sensors. (Mohanty 2015, p. 52.) Transducers provide an analog electrical signal. This signal is proportional to instantaneous magnitude of the parameter that is being measured. The actual vibration magnitude is obtained by multiplying output voltage with the calibration factor of the transducer. (SFS-ISO 13373-2 2005, p. 1-2.) Power supplies to transducers, pre-amplifiers, amplifiers, integrators and different types of filters are part of signal conditioning equipment (SFS-ISO 13373-2 2005, p. 4).

The signal conditioning system can be an integral part of the sensors or separate instrument in between sensor and data analysis system or a combination of these systems (SFS-ISO 13373-1 2002, p. 13-14). The charge amplifier is a separate instrument that does conditioning of signals from piezoelectric transducers and transmits it to an analyzer. These separate instruments are mainly used for signal conditioning and to avoid risk of picking noise due to long cables of the transducers. (Charge Amplifiers-Type 2634 2010.) When these signal conditioning functions are integral part of the transducer or separate system for certain usage, the user can be sure that it is providing right information. But if it is used in

other applications, the user has no or less choice in changing the signal conditioner setting. When there are many conditioning settings available for user, it is important to make record of setting profile used and the following measurements must also be made with the same setting. A comparison of measurement taken in different conditioning settings can lead to judgmental errors about the actual condition of the machine. With an external signal conditioning system between the transducer and measuring instruments, it is important to be aware of signal levels and dynamic range of the instrument in order to avoid introducing distortion into the measurement. To obtain valid results, frequency response characteristics of signal conditioners must be matched with remaining instruments being used for vibration measurement. (SFS-ISO 13373-1 2002, p. 13-14.)

### 3.1.1 Filtering

Filtering is an important signal conditioning process which removes noise and unwanted signals from the measurement. The measured steady state analog signal from the rotating machine by a transducer such as an accelerometer is random in nature with noise. Figure 10 shows an example of how the raw measured uniaxial acceleration vibration from rotating machine looks like.

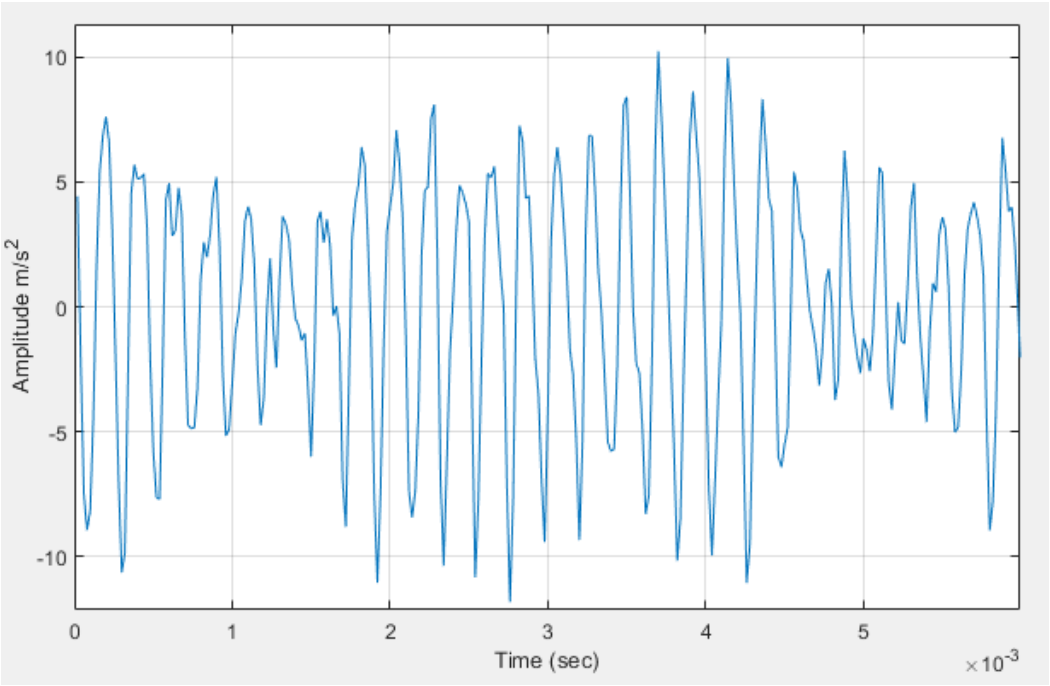


**Figure 10.** Example of raw measured acceleration vibration in $m/s^2$ for a given time in seconds.

These measured signal by a transducer is also called a composite signal. It is composed of many individual signals with different frequencies and amplitude including noise. Thus, only taking informative signals from a composite signal with the use of filters is called filtering. The filtering of the signal is important when analyzing signals that have frequencies with both high and low amplitudes. Without filtering such signals cannot be analyzed with the same level of accuracy because of limitations in the dynamic range of the signal analyzer. For signal conditioning, there are three basic types of filters. They are low pass, high pass, and bandpass filters that can be analog or digital. These are listed below. (SFS-ISO 13373-2 2005, p. 6.)

A. Low pass filters

In machine vibration, composite signals can have individual signals with frequencies above the 10 times the RPM of the machine. It can be noise or true signal but has little importance from the perspective of signal analysis. Low pass filter removes these high-frequency components from composite signals that are above filter limiting frequency or also known as the cut-off frequency of the filter. Low pass filtration can be analog or digital. (Adams 2001, p. 241.) The Figure 11 shows how high frequency noise is removed from composite signal using low pass filter.

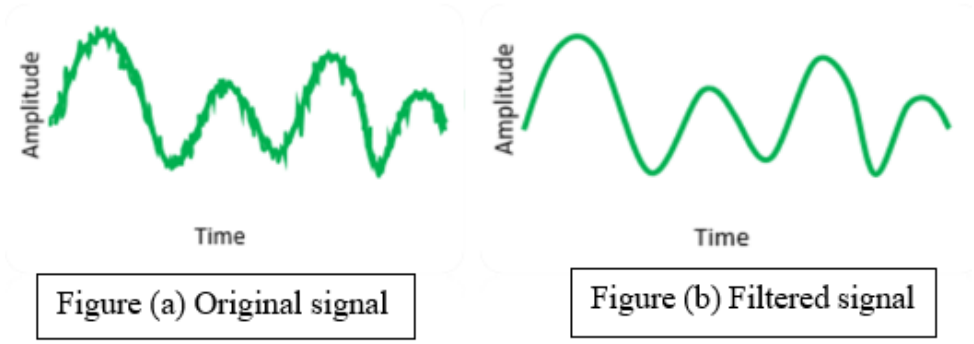


**Figure 11.** Filtration of high frequency noise with low pass filter. Figure (a) is original signal which is filtered using low pass filter to get filtered signal in Figure (b). (Mod. Siemens, 2019.)

In Figure 11, the composite original signal contains high frequency noise as shown in Figure (a). The low pass filter removes this high frequency noise from original signal to get the filtered signal as shown in Figure (b).

B. High pass filters

When a composite signal from a transducer is subjected to a high pass filter, the filtered signal will not contain individual signals with a frequency lower than the cut-on frequency. That means the filter blocks all individual signals that have frequency lower than cut-on frequency. (Mohanty 2015, p. 53.) High pass filters are mainly used to remove low-frequency transducer noise also called thermal noise and other unwanted low-frequency components before analyzing the signal (SFS-ISO 13373-2 2005, p. 6.) The common cut-on frequencies in machinery vibrations signal conditioning is 0.1 Hz or 1 Hz (Mohanty 2015, p. 53). However, cut-on frequency depends also upon the need for filtering.

C. Bandpass filters

The bandpass filter can be made by using pair of low pass and high pass filter to allow it to only pass individual signals that are in the range of the defined frequency band. (Mohanty 2015, p. 53). In other words, low pass filter and high pass filters are used in series to let it pass only the designated frequency band (Adams 2001, p. 241). Octave filter or 1/n octave filters are common bandpass filters. These are used to correlate vibration measurements with noise measurements. (SFS-ISO 13373-2 2005, p. 6.)

## 3.2 Analog to digital conversion

Analog signals from transducers can be processed using digital or analog systems. More recently, ADC is used to sample analog signals to digital values. With appropriate choice of the sampling frequency, both types of the signal contain the same information. It is important to know the sensitivity of the signal being measured regardless of signal processing system. The ratio of the actual output voltage of the signal to the actual magnitude of the parameter being measured is called sensitivity. The signal of interest must be significantly greater than that of the ambient noise level but should not be that large that the signal is distorted. For example, in such a case where the signal is very large than that of noise, peaks of signals are clipped. (SFS-ISO 13373-2 2005, p. 2-3.) Sampling rate and resolution are the two most important aspects when converting analog to digital signals by an ADC (Mohanty 2015, p. 49).

### 3.2.1 Sampling rate

The process where the sampled amplitudes of the conditioned analog signals are recorded in such a way that the recorded discrete or digital signal contains the same information as that of an analog signal is called sampling. The same information refers to the shape and amplitude of the analog signal. Defining the rate at which the number of amplitude points or samples from an analog signal to record it as a discrete signal is called sampling rate. It is also called sampling frequency and it represents the number of samples recorded per second. According to Nyquist sampling theorem, the sampling rate must be at least twice that of the interested highest frequency component for a sampled discrete signal to represent its original analog signal. The interested frequency component refers to the frequency of individual signals present in a composite signal after filtering. (SFS-ISO 13373-2 2005, p. 20.) Figure 12 shows the aliased signal that was sampled at a lower sampling rate than Nyquist frequency in order to represent the original signal.

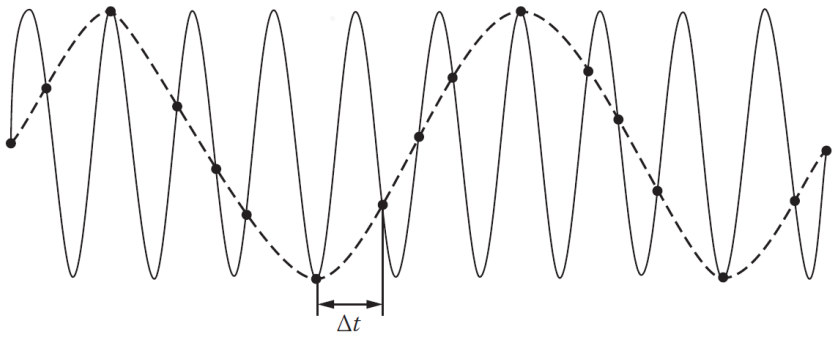


**Figure 12.** An aliased signal shown as dashed line when sampling rate at 1/Δt is smaller than Nyquist frequency of the original signal shown as solid black line (Mohanty 2015, p. 50).

In Figure 12, the original signal is represented as a black solid line and the dashed line represents the sampled signal from the original signal with a lower sampling rate than Nyquist frequency. The original signal is falsely represented as being a low frequency signal after sampling. This error of misrepresentation of original signal is called aliasing error. Thus, it is important to have a sampling rate of at least two times the frequency of the original signal. This sampling frequency is called the Nyquist frequency. (Mohanty 2015, p. 50.)

The type of analysis and anticipated frequency content of signals will determine the sampling rate. The recommended sampling rate must be about 10 times the highest frequency of

interest in the signal for the time-domain plot. (SFS-ISO 13373-2 2005, p. 4.) With a sampling rate of about 10 times the highest frequency, correct peak amplitudes can be seen in time-domain plots (Simcenter, 2019). For FFT analysis, the calculation requires the sampling rate to be greater than two times the highest frequency of interest to be measured to prevent aliasing (SFS-ISO 13373-2 2005, p. 4). The sampling rate can be fixed or variable. In a fixed sampling rate, the samples are taken from the original signal at a fixed time interval. But in synchronous sampling, external signals can be used to control the sampling rate. The sampling rate in such a case will normally be some multiple of external signal frequency. (SFS-ISO 13373-2 2005, p. 21.)

### 3.2.1 Resolution of ADC

The analog measurements are converted by ADC to digital values. These digital values are saved as binary bits according to the bit size of ADC. For instance, 3-bit ADC can save analog measurements in eight different digital values. For analog signal in range *R*, representing the measured amplitude of vibration, the amplitude resolution *AR*, of ADC can be calculated as,

$$AR = \frac{R}{2^n}, \tag{5}$$

where, *AR* is amplitude resolution of ADC, *R* is the range of analog measurements and *n* is the number of bit size of ADC. The analog values represented from ±5 V have the range of 10 V. Thus, for a 3-bit ADC, the amplitude resolution is 1.25 V. It means that ADC can convert the minimum vibration value of 1.25 V into digital values. Below this resolution threshold, ADC does not capture the amplitude of the vibration. This error is also called the digitization error. Thus, it is necessary to have higher bit-sized ADC or analog amplifiers in order to record the small change in the analog signal to provide the required accuracy needed. (Mohanty 2015, p. 51).

## 3.3 Data acquisition and processing

The analog signal that is converted to digital signal is then stored in the digital memory of ADC or these data can be also be transferred to a computer through data acquisition software. The data are transferred to computer based on computer architecture and data transfer

protocol. Digital signals can also be transmitted to remote locations for analysis via wireless network or Ethernet. (Mohanty 2015, p. 51-52.) These acquired raw digital data are then formatted in a form that is required for further analysis. Formatting refers to tasks such as filtering noises and unwanted signals, integration, differentiation, runout compensation, unit conversion, etc. Analysis of these formatted signals are done in frequency domain and time domain. How the analysis is done in these domains are explained in the subchapters 3.4 and 3.5. (SFS-ISO 13373-2 2005, p. 7.)

## 3.4 Time-domain analysis

After data acquisition and required processing, the collected data will be time indexed vibration amplitude in the respective units depending upon the sensor. It can be acceleration, velocity or displacement's composite vibration amplitudes at respective measured time. The amplitude of vibration is the most important aspect to observe in time-domain data. It can be inspected visually after plotting or inspected based on statistical features of the signal. Analysis in time domain diagnose the changing condition of the machine but the fault diagnosis that identifies the reason behind changing condition of machine from time domain is limited. (Asoke & Ahmed 2019, p. 33.) Different techniques of inspecting time domain data for analyzing machinery conditions are described in the following subchapter.

### 3.4.1 Based on visual inspection

Time domain analysis based on visual inspection refers to information provided by the formatted time domain data when these are plotted without further signal processing. The state of the machine and components can be assessed by comparing the vibration signal's amplitude from normal machine or just by observing the plotted amplitude of the signal. (Asoke & Ahmed 2019, p. 33.) Some of these time domain analyses based on visual inspection of plot are listed below.

A. Time waveforms

Time waveforms are a plot of instantaneous vibration versus the time. In the past, it was the primary method of vibration analysis. When the vibration time waveform shows that vibration amplitude is higher than normal, it indicates that there is a fault in machine. But however, it is not enough to know the cause or the condition that made the amplitude higher. (Asoke & Ahmed 2019, p. 33.) The peaks in time waveforms were useful in detecting

machinery condition. For instance, time waveforms with clipped top or bottom can indicate a rub, mechanical looseness, however, such time-domain signature provides only basic information about the condition of the machine. Machine instantaneous vibration acceptance criteria based on velocity require that the vibration velocity of the machine must be within the specified range. Time waveform helps in monitoring if the vibration goes beyond the acceptable limits. (SFS-ISO 13373-2 2005, p. 7-24.)

B. Beating

Beating is caused by superposition where the signal contains two components that are close in frequency and amplitude. Superposition refers to the vector summation of individual signals. In such a case, the composite signal has bulges and waists as shown in Figure 13. The peaks of such signals alternatively add and subtract to create bulge and waist. The length of the beat is about the same but the spacing between the peaks at the bulges is different than that of peaks at the waist. The distance between the upper and lower limits at the bulges represents the sum of the peak to peak values of the components and at waist represents the difference between the peak to peak values of the components. (SFS-ISO 13373-2 2005, p. 8-9.) Figure 13 shows how the composite signal looks like when beating occurs due to two signals close in frequency and amplitude.

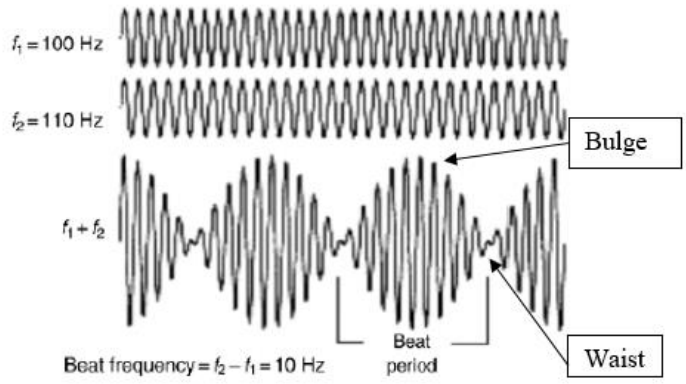


**Figure 13.** Beating vibration signal due to $f_1$ at 100 Hz and $f_2$ at 110 Hz which are close in frequency and amplitude. Bulge is section where amplitude is high, and waist is where the amplitude of beating signal is low. (Mod. Scheffer & Girdhar 2004, p. 66.)

In industrial electric motor drives, the absence of beating may indicate mechanical problems while its presence can indicate both the mechanical and the magnetic problems. For instance, in a two-pole induction motor, two beating components can have close frequencies at twice

the RPM and twice the supply frequency respectively to cause beating (Bate n.d.) In rotor dynamics, beating can occur when two successive natural frequencies are close in frequency and are excited at the same time (Friswell et al. 2010, p. 270).

C. Modulation

An amplitude modulated vibration signal is the one where only one component whose amplitude is varying with time. It looks like the beating, but the distinguishable characteristics of modulation are that the spacing of the peaks is the same at the bulges and at the waist. Also, the length of bulges may not be same. Problems in gears result in modulation of gear mesh frequency at the frequency of gear rotation. Many vibration signals contain more than two components and can have a beating and modulation present in the same composite signal. Figure 14 shows an example of the modulated signal. (SFS-ISO 13373-2 2005, p. 10.)

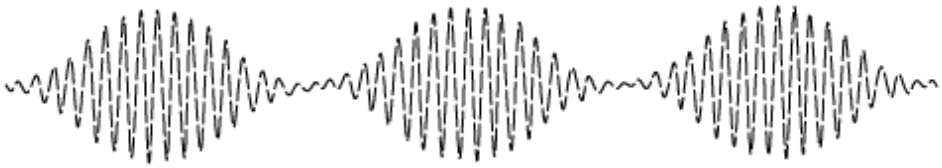

**Figure 14.** Signal modulation (SFS-ISO 13373-2 2005, p. 10).

Vibration signal is also amplitude modulated when, for example balls of ball bearing pass from a spalled bearing location (Scheffer & Girdhar 2004, p. 83). A frequency modulated vibration signal is the one where the frequency of the vibration is varying with time. Low-frequency modulation of vibration signal can happen due to misalignment in rotating machines. In electrical motors, fluctuation in torque can result in phase and frequency modulation. Torsional vibration in the rotor can also result in phase and frequency modulation of the vibration signal. (Asoke & Ahmed 2019, p. 50.)

### 3.4.2 Based on statistical functions

The formatted time domain data can be processed to extract statistical-based signal features with respect to time. Through these features, the condition of machine can be monitored through trending rather than identifying the faults in the rotating machine. There are many statistical features that can be extracted from the vibration data. Some of these are peak

amplitude or 0-p, mean amplitude, Root Mean Square (RMS) amplitude, peak to peak or p-p amplitude, crest factor (CF), kurtosis, etc. (Asoke & Ahmed 2019, p. 35-46.) Statistical features such as 0-p and p-p have been discussed in chapter 2. Some common statistical functions-based signal analysis techniques are presented in list below.

A. RMS Amplitude

The RMS amplitude of a sampled discrete vibration signal can be calculated as,

$$V_{RMS} = \sqrt{\frac{1}{N}\sum_{i=1}^{N} v_i^{\,2}}\ , \tag{6}$$

where, $V_{RMS}$ is RMS vibration amplitude, $N$ is number of discrete data points, $v_i$ is vibration amplitude of *ith* data point (Asoke & Ahmed 2019, p. 36). In order to check the acceptance criteria applicable to the specific machine, RMS vibration velocity is measured from the machine. Other reason to measure is based on condition monitoring where the RMS vibration of the machine is trended in specific frequency band and compared with the maximum and minimum allowable range. Alarms to signify the changing machine condition are created based on RMS or peak vibration. (SFS-ISO 13373-1 2002, p. 23-24). In rolling element bearing, high RMS acceleration signifies the faulty condition of bearing based on severity chart (SFS-ISO 13373-3 2015, p. 33-34). The RMS vibration values provide information regarding the diagnosis of the condition of the machine, but other methods are required for fault diagnosis (Williams, Davis & Drake 1992, p. 72).

B. Crest factor

The ratio of 0-p and the RMS of the vibration waveform is called the crest factor (CF). It is also called peak to RMS ratio. The crest factor of vibration signal is calculated as, (Asoke & Ahmed 2019, p. 36).

$$V_{CF} = \frac{V_{0-p}}{V_{RMS}}\,, \tag{7}$$

where, $V_{CF}$ is Crest factor of vibration signal and $V_{0\text{-}p}$ maximum amplitude 0-p. It is also used for trending machine condition for monitoring purpose (Scheffer & Girdhar 2004, p. 20). Impulsiveness of a vibration signal is measured by CF. Damaged bearings produce impulsive

vibration and this can be detected by the magnitude of CF. The bearings without faults have CF range of about 2.5-3.5 and in the faulty bearings, the CF is more than 3.5. Before the bearing fails, the CF factor increases, and it can get as high as about 11. But when there is no significant impulsiveness, the reliability of CF technique in detecting bearing damage is reduced. (Norton & Karczub 2003, p. 522.)

C. Kurtosis

The kurtosis of vibration signal can be calculated as,

$$V_{kur} = \frac{\sum_{i=1}^{N}(v_i - \bar{v})^4}{(N-1)\sigma^4} \ , \tag{8}$$

where, $V_{kur}$ is kurtosis, $N$ is number of discrete data points, $v_i$ is vibration amplitude of $i^{th}$ data point, $\bar{v}$ is the mean of the data points and $\sigma$ standard deviation of the data points (Mohanty 2015, p. 37). Impulse within the vibration signals are detected with the help of kurtosis. The vibration signal from the roller bearings which is in good condition without faults have kurtosis of around three. But when the bearing has faults that produces impulse, then kurtosis value of signal will be greater than four. Kurtosis analysis is limited to faults that generate the impulse. It can also be used to monitor the condition through its trending with time. (Norton & Karczub 2003, p. 522.)

## 3.5 Frequency domain analysis

The vibration measurements from rotating machines are available in time domain. This measured composite signal is summation of individual signals that were produced by different components in the machine. Each component such as gear, shaft, bearings, fans etc. produce own sine signal with specific frequency and amplitude. In other words, all components in rotating machine vibrate in their own single frequency and amplitude such that when measured by sensor, the composite signal is the summation of all these individual vibration components. Thus, it is difficult to identify the frequency and amplitude of signal produced by individual machine component in time domain analysis. In frequency domain analysis, these individual signal component's frequency and amplitude can be identified. Depending upon the signal generated by the machine component, its state can be assessed.

(Asoke & Ahmed 2019, p. 63-64.) Commonly used frequency domain analysis is done with Fourier transform as presented in following subchapter.

### 3.5.1 Fast Fourier Transform

Depending upon what type of signal, whether continuous time such as analog signal or discrete time such as sampled digital signal, there is different Fourier transformation techniques. For continuous signals, Continuous-time Fourier transform can be used to make frequency domain analysis. And for sampled digital signals, discrete-time Fourier transform can be used. But these techniques require infinitely many numbers of computations and thus are inefficient. However, Fast Fourier Transform (FFT) algorithm which computes discrete Fourier transform is computationally efficient due to reduced number of computations. Thus, FFT is commonly used signal analysis technique in digital signal processing. (Prabhu 2014, p. 1.) Figure 15 shows how FFT helps in identifying individual frequency components from composite time domain measurement.

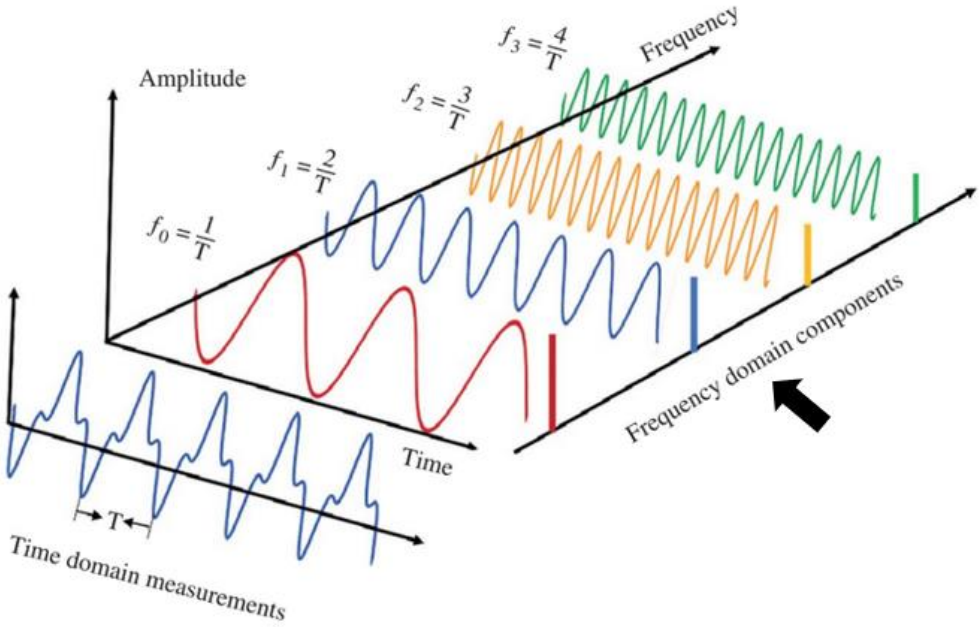


**Figure 15.** Time domain measurements into its constituent frequency components. The frequency $f_0$ is fundamental frequency and $f_1$, $f_2$ and $f_3$ are integer harmonics of fundamental frequency. (Mod. Asoke & Ahmed 2019, p. 63-64.)

These individual frequency components, including fundamental frequency and harmonics have their own amplitude, frequency and phase as shown in Figure 15. When viewed from the direction of the black arrow shown in Figure 15, the amplitude and the frequency of each

components can be identified. The fundamental frequency $f_0$, is also called once per revolution (1X) component and the harmonies are multiple of fundamental frequency.

However, before analyzing signals in frequency domain with FFT, the next process that is required after ADC is called windowing. The waveform is truncated or shortened at the start and the end of the waveform when the vibration signals are sampled at the fixed time interval. If the digital samples itself are not truncated due to the selection of sampling frequency and the fundamental frequency, it can still get truncated based on finite set of data points that are selected to do FFT. In such cases, the FFT of the discontinues or nonintegral number of cycles will show sidebands or signal components that were not present in the original signal. This is called leakage error and the reason is due to the way FFT algorithm works. The discontinues signal is seen by FFT algorithm as signal that has many signals with varying frequencies. (Scheffer & Girdhar 2004, p. 58.) Figure 16 shows the comparison of FFT when leakage occurs due to discontinuity or nonintegral number of sample cycles.

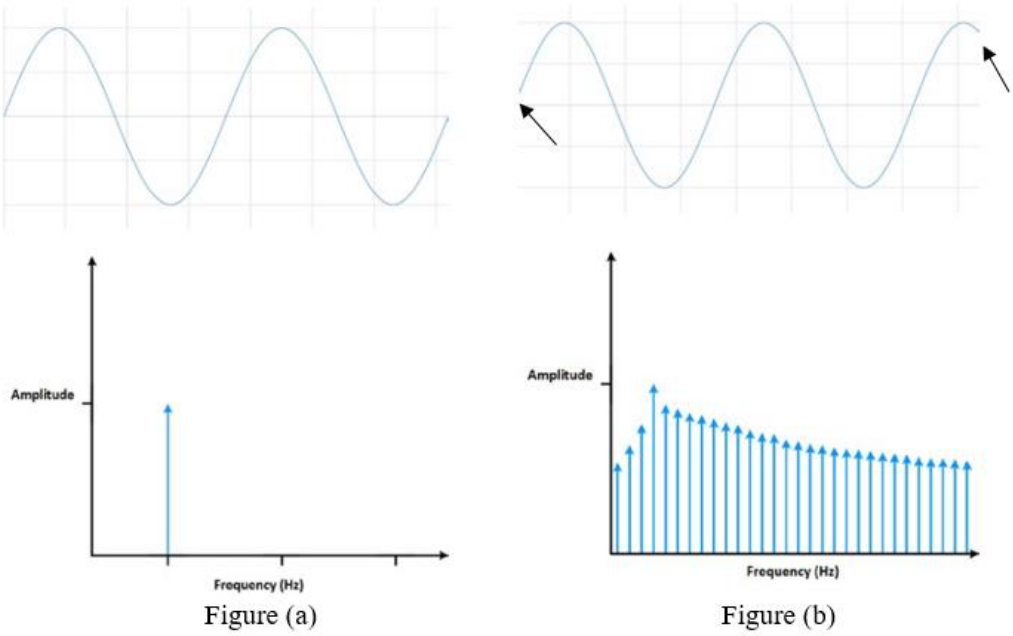


**Figure 16.** FFT of sample signal with continuous waveform or integer number of cycles in Figure (a) and signal sample with discontinues waveform as shown by black arrows or nonintegral number of cycles in Figure (b) (Mod. National Instruments n.d., p. 8-9).

The window functions are used to reduce the error by leakage. It fills the discontinuous waveform by forcing the beginning and the end of the data to be zero. This process which makes the data appear continuous is called windowing. However, windowing affects the

ability of FFT algorithm to distinguish frequencies that are close and at the same time maintain the accuracy of their amplitude. The amplitude accuracy can be optimized at loss of accuracy of frequency and vice versa. (Scheffer & Girdhar 2004, p. 58-59.) Figure 17 shows how the Hanning window function forces the discontinuous waveform to be zero at the end and start and reduces leakage error.

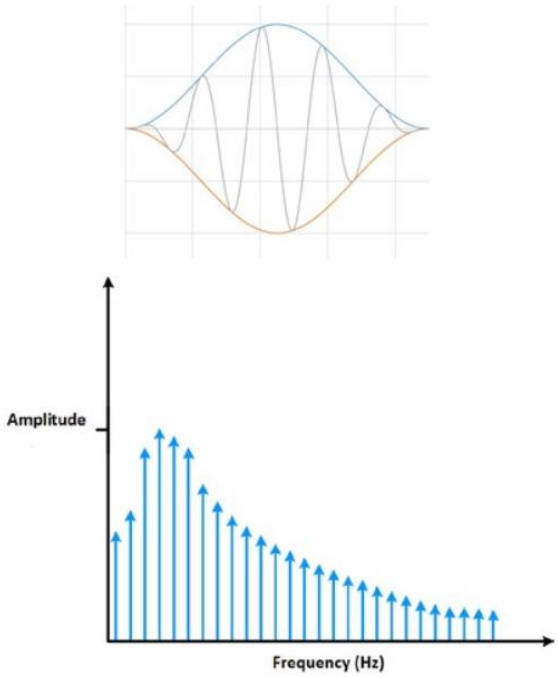


**Figure 17.** Hanning windowing and reduction in spectral leakage. (Mod. National Instruments n.d., p. 10).

There are many different types of window functions such as Hanning, Rectangular, Flat Top, Hamming, Blackman, Barlett, Kaiser Bessel etc. Which window to use depends upon signal itself and the intent of use. For example, intent could be to identify the signal component or a peak at certain frequency accurately or to identify accurately the magnitude of the frequency component. (Scheffer & Girdhar 2004, p. 59-60.) Since there is no universal approach in selecting the windowing functions, it can also be selected best on comparison of performance of windows that best serves the intent. However, the first choice of the window function can be selected based on the kind of signal it is tailored for. The Hanning window is initial choice when signal contains sine wave or combination of sine waves which are periodic or non-periodic. If the intent is to find the accurate amplitude of the signal that contains sine wave, then Flat Top is the initial choice. (National Instruments n.d., p. 14-15.)

After windowing, important factors such as the bandwidth of frequency lines or bins, frequency span and the length of sample must be considered before making FFT analysis. It requires that the interested frequency range must be divided into a finite number of sections. Within these sections, the vertical line represents the amplitude of the vibration. The number of sections is also called number of lines of resolution (LOR). Within frequencies of a single LOR bin, there can be more than one frequency component. FFT includes the total energy of all components and displays it as a single line at the center frequency of the bin. To distinguish closely spaced frequency, it is important to have enough LOR to separate these frequencies into different bins. Relationship between number of LOR, the maximum frequency of interest and bandwidth or line spacing is given by,

$$N_{LOR} = \frac{f_{\max}}{B}, \tag{9}$$

where, $N_{LOR}$ is the number of LOR, $f_{max}$ is the maximum frequency of interest in Hz and $B$ is bandwidth or line spacing in Hz. For the same frequency range, finer the resolution, smaller is the bandwidth or line spacing. (SFS-ISO 13373-2 2005, p. 16-18.)

For one complete FFT analysis, the minimum length of sample or record length ($T$) required is dependent on bandwidth and is calculated as,

$$T = \frac{1}{B}, \tag{10}$$

where, $T$ is the minimum record length in seconds. In other words, if $f_{max}$ is 100 Hz and resolution is 400 lines, then from equation (9), the bandwidth ($B$) is obtained to be ¼ Hz. Then from equation (10), the record length is calculated to be four second. Thus, four second of record length is minimum length required to be measured for one FFT analysis. And the number of sample points within four seconds depends upon sampling rate which must be greater than Nyquist frequency or two times the 100 Hz in this case. However, in order to represent the amplitude of frequency component accurately, the sampling rate and the record length are very critical selection before making FFT. In industry, the practical sampling frequency is about 2.56 times that of maximum frequency of interest. (SFS-ISO 13373-2 2005, p. 18-20.)

### 3.5.2 Interpretation of state of the machine or components

The state of machine or its components can be identified based on the amplitude, frequency and phase of the signal generated by the individual component or change in machine condition. When vibration measured are transformed using FFT, the change in condition due to machine or component's faults can be identified based on change in amplitude, phase and the frequency at which it occurs. These analyses are presented in following subchapter.

A. Unbalance

The unbalance is the uneven distribution of mass in the rotor about its rotating centerline. The unbalance creates centrifugal force in rotating machine that causes vibration, which is given as,

$$F_{ub} = me\omega^2, \tag{11}$$

where, $F_{ub}$ is centrifugal force in N, $m$ is unbalance mass in kg and $e$ is eccentricity in m. The quantity $me$ is called unbalance. (Matsushita et al. 2017, p. 105.) When the radial absolute displacement vibration measured at rotor is transformed using FFT, the amplitude of 1X component represents the maximum rotor displacement and the frequency represents the rotation speed of the rotor in Hz. The 1X amplitude due to unbalance is proportional to the rotation speed and increases as the speed increases. Any increase in maximum absolute displacement amplitude at constant speed indicates that the unbalance in the rotor is perhaps increasing. It is a possibility because, it may be due to other reasons such as crack in the rotor or structural looseness in the machine. However, when other reasons are eliminated, then it can then be identified if the unbalance is indeed increasing. (Mohanty 2015, p. 90-132.)

B. Other faults

Other faults in rotating machine or its components that can be identified through FFT are rotor rub, crack, misalignment, looseness, bearing failures etc. The fault identification of other failure related to rotating machines or components through FFT is presented in Appendix I. (Mohanty 2015, p. 217.)

# 4 MATHEMATICAL MODELLING OF ROTOR SYSTEM

An abstract and simplified model that mimics the reality of the system with the use of mathematical equations that govern the system being modeled is called mathematical model. Depending upon the design and purpose of the model, it can have parameters whose effects are neglected in the model, input or independent variables that affect the model but is not designed to study their behavior from the model and output or dependent variables that are designed to study the system's behavior through the model. (Bender 1978, p. 1-3.)

The rotor system of rotating machines consists of many components such as bearing, rotor, support, lamination, fan and other components that are assembled on the rotor to perform the specific function of the machine. These components affect the dynamic behavior of the rotor system. Mathematical modelling of such a system is the formulation of the variable's representation of the rotor system's properties and equation of motion that describes the dynamic behavior of the rotor system. The mathematical model of the same physical rotor system can be different depending upon modelling purpose, assumptions made in modelling, components being considered for modelling, independent and dependent variables considered while modelling, etc. For instance, due to manufacturing tolerances, the rotor system can have non-idealities such as uneven mass and stiffness distribution. Depending upon the modelling purpose these non-idealities can be considered or are excluded from the modelling. (Sopanen 2004, p. 15-30.)

## 4.1 Rotor model

A simple model can be made and used if the purpose of the model is to study the critical speeds of the rotor system. Depending upon the reliability of the study and ease of calculation, other assumptions such as rigidity of bearing, bearing damping and other independent variables that affect the dynamics can be considered in the model. (Krämer 1993, p. 19-24.) Depending upon the purpose, partial differential equations can be used to model and study simple rotor systems. But for complex rotor systems, the transfer matrix method or the FE method can be used to model the rotor system. These methods represent the rotor system and equation of motion in terms of the matrix. (Childs 1993.)

Modelling the rotor system and its dynamics has been done successfully by using the FE method. Other independent variables such as rotary inertia, gyroscopic moments, and shear deformation of the rotor and rotor asymmetry can also be considered and implemented in the FE method. (Sopanen 2004, p. 15-19.) This approach is suitable and effective when rotation around the radial axis is large (Kärkkäinen 2007, p. 21.)

## 4.2 Finite element model of the rotor system

FE modelling of the rotor system is done in two steps. The first step is to describe the physical system's properties in terms of abstract description by using independent quantitative variables for physical properties and dimensions. These variables are assembled in matrix form to describe the dynamic behavior of the actual system. The second step is to get the required solutions after solving equations of motion. These two steps are described in the following subchapters. (Friswell et al. 2010, p. 126.)

### 4.2.1 Abstract model description

The abstract model description defines the physical system in a way that says where forces and moments are present in the rotor and how these affect the movement and rotation of different sections within the rotor. In other words, it defines how the rotor section could dynamically behave due to forces and moments present in the physical system and how these movements are measured. In FE modelling, the physical rotor system is represented as a mathematical model by discretizing the physical system into simple geometry called elements. The type of element that can be used depends on the profile of the physical rotor. For modelling rotors, one-dimensional bar or beam element models are often used. (Friswell et al. 2010, p. 125-126.) Beam elements are a geometrical structural member which are assumed to be uniform straight bar that represents the structure and its behavior under applied loads. Based on what effects are considered in the element, it can be different. The model of the beam element where the effect of rotary inertia and shear deformation is considered is called Timoshenko beam element. However, in classical beam element, the effect due to shear forces are neglected. (Ishida & Yamamoto 2012, p. 49.) Figure 18 shows an example of rotor modelled using three-dimensional (3D) beam element.

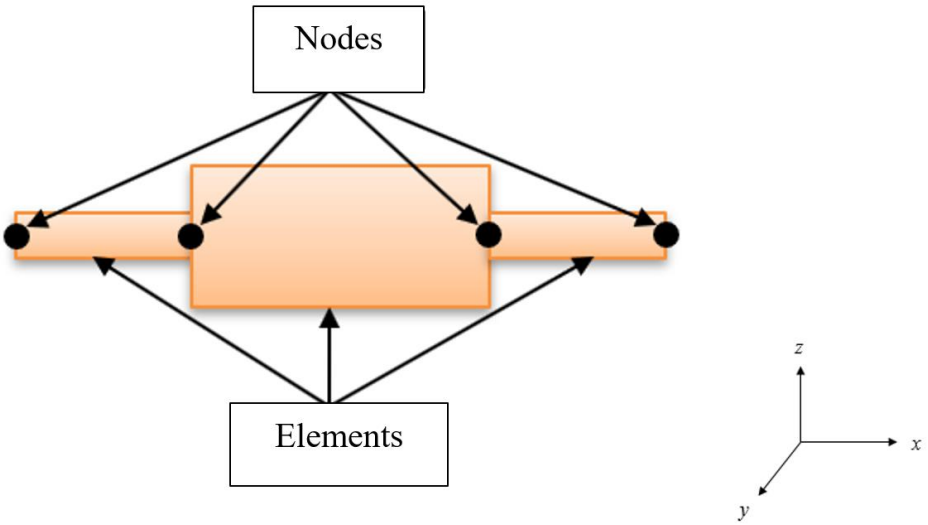


**Figure 18.** Rotor modelled with total of three 3D beam elements shown as orange straight uniform bar and four nodes shown as black dots at the end of each elements.

In the beam element model, the whole system is divided into multiple beam elements that are connected with each other at endpoints with nodes as shown in Figure 18. The forces and the moments at each element are expressed in terms of local coordinates of the system. The local coordinate is a coordinate system that is fixed with the system and is also called the body coordinate system. This local coordinate represents the translation and rotation at the nodes of the elements. The equivalent forces and moments at the node represent the distributed forces and moments. Then the forces and moments from all elements are assembled to get equivalent generalized forces in terms of generalized coordinates. For small deflection of elements, its elastic deformation produces forces and moments which are based on changes in generalized coordinate which are collectively called generalized forces. The generalized coordinate is an independent coordinate that can define the configuration of the system. These generalized forces are assembled to form an equation of motion of the system as presented in the following subchapter. The accuracy of the abstract model depends on underlying assumptions made when modelling such as choice of elements, degrees of freedom (dof) of elements, etc. (Friswell et al. 2010, p. 125-127.)

### 4.2.2 Equation of motion

In generalized matrix form, for the rotor system with variable rotational speed, its equation of motion is given as,

$$\boldsymbol{M\ddot{q}} + (\boldsymbol{C} + \Omega\boldsymbol{G})\dot{\boldsymbol{q}} + (\boldsymbol{K} + \tfrac{1}{2}\dot{\Omega}\boldsymbol{G})\boldsymbol{q} = \Omega^2\boldsymbol{Q}_1 + \dot{\Omega}\boldsymbol{Q}_2 + \boldsymbol{F}\,, \tag{12}$$

where, $\boldsymbol{M}$ is a matrix that represents mass of the system, vector $\boldsymbol{q}$ is the vector representing the nodal coordinates of the system, $\Omega$ is the rotation speed of the rotor, $\boldsymbol{G}$ is the gyroscopic matrix, $\boldsymbol{K}$ is the stiffness matrix of the system, $\boldsymbol{C}$ is the system's damping matrix, and $\boldsymbol{F}$ is the vector that represents externally applied forces in the system. $\boldsymbol{Q}_1$ is the unbalance force vectors that are related to the constant rotational speed of the rotor which is due to mass unbalance and are proportional to square of rotational speed and $\boldsymbol{Q}_2$ is also an unbalance force vector that is related to the variable rotational speed of the rotor related to static forces. $\boldsymbol{Q}_1$ and $\boldsymbol{Q}_2$ are obtained from the following equations as,

$$\boldsymbol{Q}_1 = [\boldsymbol{q}_1^c \quad \boldsymbol{q}_2^c \quad \cdots \quad \boldsymbol{q}_n^c]^T\,, \tag{13}$$

$$\boldsymbol{Q}_2 = [\boldsymbol{q}_1^{nc} \quad \boldsymbol{q}_2^{nc} \quad \cdots \quad \boldsymbol{q}_n^{nc}]^T, \tag{14}$$

where, *n* represents the number of nodes, $\boldsymbol{q}_n^c$ represents the unbalance vector of a specific node related to constant speed, $\boldsymbol{q}_n^{nc}$ represents the unbalance vector of specific nodes related to non-constant rotational speed. The unbalance vectors $\boldsymbol{q}_n^c$ and $\boldsymbol{q}_n^{nc}$ for the *nth* node at time *t* can be calculated.

$$\boldsymbol{q}_n^c = \begin{pmatrix} m_{ub}e_{ub}\cos(\Omega t + \alpha) \\ m_{ub}e_{ub}\sin(\Omega t + \alpha) \\ 0 \\ 0 \end{pmatrix} \tag{15}$$

$$\boldsymbol{q}_n^{nc} = \begin{pmatrix} m_{ub}e_{ub}\sin(\Omega t + \alpha) \\ -m_{ub}e_{ub}\cos(\Omega t + \alpha) \\ 0 \\ 0 \end{pmatrix} \tag{16}$$

In equation (15) and (16), $\alpha$ is the phase angle of the unbalance in radian, $m_{ub}$ is unbalance mass in kg and $e_{ub}$ is the eccentricity of the unbalance at node *n* in m. Figure 19 describes the unbalance forces of the decelerating rotor at node *n*. (Kärkkäinen 2007, p. 30-31.)

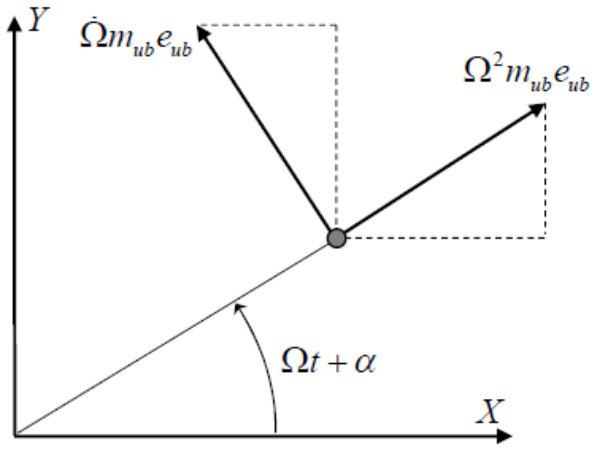


**Figure 19.** Unbalance forces at node *n* when the rotor is decelerating ($\dot{\Omega}$<0) (Kärkkäinen 2007, p. 31.)

When the rotational speed of the rotor is constant, equation of motion presented in equation (12) can be simplified.

$$\boldsymbol{M\ddot{q}} + (\boldsymbol{C} + \Omega\boldsymbol{G})\dot{\boldsymbol{q}} + \boldsymbol{Kq} = \Omega^2\boldsymbol{Q}_1 + \boldsymbol{F} \qquad (17)$$

The expression $\Omega^2\boldsymbol{Q}_1$ is force due to rotating mass unbalance as shown in equation (17). The equation of motion presented in equation (17) is used to calculate dynamics responses of the system in RoBeDyn as explained in the following subchapter.

4.3 RoBeDyn and its objectives

RoBeDyn stands for Rotor-Bearing Dynamics. It is FE based mathematical modelling tool for rotor-bearing systems coded in MATLAB software. It has been developed in LUT University to study the dynamic behavior of rotor systems. In the RoBeDyn model, the rotor is modeled in such a way that the rotor axis or length of the rotor is parallel to the *x*-axis and *y*- and the *z*-axis are the radial axes. The 3D Timoshenko beam element is used to make the FE model of the rotor with two nodes, cross-sectional and material properties. Each beam element has 12 degrees of freedom but the displacement of nodes in the rotor's axial direction and rotation of nodes around axial direction is constrained. Spring-damper elements can also be defined between two nodes or between a node and ground. The discs, impellers and bearing housing installed in rotor are modeled as rigid mass point elements. These elements can be connected to the specific node as a rigid body and have six dof with

mass and inertia properties. Ball and journal bearing can also be defined at the nodal location. Bearings can also be defined in terms of speed-dependent stiffness and damping matrix. Unbalance masses can be defined in terms of location and its value. Only linear and isotropic material properties can be defined in RobeDyn. (Sopanen 2009.)

The model data are defined in input data structural array which contains model data such as nodes, elements, cross-sectional properties, element material properties, nodal constraints, properties of rigid mass elements, unbalance properties, properties of spring-damper elements, modal damping properties and bearing properties. Functions that are part of RoBeDyn code constructs also system mass matrix, stiffness matrix, damping matrix, gyroscopic matrix and unbalance force vectors as shown in equation (17). Based on this equation of motion, different functions calculate free-free vibration mode shapes, Campbell diagram, steady-state response due to unbalance, threshold speeds of rotor dynamic stability, etc. Different plotting functions plot modeled rotor system, Campbell diagram, mode shape and displacement of nodes due to unbalance response. Calculation of these rotor system's dynamic parameters while using less computing time compared to commercial FE software's solid elements-based model are the objectives of the mathematical model of the rotor-bearing system based on RoBeDyn code. (Sopanen 2009.)

# 5 CASE STUDY: SINGLE PLANE RESIDUAL UNBALANCE

The purpose of the case study is to identify the magnitude and location of a single plane residual unbalance of the physical rotor system of standard 3 phase 11 kW induction motor that could be used as unbalance definition in the FE model. The task process of the case study in identifying the location and magnitude of single plane residual unbalance is presented as list below.

1. Make the RoBeDyn model of the studied physical rotor with available rotor information.
2. Tune and validate the dynamics of the RoBeDyn model of the rotor from the experimental and eigenvalue analysis of the physical rotor.
3. Find the maximum and minimum amplitude 0-p of radial absolute vibration displacement of the rotor at the measured location at different speeds from the relative displacement of the rotor and absolute acceleration vibration of the end shield.
4. Find the maximum permissible residual specific unbalance from the reported balance grade of the physical rotor.
5. Simulate the RoBeDyn model with minimum and maximum range of residual unbalance magnitude at each node, at different measured speeds to calculate the absolute radial displacement of the rotor at measured nodes.
6. Compare the maximum and minimum measured radial absolute displacement and the simulated displacement at each speed and identify single plane residual unbalance, such that simulated displacement at the measured location is in the range of measured maximum and minimum absolute displacement.

The physical rotor system of standard 3 phase 11 kW induction motor was studied. The experimental modal analysis of the physical rotor was conducted in earlier study to get free-free modes of the rotor with a scanning vibrometer by Polytec (Kastinen 2019, p. 34-36). Then the FE model of the rotor was made in RoBeDyn based on known material properties, inertia properties, and dimensions. Model tuning was done to match the mass and inertia properties of the FE model and the physical rotor. The uncertainties in the FE model were verified by tuning the material and physical properties of lamination and short-circuiting

rings. Further tuning was done by comparing free-free modes and their respective natural frequencies from eigenvalue analysis of the FE model and experimental modal analysis of the physical rotor. The absolute radial acceleration vibration of end shield and relative vibration displacement measurements from the physical rotor were taken at different rotation speeds with and without additional hubs and known unbalance masses attached at hubs. These additional hubs and known unbalance were then included in the FE model. Then the simulation to find the single plane residual unbalance was done by using the FE model. These processes are explained in the following subchapter in detail.

## 5.1 Rotor system

The typical structure and components of the induction motor are shown in Figure 20.

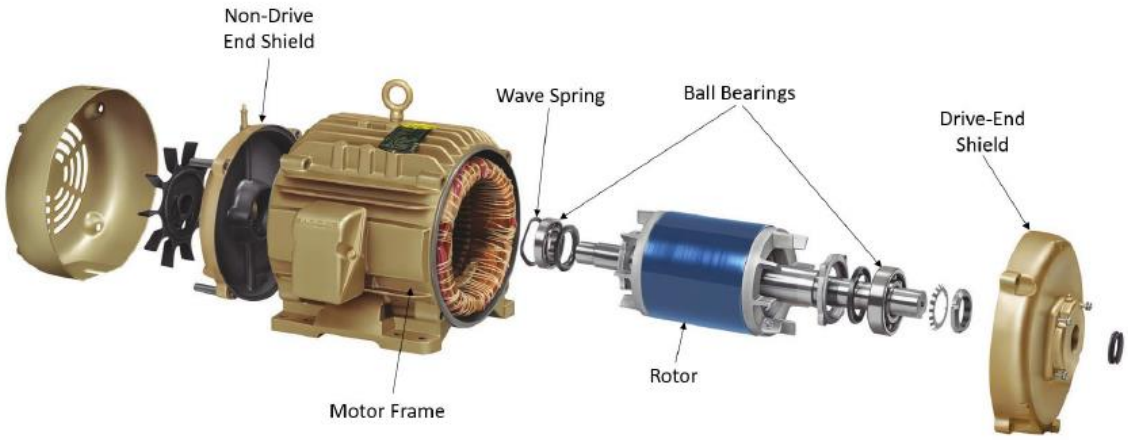


**Figure 20.** Exploded view of the standard induction motor (Kastinen 2019, p. 34).

The typical induction motor, for example, consists of rotor, bearings, stator, lamination, end shields and other components as shown in Figure 20. Figure 21 shows the structure of the lamination on the rotor with short-circuiting rods at both ends of the lamination.

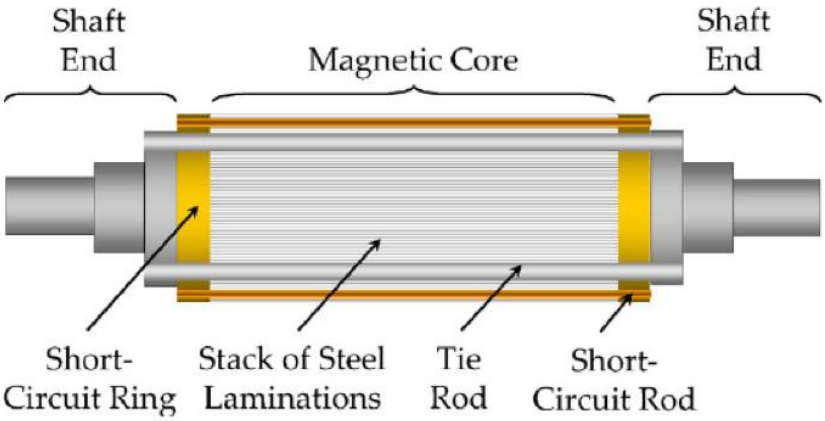


**Figure 21.** The structure of a squirrel cage induction motor (Mogenier et al. 2010, p. 281).

The induction motor works on the principle of electromagnetic induction. The current in stator winding produces a magnetic field in the slots of the stator which induces a current in the rotor. This current in the rotor produces own magnetic field around the rotor. These two magnetic fields in rotor and stator interact to produces torque that in turn rotates the rotor. (Electrical4U 2019.) The studied rotor consists of a rotor, stack of lamination and short-circuiting rings. The rotor lamination was made from steel sheet with an insulation layer on the top and the short-circuiting rings were made of aluminum.

## 5.2 Experimental Modal analysis

Experimental modal analysis of the physical rotor was conducted in earlier study in the machine dynamics laboratory at LUT. The scanning vibrometer with PSV-500 scanning head, OFV-505 reference laser and AS-1220 excitation hammer from Alpha Solutions were used for the experimental modal analysis. A total of 12 measuring points on the rotor was marked with reflective tape to prevent scattering of the laser beam. The data acquisition software used was PSV 9.2. For each point on the rotor, three repeated measurements were taken for FFT. The reference laser velocity of 50 mm/s was used for the scanning. The selected frequency range for experimental modal analysis was from 0 to 2500 Hz. The hammer was excited with a square wave at 0.2 Hz frequency and with a corresponding amplitude of 4.8 Volts (V). The natural frequencies for bending modes of the physical rotor in the respective axis are presented in Table 2. (Kastinen 2019, p. 34-36.)

*Table 2. The natural frequency of respective bending modes in the y-axis and z-axis in Hz obtained from experimental modal analysis (Kastinen 2019, p. 34).*

| Natural frequency | *y*-axis [Hz] | *z*-axis [Hz] |
|---|---|---|
| First bending mode | 595.3 | 595.3 |
| Second bending mode | 1453.9 | 1446.9 |
| Third bending mode | 2099.2 | 2085.2 |

The *x*-axis is along the length of the rotor and the *y*- and *z*-axis are the radial axes. *Y* is the radial vertical axis and *Z* is radial horizontal axis. The natural frequency of the first bending mode of the rotor was equal in the *y*- and *z*-axis. But natural frequency for second and third bending modes were not equal in z- and *y*-axis. The mode shape of the bending modes is presented in appendix II (Kastinen 2019).

## 5.3 Modelling rotor in Robedyn

The FE model of the rotor system was made in RoBeDyn. The rotor was modeled as the 3D Timoshenko beam element with its given dimensions, material, and inertial properties. The lamination and both the short-circuiting rings of the rotor system were modeled together as one-second layer hollow disc element over the rotor, with the same mass and the inertia properties as that of lamination plus the short-circuiting rings of the physical lamination.

The equivalent outer diameter of the modeled lamination and short rings was calculated using the following equation. (Friswell et al. 2010, p. 499.)

$$I_p = M(D^2 + d^2)/8 \tag{18}$$

In equation (18), $I_p$ is the polar mass moment of inertia of hollow disc, $M$ is mass of the hollow disc, $D$ is outer diameter and $d$ is the inner diameter. From equation (18), with given mass of the lamination plus the short-circuiting rings, inner diameter, and total polar mass moment of inertia of the lamination with rings, the equivalent outer diameter was calculated. It was found to be around 209 mm which is not equal to the outer diameter of the lamination of the physical rotor. This calculated outer diameter was used to calculate the equivalent density of the modeled hollow disc with the following equation (Friswell et al. 2010, p. 499).

$$M = \rho\pi h(D^2 - d^2)/4 \tag{19}$$

In equation (19), $\rho$ is the equivalent density of the modeled hollow disc and $h$ is the length of the disc. The calculated equivalent density of the hollow disc that represents the lamination with the short-circuiting ring was found to be around 2379 kg/m$^3$. Figure 22 shows the wireframe plot of the FE model of the rotor and Figure 23 shows the three-dimensional plot of the rotor from RoBeDyn.

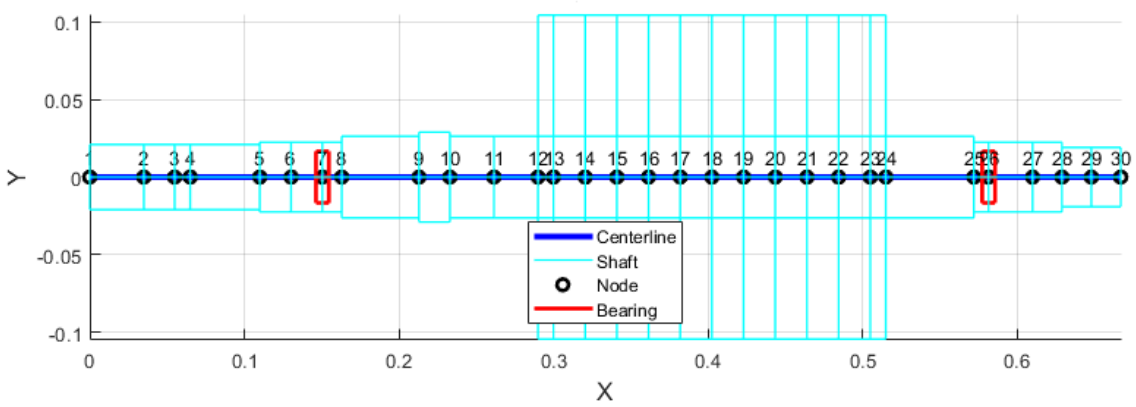


**Figure 22**. Wireframe plot of FE model of the modelled rotor from RoBeDyn.

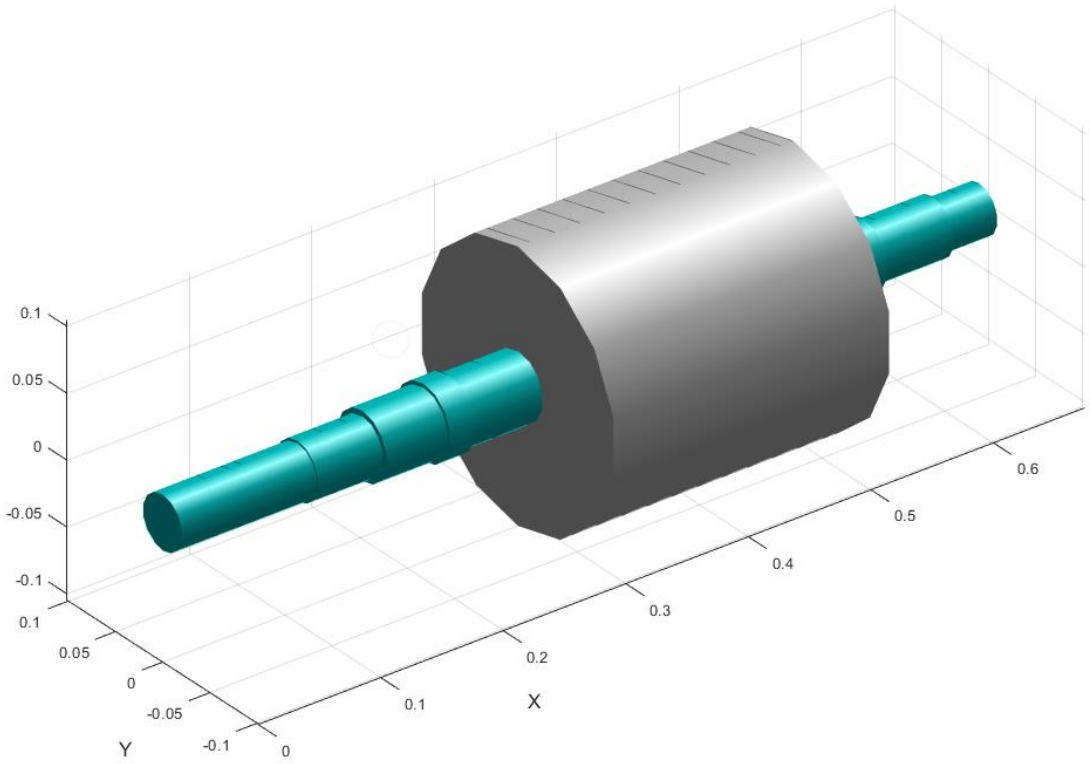


**Figure 23.** Three-dimensional plot of the modeled rotor in RoBeDyn.

Figure 22 shows that the model consists of 30 nodes. In Figure 23 the light grey hollow component represents the lamination and the short-circuiting rings. The six by six rigid body mass matrix showed that total mass and the polar mass moment of inertia around the *x*-axis of the FE model were equal to that of the physical rotor system.

## 5.4 Tuning dynamics of RoBedyn model

Both experimental and eigenvalue analysis reveals the inherent dynamic responses of the rotor system and FE model it represents respectively that is independent of external loads. Modal analysis reveals the natural frequency and the relative displacement of nodes called mode shape at respective natural frequencies. The mode shape reveals that if the system is excited at the corresponding natural frequency of the mode shape, what will be the relative displacement of the nodes in the respective axis of the system. (Peter 2018, p. 3-5.) The experimental and eigenvalue analysis helps to validate the dynamic characteristics of the FE model. If the results of the modal analysis are satisfactory based on the magnitude of natural frequency and respective mode shapes, then such FE model can be used for diagnostics and forecasting the machine dynamic behavior during operation. (Agnieszka 2005, p. 75.) But however dynamic characteristics of the machine can be different at other speeds and only modal analysis does not predict the machine's characteristics at other speeds (SFS-ISO 13373-3 2015, p. 8).

Eigenvalue analysis was done for the FE model that was created in RoBeDyn without modal damping ratios for free-free modes. It is because no information regarding model damping was provided from the experimental modal analysis. The model created in RoBedyn was tuned to make the natural frequencies and the bending modes of the FE model like that were obtained from experimental modal analysis in the respective axis. All the parameters that were associated with modeled lamination and the short-circuiting rings were tuned such that natural frequencies were equal or close to that were obtained from the experimental modal analysis. The Poisson's ratio, modulus of elasticity, density, and outer diameter were the tuned parameters of the modeled lamination and short-circuiting rings. Table 3 shows the natural frequencies in the *z*- and *y*-axis for the first, second and third bending modes that were obtained from eigenvalue analysis of the FE modal.

*Table 3. The natural frequency of respective bending modes in the y-axis and z-axis in Hz obtained from eigenvalue analysis.*

| Bending modes | *z*-axis (Hz) | *y*-axis (Hz) |
|---|---|---|
| First bending mode | 595 | 595 |
| Second bending mode | 1328 | 1328 |
| Third bending mode | 2140 | 2140 |

The natural frequencies obtained from the eigenvalue analysis of the FE model are the same in *z*- and *y*-axis as shown in Table 3. The free-free modes obtained from eigenvalue analysis of the FE model are presented in Appendix III. The mode shape obtained from experimental modal analysis must be compared to the ones obtained from eigenvalue analysis from the FE model to reduce the uncertainties in the FE model (Sopanen 2009, p. 18). Figure 24 shows the first bending mode in *z*-axis represented as a dotted blue line obtained from eigenvalue analysis. Figure 25 shows the first bending mode in *z*-axis obtained from the experimental modal analysis (Kastinen 2019, p. 34).

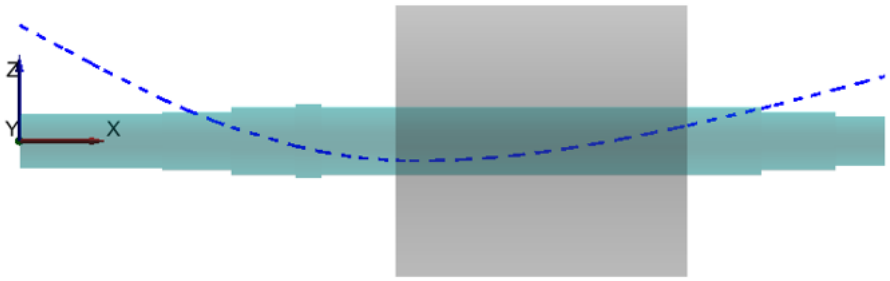


**Figure 24.** The first bending mode in the z-axis represented as dotted blue line at 595 Hz from eigenvalue analysis.

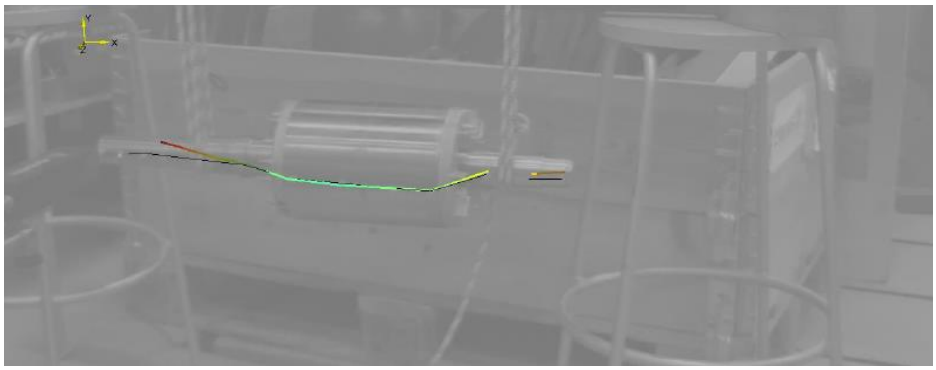

**Figure 25.** The First bending mode in the *z*-axis at 595.3 Hz from experimental modal analysis (Kastinen 2019, p. 34).

Figure 24 shows that lamination with short-circuiting rings can deflect but Figure 25 shows that lamination is not deflecting. This indicates that the rotor in the FE modal behaves dynamically as if it is one rigid component. Thus, it can be concluded that the FE model is not going to accurately depict the dynamic characteristics of lamination. But however, the relative displacement of the rotor ends excluding the lamination has a similar mode shape. In both cases, the rotor ends are bending towards the *z*-axis as an arch. The natural frequency of first bending mode obtained from experimental modal analysis and eigenvalue analysis are about equal. These two facts may indicate that the FE model could predict the displacement of the rotor excluding the lamination section. Thus, this was considered a satisfactory FE model.

## 5.5 Unbalance response measurements

The steady-state unbalance response with only residual unbalance and known additional unbalance were measured for different constant rotational speeds. The following subchapter explains how the hubs were attached to facilitate the attachment of additional unbalance masses, how the measurements were taken with and without additional unbalance masses.

### 5.5.1 Without additional unbalance

The radial and axial absolute acceleration vibration of end shield, relative displacement of the rotor, and phase and rotation speed of rotor were measured with only residual unbalance of the rotor without external load. These measurements were taken in DE and NDE of the rotor at rotational speeds of 500, 1500, 2500, 3500 and 4500 RPM.

### 5.5.2 With additional known unbalance

The relative displacement vibration of the rotor and only axial acceleration vibration of the end shield were measured with additional known unbalance at DE and NDE at rotational speeds of 500, 1500, 2500, 3500 and 4500 RPM. Two coupling hubs were added at the DE and NDE of the rotor to facilitate the addition of the known unbalance masses at the radial holes on the hubs. The known additional unbalance masses of 14, 22, 30 and 37 g were bolted on one outer hole on each of the hubs. Figure 26 shows the hubs that were attached to the rotor to facilitate the addition of known unbalances.

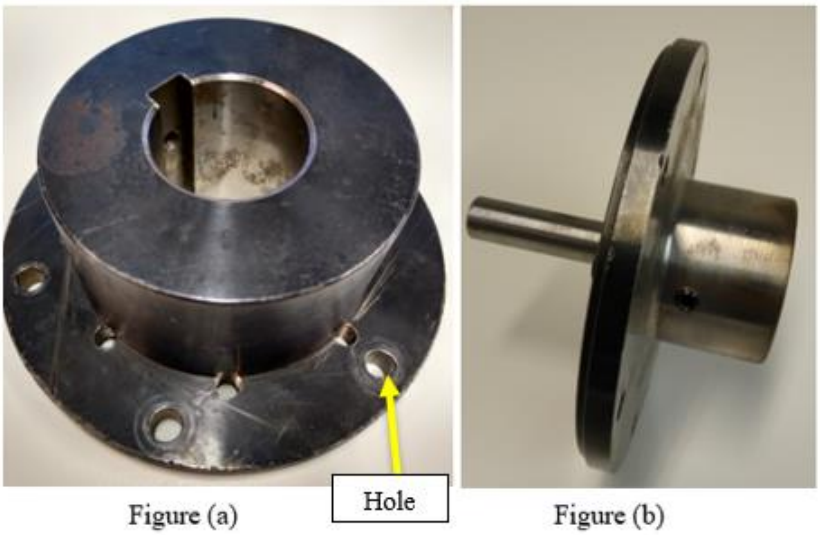


**Figure 26.** Hub that was attached in DE is in Figure (a) and the hub that was attached in NDE is in Figure (b). The hole where the additional mass in DE was attached is shown with arrow in yellow colour in Figure (a).

Figure 26 shows that the hub in NDE has a protruding shaft and disc in DE has a keyhole. The mass of the hub attached in DE of the rotor is 3494 grams and the mass of the hub attached in NDE is 2049 grams. The mounting hole for additional unbalance mass were at the radius of 60 mm from the center of both hubs as shown in Figure 27.

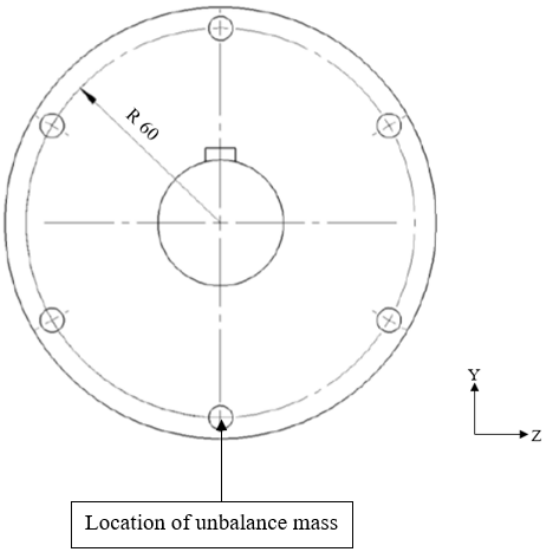


**Figure 27**. Location of the single hole where additional unbalance mass was attached to the hub at DE (Mod. Kastinen 2019).

In both hubs, the equal amount of unbalance masses was attached for each measurement case in the location shown in Figure 27. The diameter of the hole is 8 mm. The same pair of nuts and bolts were used as known test unbalance masses that were mounted on each hub. These unbalance masses were at the phase of π radian with respect to the positive *y*-axis. In other words, the unbalance masses were at negative *y*-axis as shown in Figure 27. The hub at DE was attached such that the disc section was towards the center of the rotor and the hub at NDE was attached the opposite way as shown in Figure 28.

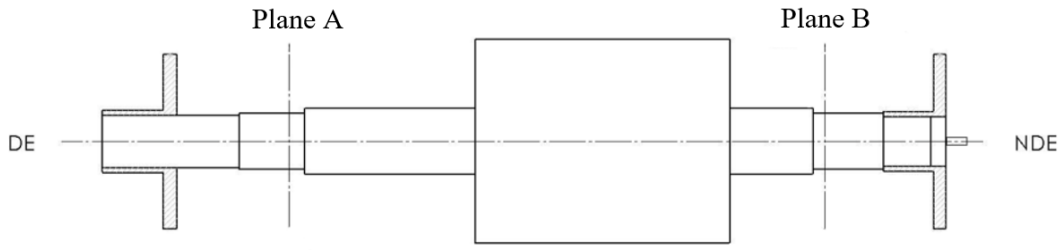


**Figure 28**. Coupling hubs in DE and NDE of the rotor. The transverse plane A is DE bearing centreline and the transverse plane B is NDE bearing centreline. (Mod. Kastinen 2019.)

### 5.5.3 Adding hubs in RoBeDyn model

The 3D models of both the coupling hubs were modeled in Solidworks 2017. The dimensions required to model the hubs were measured by using Vernier caliper. The measurement tolerance of the caliper was ±0.05 mm. The mass properties of the hubs were defined such that the total mass of the hubs was equal to their respective measured masses. Both hubs were added in the FE model as a rigid mass point element at respective nodes where they were in the physical rotor. Figure 29 shows the wireframe plot of the modeled rotor in RoBeDyn with added hubs in DE and NDE.

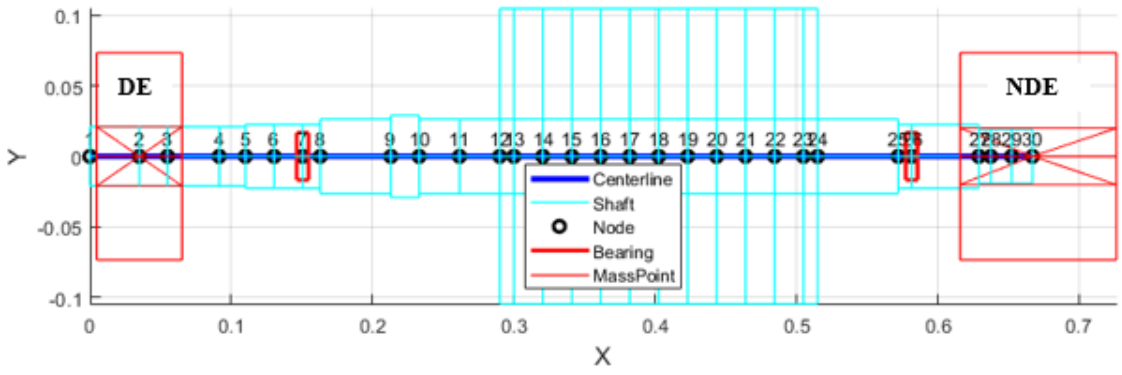


**Figure 29.** Wireframe plot of FE model of the rotor from RoBeDyn with added hubs.

The hub in DE was added at node 2 which is the center of mass location of the DE hub. The hub in NDE was added at node 30 with the center of mass offset of 4.08 mm. The appearance of the hubs due to dimensions in Figure 29 is for graphical plots and it does not affect the solution given by RoBeDyn functions (Sopanen 2009, p. 8).

### 5.5.4 Adding bearing and support parameters

The motor was mounted on a steel frame to make the measurements. The frame itself was mounted to the ground. But however, the frame was mounted only on one side as shown in Figure 30. (Kastinen 2019, p. 39.)

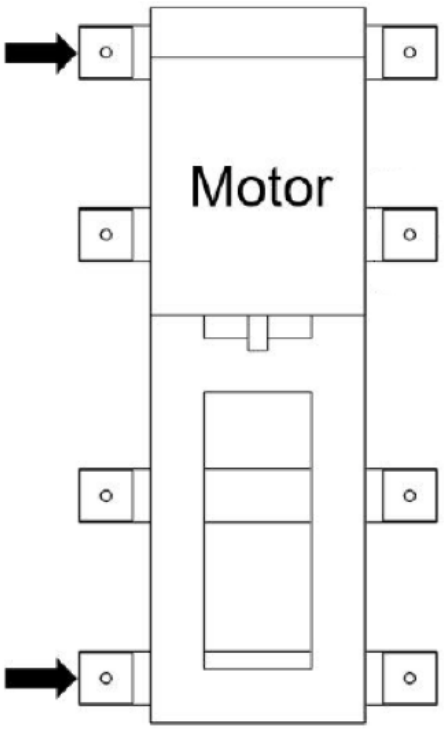


**Figure 30.** Steel frame mounted on the ground from one side (Mod. Kastinen 2019, p. 39).

In Figure 30, the dark arrow indicates that the steel frame was mounted to ground at only one side at two locations. The stiffness and the dynamics of the steel frame were not accounted for in the RoBeDyn model because this information regarding the frame was not available. The rotor was supported by two deep groove ball bearing at DE and NDE. The stiffness of the bearings used in the RoBeDyn model for the *y*-axis and *z*-axis in DE and NDE are presented in Table 4 (Kastinen 2019, p. 43).

*Table 4. Stiffness of respective bearing in y- and z-axis (Kastinen 2019, p. 43).*

| Bearing location | $K_{yy}$ [N/mm] | $K_{zz}$ [N/mm] |
|---|---|---|
| DE | 208133 | 208133 |
| NDE | 189992 | 189992 |

The stiffness of both bearings on the *x*-axis was zero. For each bearing, one node was attached to respective nodal location at rotor and the other was attached to the ground. The damping coefficient of both bearings in the FE model was $10^{-5}$ times that of stiffness in respective bearing in respective axes.

5.6 Measurement parameters and sensors used

As mentioned in chapter 2.5, there is a total of five parameters that are required to be measured for interpretation of machinery condition through analysis of vibration measurement. However, the studied rotor does not have journal bearings and thus it only requires four parameters to be measured. Figure 31 shows the location where the sensors were mounted in studied rotor to measure these parameters.

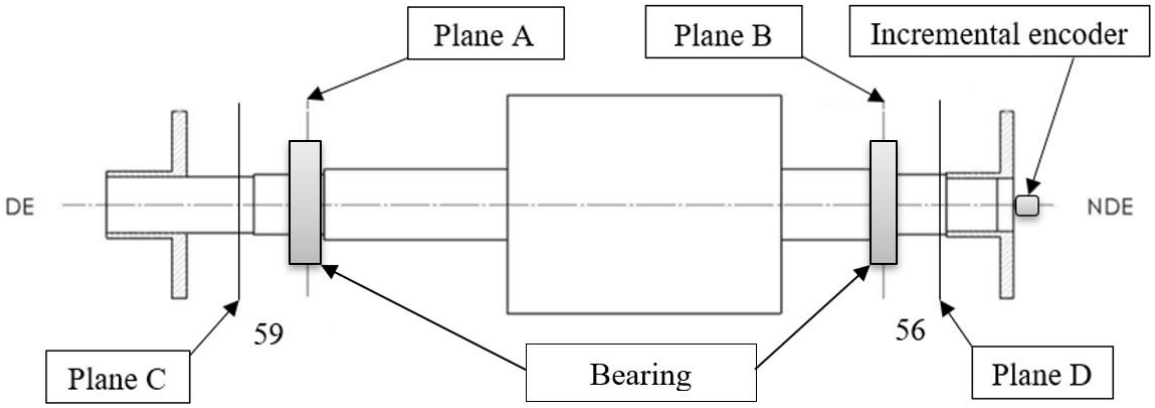


**Figure 31.** The location where the sensors were mounted in the studied physical rotor (Mod. Kastinen 2019).

The radial and axial accelerometers were mounted in transverse planes A and B, transverse flux capacitive sensors were mounted at plane C and D and incremental encoder was mounted at protruding shaft on NDE hub as shown in the Figure 31. The vibration parameters measured, and sensors used in measuring them are explained in the following subchapters.

### 5.6.1 Absolute radial acceleration vibration of the non-rotating part

The non-rotating part in the induction motor is the motor cover. The motor assembly does not have external bearing housing. The outer race seat of bearing is located at the end shield of the cover. Two radial holes were drilled at the centerline of both bearing locations to measure the absolute radial vibration of the end shield. Although axial vibration of the end shield was not required to be measured for the purpose of condition monitoring, two axial holes were also drilled on end shields to measure the axial absolute vibration of the end shield. In total, six accelerometers were used to measure the absolute vibration of the end shield in radial and axial direction in DE and NDE. Figure 31 shows the transverse plane where the radial accelerometers were screw mounted to the respective end shields. The transverse plane A is the centerline of bearing in DE which is 25 mm in width. Transverse plane B is the centerline of bearing in NDE which is 19 mm in width. The location of plane A from the DE of the rotor is at 150.5 mm and the location of plane B is at 581.5 mm from DE. The accelerometers were placed in radial *y*-and radial *z*-axis at each transverse plane. Figure 32 shows the orientation of radial accelerometers in both transverse planes A and B.

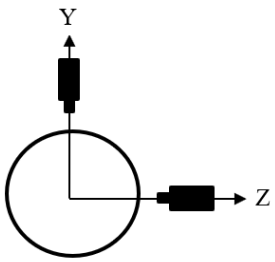


**Figure 32**. The orientation of accelerometer used in measurement for absolute radial acceleration vibration of end shields at planes A and B at bearing centreline.

Six accelerometers used were PCB piezo electronics and the model used was 622B01. The sampling rate of the accelerometers used was 50 kHz. It uses piezoelectric crystal as a sensing element. (PCB Piezotronics 2019.)

### 5.6.2 Relative radial vibration displacement of the rotor

As explained in chapter 2.7, the criteria of the vibration measurement and the 20% rule determine whether to use or measure relative or absolute vibration displacement of the rotor for signal analysis. But however, in order to check the 20% rule, it is required to measure the relative radial vibration displacement of the rotor.

The relative radial vibration of the rotor was measured using a transverse flux capacitive sensor that was developed in LUT in collaboration with ABB. Two similar transverse flux capacitive sensors were used to measure relative radial vibration displacement of the rotor in *y*- and *z*-axis at two locations at DE and NDE. (Pelli 2018, p. 6.) Figure 31 shows the transverse planes C and D where the capacitive sensors were attached to the end shield. The distance between the transverse plane where accelerometer was mounted and where capacitive sensors were mounted is 59 mm in DE and 56 mm in NDE as shown in Figure 31.

The capacitive sensor measures the radial relative displacement vibration of the rotor in four locations with four capacitive plates positioned at *y*- and *z*-axis as shown in Figure 33. It processes these measurements and gives raw rotor displacement in *y*- and *z*-axis. (Pelli 2018, p. 6.) In other words, the capacitive sensor measures the radial relative vibration displacement of the rotor center point at transverse planes C and D.

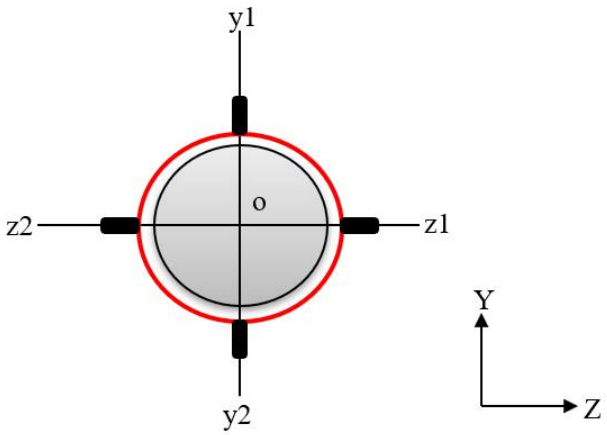


**Figure 33**. Four capacitive plates around the rotor to measure the relative displacement of the rotor in y- and z-axis.

Figure 33 shows how the radial relative vibration displacement of the rotor at the respective location is measured by the capacitive sensors. In Figure 33, the grey circle represents the rotor at the measuring plane, the red circle represents the capacitive sensor with four measuring plates around the rotor surface. The point ‘o’ represents the center of the rotor. Measurements *y1* and *y2* is processed to give the relative displacement in *y*-axis as,

$$Y = y1 - y2, \tag{20}$$

where, *Y* is relative displacement in the *y*-axis, *y1* and *y2* are displacement measurements at rotor surface in *y*-axis. Measurements *z1* and *z2* are processed to give the relative displacement in the *z*-axis as,

$$Z = z1 - z2, \tag{21}$$

where, *Z* is relative displacement in *z*-axis, *z1* and *z2* are displacement measurements at the rotor surface in *z*-axis. These measurements in *y*- and *z*-axis were scaled according to the sensor's calibration factor to get the relative displacement of the rotor in the respective axis in µm. (Liukkonen 2019.) Figure 34 shows how the capacitive sensor was attached to the end shield at DE.

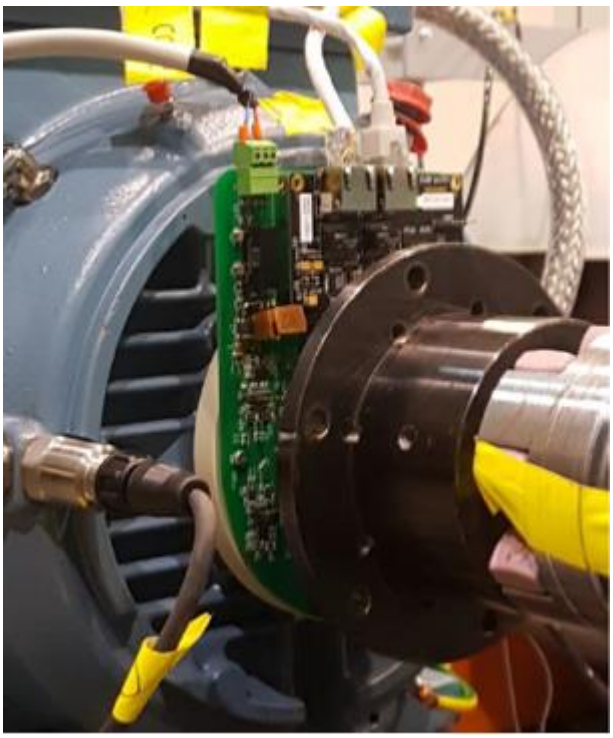

**Figure 34**. Capacitive sensor with preprocessing circuit board at DE to measure relative displacement at plane C (Kastinen 2019, p. 38).

The printed circuit board is attached with a plastic plate and these were both screwed to the end shield of the motor (Liukkonen 2019). The used capacitive sensors have a resolution of 0.16 µm. The range of measurement is from -1 to +1 mm in each measuring axis. The sampling rate of the sensor is 20 kHz and bandwidth is 10 kHz. The resonance frequency of the sensor is 430 MHz. (Pelli 2018, p. 22-25.)

### 5.6.3 Phase reference and rotation speed of the rotor

The rotary incremental encoder from Leine & Linde was used to measure the rotation speed and the phase. The phase reference point was the keyhole and the reference mark made on the top of the motor frame at the DE. The incremental encoder was inserted around the protruding shaft of the coupling hub at the NDE as shown in Figure 31. The resolution of the encoder is 0.352 degrees. The sampling rate of the rotatory incremental encoder was 50 kHz. (Kastinen 2019, p. 32.)

## 5.7 Measurements

Measurements from the sensors attached were taken at a respective fixed sampling rate at a constant rotational speed. The ABB ACS800 variable frequency converter was used to control the rotation speed of the rotor. The measurements were taken without external loads on the rotor. The steady-state measurements were taken at the rotational speed of 500 RPM to 4500 RPM with a speed increment of 1000 RPM. The measurements were taken with and without additional unbalance masses. The additional unbalance masses that were used for relative rotor displacement vibration are 14, 22, 30 and 37 grams. For each measurement, the keyway of the rotor was aligned to the reference point on the motor frame. The record length of each measurement ranges from 13 to 26 seconds. (Kastinen 2019, p. 39.)

## 5.8 Data acquisition, conditioning, and processing

All the sensor data were collected via the ABB AC500-CMS programmable logic controller with Ethernet for Control Automation Technology (EtherCAT) connection. These raw signals were then conditioned and processed in MATLAB (2018b). The raw relative displacement signals were scaled with calibration factor to get rotor relative displacement at the respective axis in µm. Mechanical run out was calculated from the displacement measured at 500 RPM without additional unbalance. The conditioned data were then filtered using a bandpass filter with a range of rotation speed in Hz ±0.001 Hz. The actual rotation speed was calculated from the signal from incremental encoder and phase reference. By using FFT, the maximum amplitude of relative displacement of rotor and phase at 1X was calculated for all speeds with and without additional unbalance. The raw acceleration data measured by accelerometers were scaled to get the radial and axial vibration acceleration of end shield in $m/s^2$. These scaled signals were then filtered through the bandpass filter of rotation speed in Hz ±0.001 Hz. These filtered acceleration signals were mathematically

double integrated and transformed into the frequency domain by using FFT to get maximum absolute displacement in mm. The double integration was done by using MATLAB code provided by Tom Irvine (Irvine 2019).

## 5.9 Scanning single plane residual unbalance

In order to predict the absolute displacement at the measured location in the physical rotor by using the FE model, the information regarding the residual unbalances in the physical rotor must be considered. For the purpose of the thesis here on, the process of determining the single plane residual unbalance by simulation of the FE model in RoBeDyn is called scanning for unbalance and the algorithm used is called scanning code. The five-step process of unbalance scanning is explained in Figure 35.

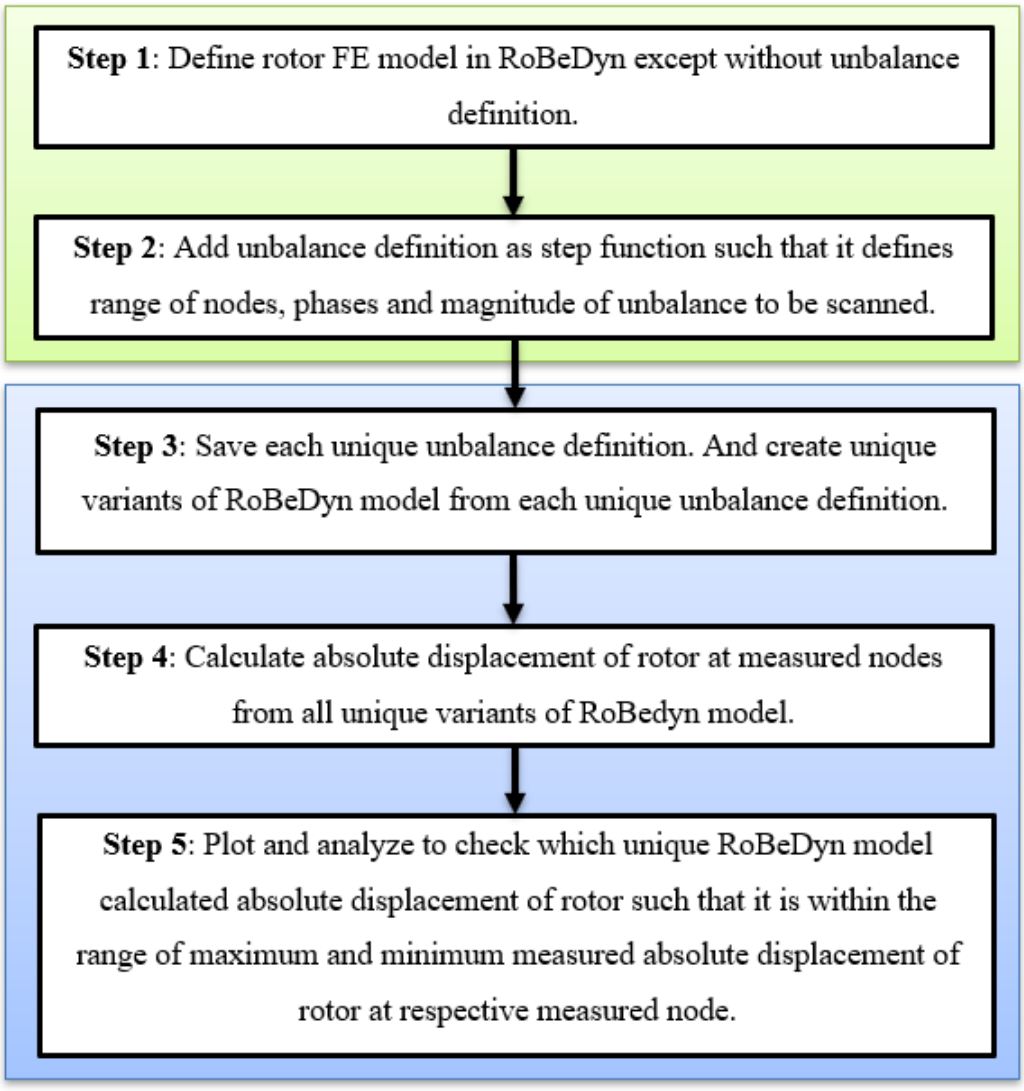


**Figure 35.** Five step process of scanning single plane residual unbalance.

In the unbalance scanning process as shown in Figure 35, first step is to define the rotor model and second step is to define the possible location, phase and the magnitude of unbalance as a step function. These definition steps are represented in green background in the Figure 35. The definition of unbalance in step two will define how many FE model variants will be created. The third, fourth and fifth step as represented in blue background in Figure 35 and it represents simulation process.

Due to reasons related to design, manufacturing, material, and assembly, every rotor has initial unbalance masses distributed along its rotor length. These unbalance needs to be corrected by adding, removing or relocating materials in order to correct the unbalance tolerance. Unbalance tolerance is defined based on balancing grade of the rotor and it defines the maximum permissible residual unbalance a rotor can have in gm·mm per kg mass of the rotor. Based on the balancing grade of the rotor, the total residual unbalance in the rotor is less than that of the permissible residual unbalance. Figure 36 shows the balance grade and permissible residual unbalance ($e_{per}$) based on service speed ($n$) in RPM. (SFS-ISO 21940-11 2017, p. 13).

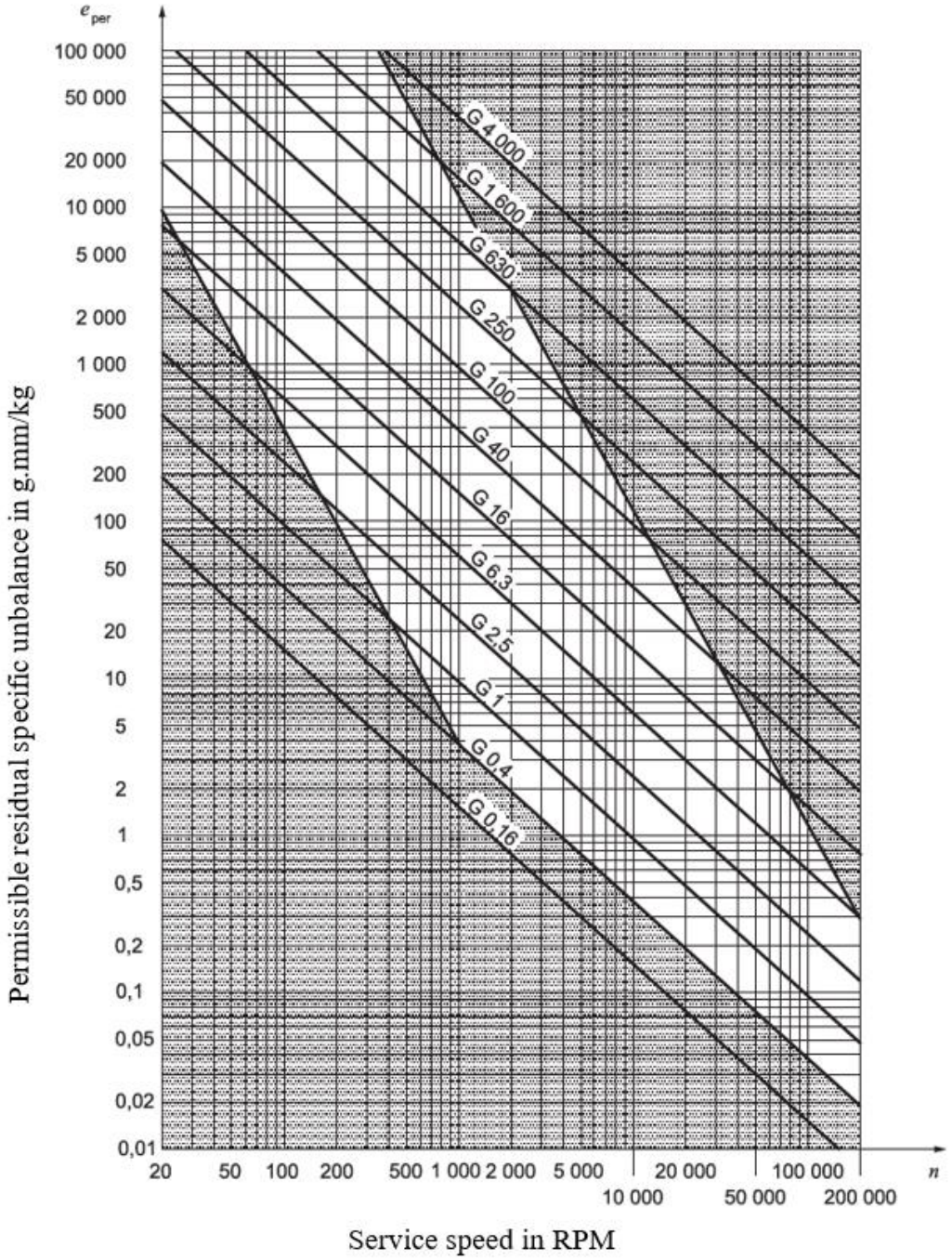


**Figure 36.** Balance grade and permissible residual unbalance ($e_{per}$) based on service speed ($n$) (SFS-ISO 21940-11 2017, p. 13).

From Figure 36, based on the balance grade reported by the manufacturer for the reported service speed, the total permissible residual unbalance can be calculated for a given rotor. According to the motor guide from ABB, the motors manufactured are balanced to grade G2.5 (Low voltage motor guide 2014, p. 75). For the studied rotor the permissible residual unbalance magnitude ($e_{per}$), is calculated as shown in Table 5.

*Table 5. Permissible residual unbalance magnitude ($e_{per}$) of studied rotor.*

| RPM | Unbalance class G 2.5 | Permissible residual unbalance $e_{per}$ [gm·mm/kg] | Residual unbalance magnitude [kg·m] |
|---|---|---|---|
| 1500 | G 2.5 | 18 | 0.00048924 |

This reported residual unbalance magnitude of 0.00048924 kg·m is the final maximum residual unbalance magnitude that the studied rotor has after unbalance correction. This total residual unbalance is reported as being in the plane of the center of mass. (SFS-ISO 21940-11 2017, p. 9-14.) Since, due to lack of information regarding the exact magnitude of residual unbalance, added mass or masses, plane or planes and phase for unbalance correction done in the physical rotor, it is difficult to further tune FE model to predict the displacement at measured nodes.

Thus, the FE model was scanned to find the single-plane residual unbalance from nodes 15 to 21 at 1500, 2500 and 3500 RPM. The magnitude of the single plane residual unbalance can thus be input as only residual unbalance in FE model to predict the absolute displacement of the physical rotor through the FE model.

# 6 RESULT AND ANALYSIS

The acceleration vibration signal at the radial *y*-axis from the end shield at DE and NDE was mathematically double integrated with respect to time to get absolute displacement. The integration was done by using function cumtrapz in MATLAB (2018b). It is cumulative trapezoidal method for numerical integration. It has error when calculating the integral based on the created trapezoid figure at each time step. Thus, it does not give accurate absolute displacement compared to direct measurement of end shield. (Quarteroni & Saleri 2006, p. 108-109). After double integration, the FFT was used to find the maximum absolute displacement at the radial *y*-axis at different speeds without additional unbalance. The measured maximum 0-p relative displacement vibration amplitude of the rotor in DE was higher in *y*-axis than in *z*-axis with 0 gm added unbalance in all measured speeds. The relative displacement measurements of the rotor from 500 RPM was used for runout compensation for other speeds. But however, relative displacement measured at 500 RPM was not used in the analysis because it was not conclusive if the runout was compensated from the measurement at 500 RPM itself (Kastinen 2019, p. 39-40.) The unbalance scanning method was only used with measurements from 1500, 2500 and 3500 RPM. Thus, only results from these speeds at *y*-axis with 0 gm unbalance are presented in the following subchapters.

## 6.1 Measured absolute vibration of end shield at DE

The FFT of the radial acceleration vibration data in the *y*-axis of end shield at DE at 1500 RPM or 25 Hz with 0 gm added unbalance is shown in Figure 37.

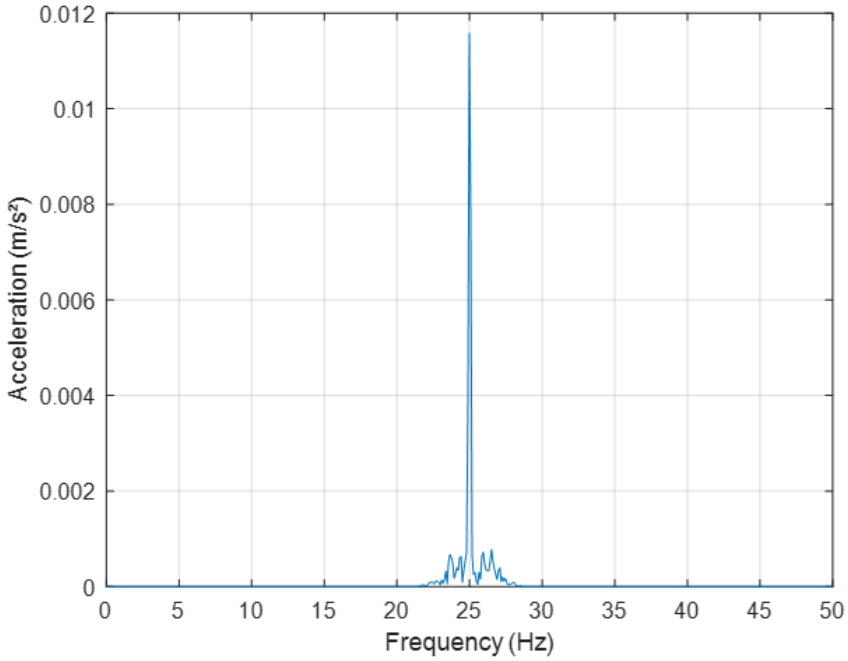


**Figure 37.** FFT of filtered acceleration data at 1500 RPM at DE in y-axis with 0 gm added unbalance.

The amplitude and phase of the acceleration signal at 24.99 Hz were found to be 0.01158 m/s² and 42.39º respectively. There were no other peaks beyond 50 Hz. Similarly, FFT of measured acceleration vibration data at DE in the *y*-axis at 2500 and 3500 RPM with 0 gm added unbalance were done. These acceleration data were then double integrated with respect to time to get the displacement. The displacement data was transformed in the frequency domain using FFT to find the maximum 0-p amplitude of absolute displacement vibration of end shield at DE in *y*-axis at 1500, 2500 and 3500 RPM with 0 gm additional unbalance as presented in Table 6.

*Table 6. The maximum measured 0-p absolute vibration displacement, phase, and frequency of end shield in y-axis at DE with 0 gm additional unbalance.*

| RPM | Maximum measured 0-p absolute displacement, phase, and frequency of DE shield in the *y*-axis | | |
|---|---|---|---|
| | [µm] | [-180º to +180º] | [Hz] |
| 1500 | 0.47 | -137.40 | 24.99 |
| 2500 | 2.43 | -85.51 | 41.68 |
| 3500 | 1.46 | -175.30 | 58.36 |

Low frequencies typically have larger amplitude and high frequencies have lower amplitude. The low frequencies have most of the vibration energy compared to high frequencies. Thus, low frequencies are more interesting from the perspective of vibration analysis. Table 6 shows that the maximum measured displacement amplitude of end shield at DE increases from 1500 to 2500 RPM. Then from 2500 to 3500 RPM, the displacement amplitude decreases.

6.2 Measured relative displacement of the rotor at DE

The maximum measured amplitude 0-p of relative displacement of the rotor with 0 gm additional unbalance at DE for different speeds are presented in Table 7.

*Table 7. The maximum measured relative displacement amplitude 0-p of the rotor at DE (Kastinen 2019, p. 44).*

| RPM | The maximum measured relative displacement amplitude 0-p of the rotor, phase, and the frequency at DE in *y*-axis | | |
|---|---|---|---|
| | [µm] | [-180º to +180º] | [Hz] |
| 1500 | 7.22 | 75.59 | 24.99 |
| 2500 | 6.00 | 54.14 | 41.68 |
| 3500 | 5.10 | 48.87 | 58.36 |

Table 7 shows that the relative displacement of the rotor in *y*-axis at DE is decreasing when rotation speed is increasing. The excitation due to residual unbalance present in rotor is proportional to rotational speed and thus the absolute vibration of rotor must increase. However, decreasing relative vibration displacement of rotor suggest that absolute radial vibration of DE in *y*-axis is either decreasing or is out of phase. These conditions can be seen for example from the Table 6 and Table 7 at 3500 RPM.

6.3 Comparison between the vibration of the rotor and end shield at DE

As explained in sub chapter 2.7, in the context of case study, if the absolute vibration of the end shield is smaller than 20% of the relative vibration of the rotor, then either of these vibration measurements can be used as a measure of rotor vibration. However, if it is greater than 20%, then the absolute vibration of the rotor must be measured. In other words, it must be calculated from relative rotor vibration and absolute vibration of the end shield. The

comparison between 20% of maximum measured 0-p relative rotor displacement vibration to measured absolute displacement vibration of the end shield in the *y*-axis at DE with 0 gm additional unbalance at different speeds is presented in Table 8.

*Table 8. The comparison between 20% of measured relative rotor displacement vibration to measured absolute displacement vibration of the end shield in the y-axis at DE with 0 gm additional unbalance.*

| RPM | The maximum measured relative displacement 0-p at DE of the rotor in *y*-axis [µm] | The 20% of maximum measured relative displacement 0-p at DE of the rotor in the *y*-axis [µm] | The maximum measured absolute displacement 0-p of end shield at DE in *y*-axis [µm] |
|---|---|---|---|
| 1500 | 7.22 | 1.44 | 0.47 |
| 2500 | 6.00 | 1.20 | 2.43 |
| 3500 | 5.10 | 1.02 | 1.46 |

As shown in Table 8, only in the case of 1500 RPM, maximum absolute displacement 0-p of end shield in the *y*-axis is smaller than the 20% of maximum relative displacement 0-p of the rotor in *y*-axis at DE. Thus, for other speeds, it is required to measure the absolute displacement of the rotor.

6.4 Maximum and minimum absolute displacement of the rotor at DE

The maximum absolute vibration displacement of the rotor can be obtained by vector addition of relative vibration displacement of the rotor and the absolute vibration displacement of the end shield. For such signal operation, it is necessary to know the phase relation between these vibration signals which are presented in Table 6 and Table 7. Without the phase relation between these signals, the maximum 0-p amplitude of absolute displacement of the rotor in any axis cannot be higher than the scalar sum of 0-p amplitudes of relative displacement of the rotor and absolute displacement of end shield. This is the case when these two-displacement vibrations are in phase. But when these displacements are out of phase with each other, the minimum displacement 0-p amplitude of absolute displacement of rotor in any axis cannot be less than the scalar difference of 0-p amplitudes of relative displacement of the rotor and absolute displacement of end shield.

Table 9 shows the maximum and minimum 0-p absolute rotor displacement vibration amplitude in the *y*-axis at DE after the scalar addition and subtraction of the 0-p amplitude of absolute displacement of end shield and relative displacement of rotor respectively.

*Table 9. The minimum and maximum absolute displacement amplitude 0-p of the rotor at DE in the y-axis at different speeds with 0 gm additional unbalance.*

| RPM | The minimum and maximum absolute displacement amplitude 0-p of the rotor | |
|---|---|---|
| | Minimum [µm] | Maximum [µm] |
| 1500 | 6.75 | 7.69 |
| 2500 | 3.57 | 8.43 |
| 3500 | 3.64 | 6.56 |

Depending upon the phases of relative rotor displacement and the absolute displacement of the end shield, the absolute displacement vibration of the rotor at DE in *y*-axis is in the range of minimum and maximum values presented in Table 9 for respective speed.

6.5 Maximum and minimum absolute displacement of the rotor at NDE

In a similar process as presented in previous sub-chapters from 6.1 to 6.4, the maximum and minimum absolute displacement of the rotor at NDE were calculated. The maximum 0-p amplitude of absolute displacement vibration of end shield at NDE in *y*-axis at 1500, 2500 and 3500 RPM with 0 gm additional unbalance as presented in Table 10.

*Table 10. The maximum measured 0-p absolute vibration displacement, phase, and frequency of end shield in the y-axis at NDE with 0 gm additional unbalance.*

| RPM | The maximum measured 0-p absolute displacement, phase, and frequency of NDE end shield in *y*-axis | | |
|---|---|---|---|
| | [µm] | [-180º to +180º] | [Hz] |
| 1500 | 0.45 | -178.30 | 24.99 |
| 2500 | 1.91 | 130.00 | 41.68 |
| 3500 | 3.81 | -126.50 | 58.36 |

The Table 10 shows that the maximum measured 0-p absolute displacement of the end shield in *y*-axis is increasing with speed in NDE. The maximum measured relative displacement of the rotor at NDE in *y*-axis is presented in Table 11.

*Table 11. The maximum measured relative displacement 0-p of the rotor at NDE with 0 gm additional unbalance (Kastinen 2019, p. 44).*

| RPM | The maximum measured relative displacement amplitude 0-p, phase, and the frequency of rotor at NDE in *y*-axis | | |
|---|---|---|---|
| | [µm] | [-180º to +180º] | [Hz] |
| 1500 | 2.58 | 96.15 | 24.99 |
| 2500 | 2.90 | 84.73 | 41.68 |
| 3500 | 2.73 | 119.18 | 58.36 |

From Table 10 and Table 11, the maximum and minimum 0-p absolute rotor displacement vibration amplitude in the *y*-axis at NDE after scalar addition and subtraction of the 0-p amplitude of absolute displacement of end shield and relative displacement of rotor respectively were calculated. It is presented in Table 12.

*Table 12. The minimum and maximum absolute displacement amplitude 0-p of the rotor at NDE in y-axis at different speeds with 0 gm additional unbalance.*

| RPM | The minimum and maximum absolute displacement amplitude 0-p of the rotor at NDE in *y*-axis at different speeds with 0 gm additional unbalance | |
|---|---|---|
| | Minimum [µm] | Maximum [µm] |
| 1500 | 2.13 | 3.03 |
| 2500 | 0.99 | 4.81 |
| 3500 | 1.08 | 6.54 |

Depending upon the phases of relative rotor displacement and the absolute displacement of the end shield, the absolute displacement vibration of the rotor in NDE in *y*-axis is in the range of minimum and maximum values presented in Table 12 for respective speed.

## 6.6 Scanning single plane location for residual unbalance

The rotor and the lamination were modeled in Solidworks 2017 and the center of the mass of the rotor was found to be at 382 mm from the DE. In RoBeDyn model, the center of the mass of the rotor corresponds to location of the node 17. However, before scanning the FE model for magnitude and location of residual unbalance, it is important to know if there is any critical speed within the scanning RPM range in the physical rotor. The critical speed in traditional sense is the speed of the rotor which is equal to its natural frequency due to unbalance excitation when resonance occurs. The occurrence of resonance is critical physical phenomenon and the corresponding speed is called the critical speed. However, in general sense, critical speeds also occur when there are excitations at multiple or fraction harmonics of one of its natural frequencies. These critical speeds can be identified from the Campbell diagram. It is obtained when damped natural frequencies of the rotor system are plotted against the rotational speed of the rotor. (Chen & Gunter 2005, p. 60-61.)

In order to know the critical speed from the FE model, the magnitude of maximum permissible residual unbalance calculated in Table 5 was used. The phase of the unbalance was 0 radian with respect to positive *y*-axis. The damping coefficient of both bearings in the FE model was $10^{-5}$ times that of stiffness in respective bearing in respective axes as shown in Table 4. The model damping ratios for individual free-free modes were not available from the experimental analysis. Thus, no modal damping ratios for bending modes were used to obtain the Campbell diagram. Figure 38 shows Campbell diagram obtained from FE model without damping ratios of first two bending modes with the location of maximum permissible residual unbalance at node 17.

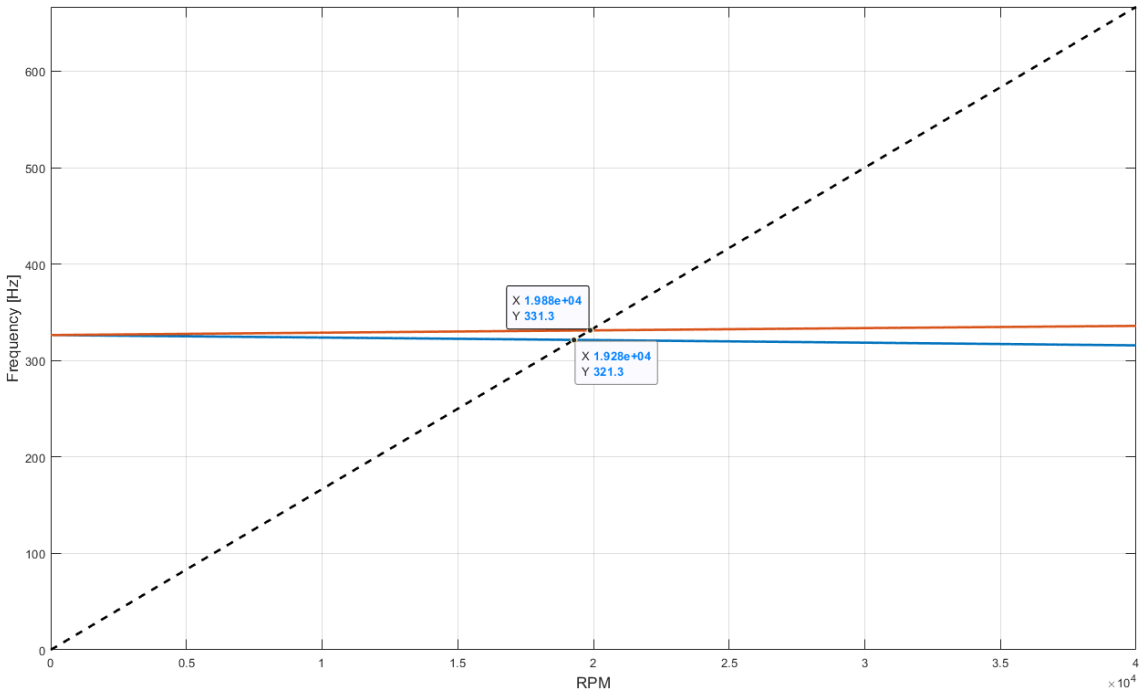


**Figure 38.** Campbell diagram from FE model of the rotor in speed range of 40000 RPM without damping ratio of first two bending modes.

The critical speed where the black dotted line intersects with the lines of damped natural frequencies of bending modes shown in orange and blue colour in Campbell diagram shown in Figure 38 are the critical speed of the FE model. The first critical speed of the system is 19280 RPM for first bending mode which is backward whirl mode (BW) and the second critical speed is at 19880 RPM for second bending mode which is forward whirl mode (FW). In forward mode, its frequency increases with increase in rotational speed and vice versa with backward mode. In other words, Campbell diagram shows that there is no critical speed in the range of measured speed from 500 to 3500 RPM. Thus, it can be safely assumed that simulated absolute displacement of rotor could be in the range of measured maximum and minimum displacement. The absence of critical speed in the range of the measured speed in FE model, does not mean that the physical rotor does not have one. The speed at which the motor was rotated to measure vibration was 3500 RPM and the first critical speed is at 19280 RPM. There is safety factor of 5.5 when machine rotates at 3500 RPM. The studied motor is designed in such a way that there is no critical speed within the operating range.

The scanning code was used to scan possible location and magnitude of single plane residual unbalance being in nodes from 15 to 21 in the model. Nodes from 12 to 24 represent the

lamination and short-circuiting rings in the rotor. The phase of the unbalance when scanned was taken as 0 because of being only interested in maximum 0-p absolute displacement amplitude of the rotor at the nodes. The displacement in the physical rotor was higher in *y*-axis compared to *z*-axis. Thus, simulated results were only analyzed to see if simulated absolute displacement of rotor is within the range of maximum and minimum measured absolute displacement of rotor in *y*-axis. The RoBeDyn model calculated equal displacement in *y*- and *z*- axis because of bearing stiffness being equal in these axes in DE and NDE bearing. Thus, only unbalance scanning results from *y*-axis are compared to measured results in *y*-axis. Table 13 shows the possible nodal location and magnitude of unbalance where the simulated absolute displacement of rotor is close to or within the range of the absolute minimum and maximum rotor displacement 0-p amplitude that was measured at DE.

*Table 13. The possible location of single plane unbalances and its magnitude and simulated absolute displacement of the rotor in y-axis for respective rotation speed at DE.*

| Node | Unbalance [kg·m] | Simulated maximum absolute displacement of the rotor in *y*-axis at the respective rotational speed [RPM] in [µm] at DE | | |
|---|---|---|---|---|
| | | 1500 | 2500 | 3500 |
| 15 | 0.0190 | 1.1440 | 3.2170 | 6.4230 |
| 16 | 0.0200 | 1.2420 | 3.4910 | 6.9670 |
| 17 | 0.0190 | 1.1890 | 3.3410 | 6.6670 |
| 18 | 0.0190 | 1.1740 | 3.2990 | 6.5810 |
| 19 | 0.0210 | 1.2570 | 3.5330 | 7.0460 |
| 20 | 0.0220 | 1.2530 | 3.5200 | 7.0200 |
| 21 | 0.0240 | 1.2750 | 3.5830 | 7.1460 |

Table 13 shows that not one simulated response is in the range of measured absolute displacement at any RPM. For node 17, the simulated absolute displacement at 2500 and 3500 RPM is very close to the range of measured maximum and minimum absolute displacement. It is also evident that to get the absolute displacement of the rotor in the range of measured absolute displacement, the FE model must have unrealistically higher amount of residual unbalance. This is because, the stiffness of the FE model, which has only the bearing stiffness is much higher than the equivalent stiffness of the physical rotor in the test

rig. In other words, it concludes that model is so inaccurate that the maximum reported residual unbalance at node 17 does not produce absolute displacement as measured.

It is evident that single plane unbalance is not able to define the measured responses by the FE model for all the speeds measured. Thus, three different unbalance magnitude for each speed were selected. These selected unbalances at node 17, when used in FE model resulted in simulated absolute displacement of rotor to be in the range of measured minimum and maximum absolute rotor displacement. The magnitude of unbalance for respective speed are called here as speed specific unbalance. The absolute displacement of rotor for this speed specific unbalance magnitude at node 17 for respective speed are presented in Table 14.

*Table 14. The speed specific unbalances at node 17 and respective simulated absolute displacement of rotor at DE.*

| Speed [RPM] | Node | The magnitude of speed specific Unbalance [kg·m] | Simulated maximum absolute displacement of the rotor in *y*-axis at DE [µm] |
|---|---|---|---|
| 1500 | 17 | 0.1150 | 7.1960 |
| 2500 | 17 | 0.0340 | 5.9790 |
| 3500 | 17 | 0.0140 | 4.9120 |

In each of these cases of selected speed specific unbalance at node 17, absolute displacement of rotor calculated in *y*-axis at DE is in the range of the measured maximum and minimum absolute rotor displacement as shown in Table 9. These are in the range because these were selected where it happened. These speed specific unbalances at node 17 in DE were curve fitted using line of best fit with second order polynomial. It was done to find the function that defines the residual unbalance which is dependent on the rotation speed of the rotor as shown in Figure 39.

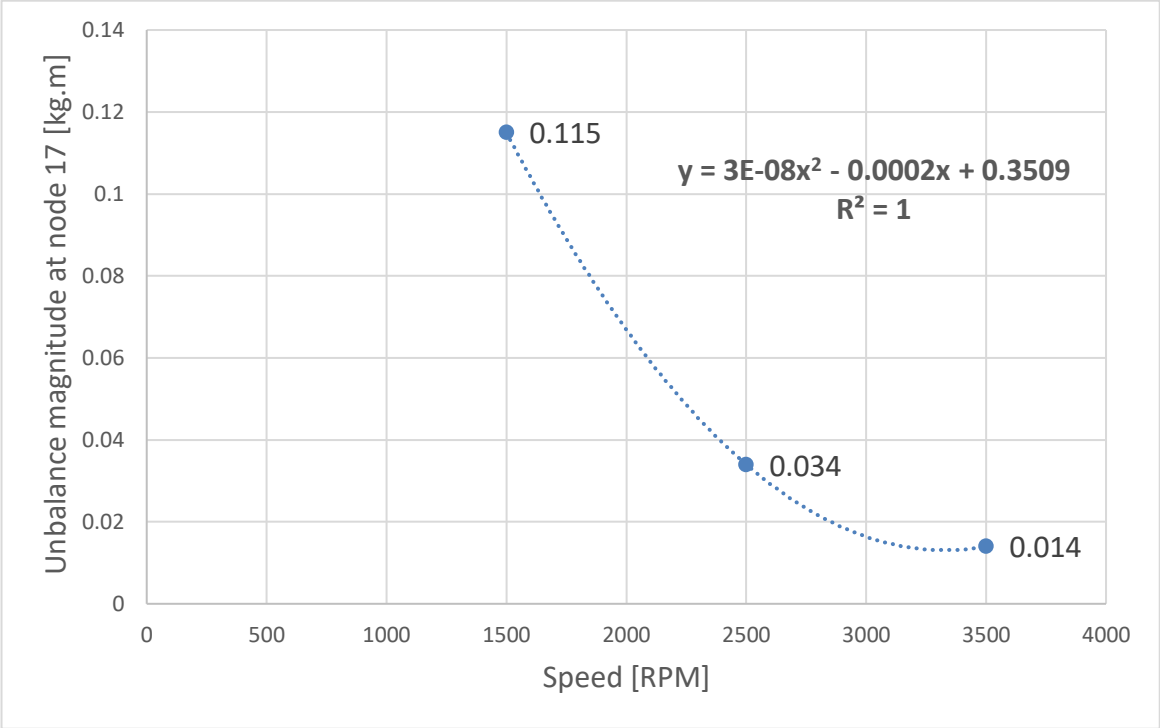


**Figure 39.** Trendline of speed in RPM and speed specific unbalance magnitude at node 17.

The speed-dependent single plane residual unbalance magnitude at node 17 can be calculated as,

$$Ub(r) = 3 \cdot 10^{-8} \cdot r^2 - 0.0002r + 0.3509, \quad (22)$$

where, *Ub(r)* is single plane speed-dependent residual unbalance in kg·m and *r* are the rotation speed of the rotor in RPM. The speed-dependent unbalance calculated by the function given in equation (22) is used to check if the absolute displacement of the rotor calculated by RoBeDyn model is within the range of measured absolute displacement in both DE and NDE.

6.7 Verification with speed-dependent unbalance function at DE and NDE

The function that defined the speed-dependent unbalance magnitude at node 17 as shown in equation (22) was used to calculate the unbalance magnitude. The calculated speed dependent unbalance magnitude was used to simulate the FE model to calculate maximum absolute displacement of rotor at DE and NDE. The comparison between the range of

measured absolute displacement to simulated absolute displacement of the rotor at DE and NDE with different speeds is presented in Table 15 and Table 16 respectively.

*Table 15. The comparison of simulated displacement using speed dependent unbalance function to a measured range of absolute displacement of the rotor at DE.*

| Speed [RPM] | Unbalance $Ub(r)$ [kg·m] | The measured minimum and maximum absolute displacement of the rotor in *y*-axis at DE [µm] | The simulated maximum absolute displacement of the rotor in *y*-axis at DE [µm] |
|---|---|---|---|
| 1500 | 0.1184 | 6.7500 – 7.6900 | 7.4090 |
| 2500 | 0.0384 | 3.5700 – 8.4300 | 6.7530 |
| 3500 | 0.0184 | 3.6400 – 6.5600 | 6.4560 |

*Table 16. The comparison of the measured range of absolute displacement of the rotor to simulated displacement using speed dependent unbalances at NDE.*

| Speed [RPM] | Unbalance $Ub(r)$ [kg·m] | Measured minimum and maximum absolute displacement of the rotor in *y*-axis at NDE [µm] | Simulated maximum absolute displacement of the rotor in *y*-axis at NDE [µm] |
|---|---|---|---|
| 1500 | 0.1184 | 2.1300 – 3.0300 | 2.9130 |
| 2500 | 0.0384 | 0.9900 – 4.8100 | 2.6370 |
| 3500 | 0.0184 | 1.0800 – 6.5400 | 2.4960 |

All the simulated absolute displacement of the rotor in *y*-axis at DE is within the range of measured minimum and maximum absolute displacement at DE. Also, all the simulated absolute displacement of rotor in *y*-axis at NDE is within the range of measured minimum and maximum absolute displacement at NDE. Thus, it can be concluded that the speed-dependent unbalance can be used to estimate the absolute displacement of the physical rotor from FE model at speed of 1500, 2500 and 3500 RPM. However, it must be verified further to predict absolute displacement of the rotor at other speeds or even within the range of those speeds. In order to predict the changes in absolute displacement due to change in unbalances magnitude in the rotor system, the phase of the speed-dependent unbalance must be found.

6.8 Verification with additional known unbalance mass at DE

The measurements from the radial accelerometers were not available for speeds when the additional known unbalances were attached in the rotor with hubs. Only at 1500 RPM, the absolute vibration of end shield at DE was less than 20% of the maximum measured relative displacement of rotor in *y*-axis. Thus, the magnitude of speed-dependent unbalance for 1500 RPM at node 17 is used to simulate the RoBeDyn model to calculate the maximum absolute displacement of the rotor at DE at 1500 RPM with 30 gm additional unbalance with added hubs. The comparison between the simulated absolute displacement and measured relative displacement at DE with added unbalance of 30 gm is shown in Table 17.

*Table 17. The comparison between maximum measured relative displacement and simulated absolute displacement of the rotor in DE at 1500 RPM with 30 gm additional unbalance.*

| Unbalances [kg·m] | | Node | Phase [rad] | The maximum measured Relative displacement of the rotor at *y*-axis in DE [µm] (Kastinen 2019, p. 44). | The maximum simulated absolute displacement of the rotor at *y*-axis in DE [µm] |
|---|---|---|---|---|---|
| $Ub(r)$ | 0.1184 | 17 | 0 | 8.0200 | 8.3410 |
| Added mass at DE 30 gm | 0.0018 | 3 | pi | | |
| Added mass at NDE 30 gm | 0.0018 | 30 | pi | | |

For all possible phases of the unbalance $Ub(r)$ at node 17 and an additional 30 gm per hub at respective nodal location, the result shows that the highest displacement was 8.341 µm at phase of 0 radian. It is higher than the maximum measured relative displacement. The phase of the maximum measured relative displacement of the rotor at *y*-axis was 235.72º (Kastinen 2019, p. 44). It was used to recreate the relative displacement signal of the rotor. The simulated absolute displacement signal from FE model and recreated relative displacement

signal were then used to calculate the absolute displacement of shield at DE. The maximum amplitude 0-p of absolute displacement of end shield at DE was found to be 7.10 µm. In subchapter 6.1, the maximum absolute displacement of end shield at DE at 1500 RPM with 0 gm added unbalance was found to be 0.47 µm. It is possible that the two additional unbalance mass and hubs have increased the resultant residual unbalance and hence the magnitude of absolute displacement of the rotor increased.

# 7 DISCUSSION

In order to make a model-based software solution that can automatically analyze and interpret the state of the rotating machine system from measured vibration, the FE model of the physical rotor must be accurate. For that reason, the FE model must be validated to match the dynamic responses of the physical rotor. Experimental and eigenvalue analysis helps to validate the natural frequencies and mode shapes. Even if the natural frequencies and the mode shapes are exactly similar for respective bending modes from the physical rotor and its FE model, it still cannot predict the displacement of nodes when it is rotating at specific speed without unbalance's information. The magnitude, location, and phase of residual unbalance present in the physical rotor must be identified from the measurements. Once this unbalance information is known and considered in FE model, then the model could predict the absolute displacement of rotor at other speeds. Then the question is if the absolute displacement of rotor predicted by the FE model is accurate or not. How accurate is the prediction depends upon, how accurate are the FE model itself and the measurements taken from the physical rotor?

The target of finding magnitude and location of single plane residual unbalance for the FE model with beam elements such that the model behaves like a physical rotor in terms of displacement measured at all speeds was not successful. In other words, single magnitude of residual unbalance was not able to predict the absolute displacement of the rotor at DE and NDE at a different speed. In theory, no matter how many unbalance vectors are distributed along the rotor length, the resultant unbalance vector can be represented as vector sum of these individual unbalance vectors. If everything were accurate from modelling, measurement process and the measurements itself, then the scanning should be able to identify single plane unbalance and location, which could predict the absolute displacement of rotor unless the rotation axis of physical rotor was not coincident with rotor centreline. Thus, it may mean that the central rotation axis has any relative position to the rotor centreline. In such case, it is required to find dynamic unbalance and it can be represented at two planes which is perpendicular to rotor centreline (ISO 1940-1 2003, p. 3). In other words, dynamic unbalance cannot be represented on single plane. The inability of finding single

plane residual unbalance may point to the fact that the unbalance in studied physical rotor perhaps is due to dynamic unbalance.

It may also be because of uncertainties in the measurement process, measurement values itself, inaccurate RoBeDyn model and any analysis and calculation error that was made. The measurement process and the test rig could have been better for taking accurate vibration measurements. It made FE modelling of the rotor more challenging and testing of the method of scanning unbalance more difficult. The steel frame where the motor was mounted could have been attached at all sides of the frame. This setup would have reduced measurement errors due to the loose side of the frame. It is hard to conclude if it would affect the relative displacement measured but it certainly does affect the calculation of absolute displacement vibration of the rotor that would require the acceleration vibration signal from end shield. The maximum measured temperature in machine during measurement was 35.2ºC (Kastinen 2019, p. 44). The measurement accuracy of the sensor can be affected by the temperature of the machine if it is not compensated for the temperature. The transverse flux capacitive sensor was mounted on end shields such that there was a 12 mm plastic plate between the end shield and the sensor (Liukkonen 2019). The damping properties of the plastic plate and rigidity of the mount affects the measurement of relative rotor displacement. Since capacitive sensors were more than 50 mm away from the bearing centreline in DE and NDE, the absolute radial vibration of rotor is not as accurate as it would have if they were closer to bearing centreline.

The modelling approach of the lamination section of rotor in RoBeDyn only represented its mass and the inertia properties. Thus, the material properties were different in physical lamination compared to that of FE model. This did affect the bending mode shapes at respective natural frequencies obtained from modal analysis. However, it is difficult to conclude how this approach affected the simulated absolute displacement of rotor at measured location. The stiffness and the dynamics of steel frame were not accounted for in FE model. This does affect the simulated absolute displacement of rotor. It is because of the deformation of steel frame (Sikanen 2014). It can also be seen in magnitude of unbalance calculated when the simulated displacement is in the range of measured minimum and maximum displacement. In other words, the RoBeDyn model is so stiff that in order to get the simulated absolute displacement within the range of measured absolute displacement of

rotor, unrealistically high amount of unbalance magnitude in the FE model is required. The equivalent stiffness of the test rig must be less stiff than RoBeDyn model which only considered bearing stiffness as support parameter. The clearance of the bearing in physical rotor also affects the vibration measured. And there are also uncertainties in the estimated bearing stiffness (Kastinen 2019, p. 44). The different amplitude of measurement in radial axis also shows that frame was not equally stiff in *y*- and *z*-axis. Regardless of all these uncertainties, there could also be errors in the analysis.

Although the magnitude and location of single plane residual unbalance was not successfully found, the speed-dependent residual unbalance function was calculated for speeds of 1500, 2500 and 3500 RPM. The function calculates speed specific single-plane unbalance for these speeds. When unbalance magnitude at node 17 is defined based on functional value rather than single constant magnitude in RoBeDyn model, it was able to predict the absolute displacement of rotor at both DE and NDE in speed range of 1500, 2500 and 3500 RPM. However, it was not verified if it can predict the displacement in speeds other than 1500, 2500 and 3500 RPM. Although the unbalance magnitude is higher compared to the reported maximum permissible unbalance, it could be used to define FE model's modelling factor such that the scanned unbalance magnitude is equal to the product of modelling factor and maximum permissible residual unbalance. The modelling factor of value one would indicate that model is theoretically accurate, less than one would indicate that the model could be practically accurate and modelling factor more than one means less accurate RoBeDyn model. This could be one possibility to estimate the accuracy of model used. The modelling factor for the FE model used was estimated to be about 242 when the unbalance magnitude is 0.1184 kg·m. It also concludes what was known that FE model is far from being theoretically or practically accurate.

Even if the single plane residual unbalance was found that could predict the absolute displacement of the rotor at DE and NDE at different speeds, it would require more work to verify if it is also true at other speeds. It would also require more work to find the exact node and the magnitude where the simulated displacement is equal to measured displacement. It is because the different magnitude of single plane unbalance at two different nodes can give equal simulated absolute displacement of rotor. But by comparing the phase of the measured

to simulated displacement, it is possible to identify the correct node and magnitude. It would thus require statistical measures to tell how precise the calculation of unbalance is.

One of the very important issues in the interpretation of the condition of machinery through vibration measurements and analysis is documentation regarding the vibration measurement location. The standard SFS-ISO 13373-1 recommends following MIMOSA (Machinery Information Management Open System Alliance) convention for identifying vibration measurement locations. It is unambiguous 14-character code with spaces that represents the type of sensor used, location where it is mounted, its angular orientation, direction of motion its measuring, etc. (SFS-ISO 13373-1 2002, p. 42-49.) Often the individual doing vibration analysis is not the one who made measurement setups and measured the vibration. In such cases, it very important to make systematic documentation on measurement setup and measurements done for unambiguous communication. The level of documentation done during measurements of the case study was not adequate and can be improved for future measurements.

# 8 CONCLUSION

The aim of the thesis work was to find answers to the research questions. These were, what to measure, why to measure, how to measure and where to measure required parameters from rotating machines to analyze and interpret the condition of the machine and or its components? What is the data format of these measurements and how these are transferred to make required analysis? What are the different signal analysis techniques and how to interpret the results from these analyses? How these measured parameters and processed results can be used to verify the mathematical model of the specific machine used in the industry?

In order to analyze and interpret the state of the rotating machine and its components through vibration analysis, it is important to measure vibration parameters from the machine. Depending upon the reason for the measuring and machine type, standard SFS-ISO 13373 recommended measuring absolute radial vibration of non-rotating parts. From rotating parts, it recommends measuring absolute or relative radial vibration displacement, radial or absolute axial vibration displacement, phase reference and rotation speed. It is important to understand that the terms, relative and absolute vibration are just the perspective based on available sensor designs, and how vibration is measured with these available sensors. For example, displacement probe measures just the displacement vibration but depending upon where it is attached, it can measure relative or absolute displacement. If it is attached to the body A to take its displacement measurement, then it is absolute displacement but if it is attached to body A to measure vibration of body B, then it is relative displacement. The displacement probe attached at bearing housing thus measures the displacement vibration of rotor with relative to the displacement of bearing housing. But if the displacement probe is attached to the ground then it measures absolute displacement of rotor.

The vibration parameters are measured on the rotating machine to monitor the state of the rotating machine and its components. The reason behind monitoring is to track and detect developing faults and failures in machine. This early detection and tracking help to prevent catastrophic failures of machines and components, estimate the remaining life of the

components, do preventive maintenance, improve safety in workplace, etc. and use the information acquired for product development of the machine and components.

The required parameters can be measured by using appropriate sensors depending upon the machine and mounting location of the sensor. The selection of the sensor depends on the magnitude range, frequency range, accuracy of measurement, mounting possibility, etc. Accuracy of measurement depends on how accurately the vibration of machine component is being transferred to the transducer. Thus, the most preferred method for attaching transducers is by rigid mechanical fastening.

The standard SFS ISO 13373-1 recommends using two accelerometers or velocity sensors per bearing housing to measure its radial absolute vibration. Two displacement probes for each bearing housing are used to measure the relative radial displacement of the rotor. The phase reference and rotation speed are measured with respect to reference mark such as keyway by using optical or inductive or eddy current based transducer at rotor. With this set up for measurement, the absolute displacement of the rotor can be calculated by vectorially adding relative displacement of rotor and absolute displacement of the bearing housing. With this set up recommended by the standard, each bearing housing requires four sensors and it measures three vibration parameters. They are absolute vibration of housing, relative and absolute vibration of rotor in radial axis. The reason for this set up is because of the available design of sensors in the market. One integrated sensor which can measure both absolute acceleration or velocity of housing and the relative displacement of the rotor does not exist, or the technical committee was not aware of it during the time. If such an ideal sensor would become available, then only two such sensors are required at radial axis instead of four individual sensors. It will make many procedures explained in standard to be outdated.

The data format or the output of the sensors depends on what is the principle behind the sensing element and what are different signal conditioning feature it has. Sensors that do not have an ADC and conditioning system give analog output in terms of charge, current, capacitance, etc. However, sensors that have built-in ADC and signal conditioning features give output in terms of digital values that correspond to measured quantity. For example, piezoelectric charge accelerometer without a built-in ADC and signal conditioning feature give an analog sample of charge in piezoelectric sensing material. But the one with ADC

and signal conditioning features such as filtering, noise reduction, linearization, etc. can give digital samples of acceleration in m/s². These measured data can be recorded in storage devices or transferred through wired or wireless communication infrastructures for signal analysis.

The vibration signals are mainly analyzed in time domain and frequency domain. The analysis of vibration in time domain for analyzing signal to interpret the state of machine or component is limited. It is mainly used for vibration trending to monitor the state of the machine rather than identifying the faults. Fault diagnosis of machine or components is mainly done in frequency domain. The faults in machine or components can be identified from frequency, magnitude and phase of the vibration signal generated by the machine or components through FFT of measured composite vibration signal.

It is not possible to verify the mathematical model in terms of its dynamic behavior without considering the residual unbalance of the physical rotor. The measured absolute displacement of the rotor can be used to determine the residual unbalance present in the specific machine. The absolute displacement obtained from the simulation of a mathematical model is compared with the measurements from the rotor to verify its dynamics. When comparisons show that the measured absolute displacement is equal to the simulated absolute displacement for different speeds, then this will verify that the dynamics of mathematical model correctly represents the dynamics of physical rotor.

The manufacturing and machine assembly processes might result in rotation axis of rotor being in relative position to the rotor centreline. In future studies, the method of scanning unbalance can be further studied to identify two-plane dynamic unbalances rather than one plane residual unbalance. The modelling of lamination can also be done with different approaches such that the deflection of lamination can be predicted from the mathematical model. That makes it possible to monitor the rotor-stator clearance through RoBeDyn model. The model can be made more accurate by considering the stiffness and dynamics of the steel frame. The test rig must be properly secured in future measurements. Further studies can be done to improve unbalance scanning algorithm.

One important process when modelling in RoBeDyn is about deciding the number of nodes in the model from the perspective of the possible location of unbalance. In physical machines, residual unbalance could be anywhere on the rotor. Thus, rather than defining nodes first and looking unbalance in those nodes, scanning algorithm can be used to define the number of nodes after the scanning process. This will help in deciding the number of nodes for the model and the unbalance can be placed at any of those nodes. This process ensures that the algorithm can scan unbalance freely in all possible rotor lengths even when the location of unbalance changes on the rotor. The statistical tool can also be implemented in the scanning algorithm that can calculate the probability of unbalance magnitude being in specific nodal locations. It can also be improved to make scanning process faster by using Newton Raphson iteration method.

The different magnitude of single plane unbalance in two nodal locations can result in equal magnitude of absolute displacement at specific measured nodes. Thus, when identifying unbalance in machine through measurements done at couple of nodes, it is difficult to be 100% certain about the identified unbalance magnitude. In such cases, the unbalance scanning method could also be used to verify the results obtained from other unbalance detection methods. Although single-plane unbalance was not found, the speed-dependent residual unbalance function was found for speeds of 1500, 2500 and 3500 RPM for studied rotor. This method can be used to estimate the absolute displacement of rotors for specific speeds. This scanning approach with modifications could also be utilized for field balancing work to determine the location and amount of mass that is needed to be attached.

**LIST OF REFERENCES**

ABB. 2015. Motors don’t just fail … do they? – A guide to prevent failure [web document]. Published 2015. [Referred 20.11.2018]. Available: https://new.abb.com/docs/librariesprovider53/about-downloads/motors_ebook.pdf?sfvrsn=4

Adams, M. L. 2001. Rotating machinery vibration: From analysis to troubleshooting. New York: Dekker. 354 p.

Agnieszka, M. 2005. Rotordynamics. United States of America. CRC press Taylor & Francis Group. 1053 p.

Asoke, K. N. & Ahmed, H. 2019. Condition monitoring with vibration signals: Compressive sampling and learning algorithms for rotating machines. USA. IEEE press. John Wiley & Sons Ltd. 440 p.

Bate, H. G. Vibration Diagnostics for Industrial Electrical Motor Drives. [web document]. [Referred 19.11.2019]. Denmark: Brüel & Kjær. 12 p.

Bender, A. E. 1978. An Introduction to Mathematical Modeling: A Wiley-Interscience Publication. John Wiley & Sons. USA. 256 p.

Charge Amplifiers-Type 2634. 2010. [www-data sheet]. Denmark: Brüel & Kjær. [Referred 04.09.2019]. Available: https://www.bksv.com/-/media/literature/Product-Data/bp0198.ashx

Cheatle, K. R. 2006. Fundamentals of Test Measurement Instrumentation. North Carolina. Research Triangle Park: ISA- Instrumentation, Systems, and Automation Society. 329 p.

Chen J. W. & Gunter E. J. 2005. Introduction to Dynamics of Rotor-Bearing Systems. Victoria, BC, Canada. Trafford Publishing. 469 p.

Childs, D. 1993. Turbomachinery Rotordynamics, Phenomena, Modeling, & Analysis, John Wiley & Sons, New York. 476 p.

Electrical4U. 2019. [web document]. Published 2019. [Referred 07.11.2019]. Available at: https://www.electrical4u.com/squirrel-cage-induction-motor/

Friswell, I. M., Penny, J. E. T., Garvey, S. D. and Lees, A. W. 2010. Dynamics of Rotating Machines. Wei Shyy and Michael J. Rycroft. II series. USA: Cambridge University Press. 526 p.

Goyal, D. & Pabla, B. 2015. The Vibration Monitoring Methods and Signal Processing Techniques for Structural Health Monitoring: A Review. In: Archives of Computational Methods in Engineering. Volume 23, Netherlands. Springer. March 1, 2015. Pp. 585-594.

Gu, L., & Chu, F. 2014. An analytical study of rotor dynamics coupled with thermal effect for a continuous rotor. In: Tham, L. G. (handling editor) Journal of sound and vibration, Volume 333. Elsevier Ltd. Pp. 4030-4050.

Higgs, P., Parkin, R., Jackson, M., Al-Habaibeh, A., Zorriassatine, F. & Coy, J. 2004. A survey on condition monitoring systems in industry. Proceedings of ESDA 2004: 7th Biennial ASME Conference Engineering Systems Design and Analysis, held at Manchester, UK July 19-22, 2004. Pp 1-16

Irvine, T. 2019. Vibration data Matlab Signal Analysis & Structural Dynamics Package. [Referred 10.08.2019]. Available: https://vibrationdata.wordpress.com/

ISO 1940-1. 2003. Mechanical Vibration- Balance quality requirements for rotors in constant (rigid) state- Part 1: Specification and verification of balance tolerances. Second edition. International Organization for Standardization. Switzerland. 27 p.

Ishida, Y. & Yamamoto, T. 2012. Linear and Nonlinear Rotordynamics: A Modern Treatment with Applications. Second enlarged and Improved edition. Singapore. Markono Print Media Pte Ltd. 447 p.

Kantoríková, E. & Fabian, P. 2019. Influence of operation temperature on rolling bearings. Defect and Diffusion Forum, 395, Pp. 64-72.

Kastinen, M. 2019. Rolling-element bearing stiffness estimation from relative rotor displacement. 68 p. Master's Thesis.

Krämer, E. 1993. Dynamics of Rotors and Foundations. New York: Springer-Verlag Berlin Heidelberg. 383 p.

Kärkkäinen, A. 2007. Dynamic Simulations of Rotors During Drop on Retainer Bearings. Lappeenranta. Acta Universitatis Lappeenrantaensis. 91 p. Dissertation.

Liukkonen, O. 2019. Research Engineer, LUT schools of Energy Systems. Lappeenranta. Oral interview. Interviewer Satish Bastakoti. Notes are occupied by the interviewer

Low voltage motor guide. 2014. [web document]. [Referred 3.11.2019]. Available at: https://new.abb.com/docs/librariesprovider53/about-downloads/low-voltage-motor-guide.pdf

Maslen, E. H. & Schweitzer, G. 2009. Magnetic Bearings: Theory, Design, and Application to Rotating Machinery. Berlin, Heidelberg: Springer Berlin Heidelberg. 535 p.

Matsushita, O., Tanaka, M., Kanki, H., Kobayashi, M. and Keogh, P. 2017. Vibration of Rotating Machinery. Wakayama, M. Basic Rotordynamics: Introduction to Practical Vibration Analysis. Japan. Springer. 360 p.

McMillan, R. B. 2004. Rotating machinery: Practical solutions to unbalance and misalignment. USA. Fairmont Press Inc., Marcel Dekker Inc. 224 p.

Mogenier, G., Dufour, R., Ferraris-Besso, G., Durantay, L. & Barras, N. 2010. Identification of Lamination Stack Properties: Application to High-Speed Induction Motors. IEEE Transactions on Industrial Electronics, 57(1), Pp. 281-287

Mohanty, A. R. 2015. Machinery Condition Monitoring: Principles and Practices. Boca Raton, Florida. CRC Press Taylor & Francis Group. 232 p.

National Instruments n.d. Understanding FFTs and Windowing. [web document]. [Referred 21.11.2019]. Available: https://download.ni.com/evaluation/pxi/Understanding%20FFTs%20and%20Windowing.pdf

Norton, M. P. & Karczub, D. G. 2003. Fundamentals of noise and vibration analysis for engineers. Second edition. USA. Cambridge University Press. 619 p.

PCB Piezotronics 2019. Model: 622B01 [www- data sheet]. [Referred 22.10.2019]. Available at: http://www.pcb.com/Products.aspx?m=622B01

Pelli, I. 2018. Capacitive Displacement Sensor's Applicability and limitations in Condition Monitoring Systems of Rotating Electrical Machines. 73 p. Master's Thesis

Peter, A. 2018. Modal testing: A practitioner's guide. Hoboken, NJ: John Wiley & Sons Ltd. 517 p.

PHOTON+ Dynamic Signal Analyzer. 2016. [www-data sheet]. Denmark: Brüel & Kjær, 2016. [Referred 04.09.2019]. Available: https://www.bksv.com/-/media/literature/Product-Data/bu3080.ashx

Piezoelectric Charge Accelerometer Types 4371 and 4371-V.2018. [www-data sheet]. Denmark: Brüel & Kjær, 2018. [Referred 04.09.2019]. Available: https://www.bksv.com/-/media/literature/Product-Data/bp2036.ashx

Prabhu, K. M. M. 2014. Window Functions and Their Application in Signal Processing. Boca Raton, Florida. CRC press, Taylor & Francis Group. 362 p.

Quarteroni, A. & Saleri, F. 2006. Scientific Computing with MATLAB and Octave. T.J. Barth, M. Griebel, D.E. Keyes, R.M. Nieminen, D. Roose, T. Schlick. Second Edition. Berlin, Heidelberg: Springer. 318 p. Texts in Computational Science and Engineering, 3

Rajendra, M., William, R. F., Hashish, E. and Kreitzer, S. 2018. Rotating Machines, The pros and cons of monitoring devices. IEEE Industry Application Magazine. 2018. Pp. 45-55.

Roivainen, J. 2009. Unit-wave response-based modeling of electromechanical noise and vibration of electrical machines. Espoo. TKK Dissertations. Helsinki University of Technology. 184 p.

Scheffer, C., & Girdhar, P. 2004. Practical Machinery Vibration Analysis & Predictive Maintenance. Series editor: Steve Mackay. The Netherlands: Newnes. Elsevier. 255 p.

SFS-ISO 13372. 2012. Condition monitoring and diagnostics of machines. Vocabulary. International Organization for Standardization. Switzerland. 15 p.

SFS-ISO 13373-1. 2002. Condition monitoring and diagnostics of machines. Vibration condition monitoring. Part 1: general procedures. International Organization for Standardization. Switzerland. 52 p.

SFS-ISO 13373-2. 2005. Condition monitoring and diagnostics of machines. Vibration condition monitoring. Part 2: processing, analysis and presentation of vibration data. International Organization for Standardization. Switzerland. 32 p.

SFS-ISO 13373-3. 2015. Condition monitoring and diagnostics of machines. Vibration condition monitoring. Part 3: Guidelines for vibration diagnosis. International Organization for Standardization. Switzerland. 39 p.

SFS-ISO 13381-1. 2015. Condition monitoring and diagnostics of machines. Prognostics. Part 1: General Guidelines. International Organization for Standardization. Switzerland. 25 p.

SFS-ISO 20816-1. 2017. Mechanical vibration. Measurement and evaluation of machine vibration. Part 1: General guidelines. International Organization for Standardization. Switzerland. 39 p.

SFS-ISO 21940-11. 2017. Mechanical vibration. Rotor balancing. Part 11: Procedures and tolerances for rotors with rigid behavior. International Organization for Standardization. Switzerland. 29 p.

Siemens. 2019. Introduction to Filters: FIR versus IIR. [web document]. Published 2019, updated August 2019. [Referred 24.11.2019]. Available: https://community.sw.siemens.com/s/article/introduction-to-filters-fir-versus-iir

Sikanen, E. 2014. Mechanical Design and analysis of modular active magnetic bearing test rig. 74 p. Master's Thesis

Simcenter. 2019. On-demand Webinar: Digital signal processing fundamentals. [web document]. Published 2019, updated August 2019. [Referred 11.11.2019]. Available: https://community.sw.siemens.com/s/article/digital-signal-processing-sampling-rates-bandwidth-spectral-lines-and-more

Sopanen, J. 2004. Studies of rotor dynamics using a multibody simulation approach. Lappeenranta. Acta Universitatis Lappeenrantaensis. 102 p. Dissertation

Sopanen, J. 2009. User Manual. RoBeDyn: Rotor-Bearing Dynamics Toolbox for Matlab. Version 2.1. Lappeenranta: February 2009. 30 p. Not available publicly

Valmet. 2015. Dual output accelerometer and temperature sensor. [web document]. Published 2015, updated April 2015 [Referred 30.08.2019]. Available: https://www.valmet.com/globalassets/products/automation/valmet-dna-dcs/condition-monitoring/br81082_en_01-rvt_tt-125.pdf

Vance, J. M. 1988. Rotordynamics of turbomachinery. New York: Wiley. 393 p.

Waide, P. & Brunner, C. U. 2011. Energy-Efficiency Policy Opportunities for Electric Motor-Driven Systems. IEA Energy Papers. 128 p.

Williams, H. J., Davies, A. & Drake, R. P. 1994. Condition-based maintenance and machine diagnostics. London. Chapman & Hall. 188 p.

Zhou, W., Habetler, T.G., & Harley, R.G. 2007. Bearing Condition monitoring Methods for Electric Machines: A General Review. In: IEEE International Symposium on Diagnostics for Electric Machines, Power Electronics and Drives Conference: Proceedings of the International Conference, held at Cracow, Poland 6-8 September 2007. Atlanta, USA. IEEE Conference Publications. 2007. Pp. 3-6

APPENDIX I: Fault identification in rotating machine and components through FFT.

| Machine Component Faults | Dominant Direction | Predominant Frequency | Remarks |
|---|---|---|---|
| *Shaft/Rotor* | | | |
| Unbalance | Radial | 1 x | Amplitude increases as square of the rotational speed |
| Misalignment | Axial | 2 x | |
| Looseness | Radial | 1/2 x, 0.5 x, 1 x, 1.5 x, 2 x and 2.5 x | Time waveform gets clipped |
| Rub | Radial | Continuous spectrum | |
| Crack | Radial | 1x, 2x, 3x | Amplitudes decrease with increase of frequency |
| *Bearings* | | | |
| Journal | Radial | 0.42 x to 0.48 x | Due to oil whirl phenomenon |
| Rolling Element | Radial | Harmonics of CDFs[a] and at 20 to 30 kHz | Detection possible by envelope analysis. High-frequency vibration is due to resonance of bearing components |
| Gears | Radial | GMFs[b] and sidebands | Cepstrum analysis is preferred to detect families of sidebands |
| Impellers/Pump | Radial | Sidebands around VPFs[c] and 20 to 30 kHz | High-frequency vibration is due to cavitations |
| Fan/Blowers | Radial | Sidebands around VPFs | — |
| Pulley/Belt | Radial | 1 and 2 times BF[d] | — |
| Electrical Motor | Radial | 2 times electrical supply frequency | — |

[a] Characteristics defect frequencies of bearing components
[b] Gear mesh frequency
[c] Vane pass frequency
[d] Belt frequency

APPENDIX II: Mode shapes and natural frequencies in the respective axis obtained from experimental modal analysis.

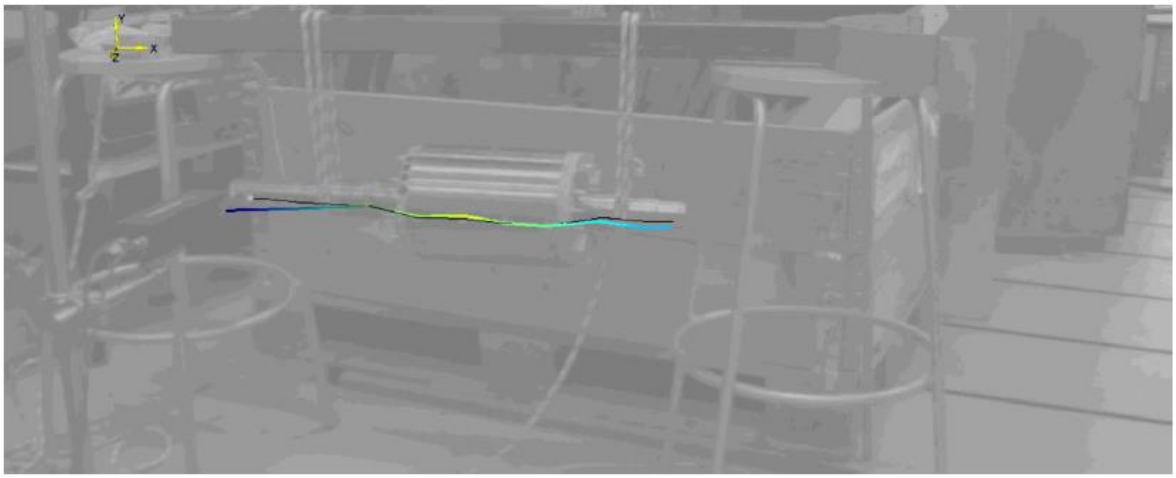

**Figure II.1.** The first bending mode in the *z*-axis at 595.3 Hz.

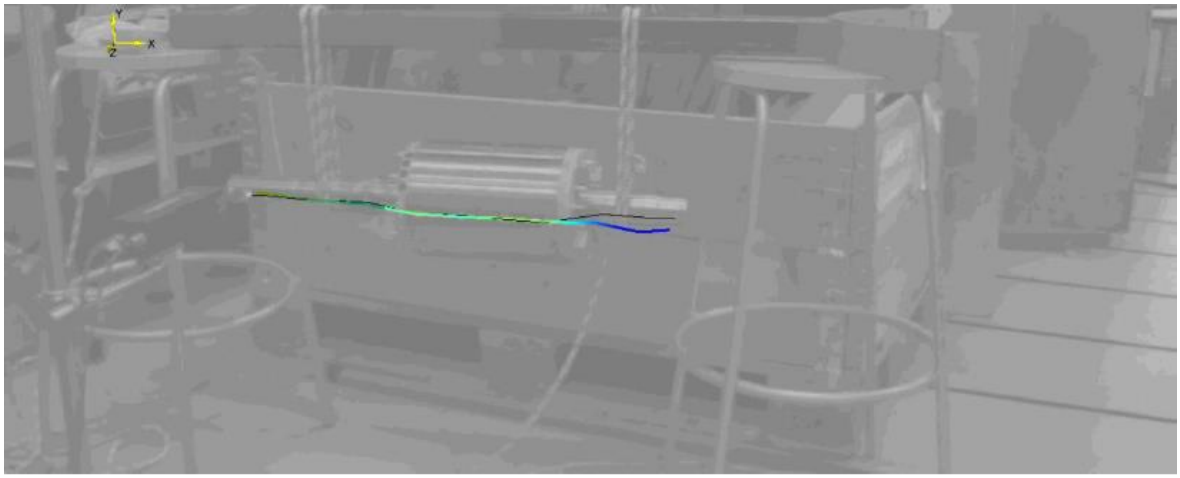

**Figure II.2.** The second bending mode in the *z*-axis at 1453.9 Hz.

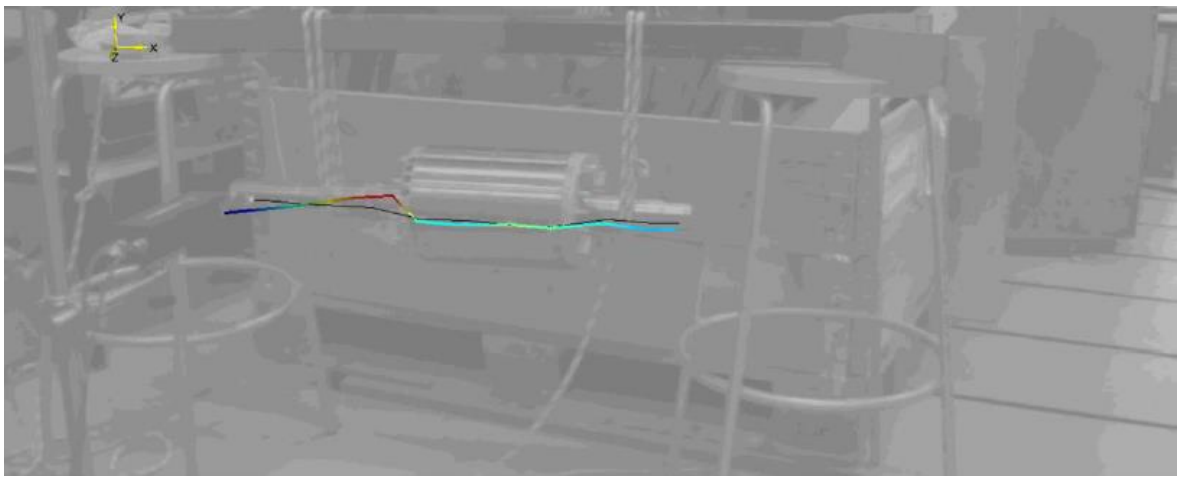

**Figure II.3.** The third bending mode in the *z*-axis at 2099.2 Hz.

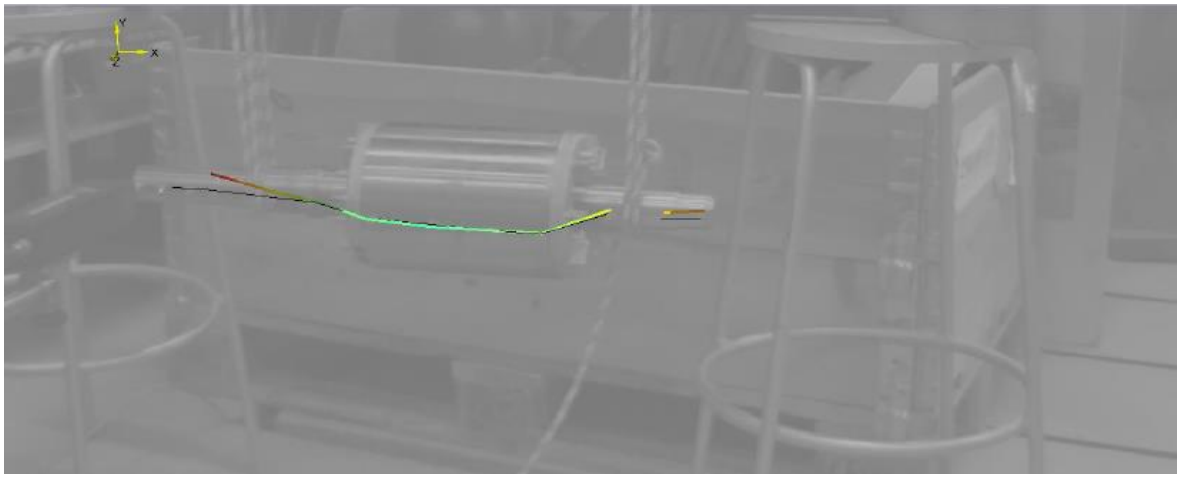

**Figure II.4.** The first bending mode in the *y*-axis at 595.3 Hz.

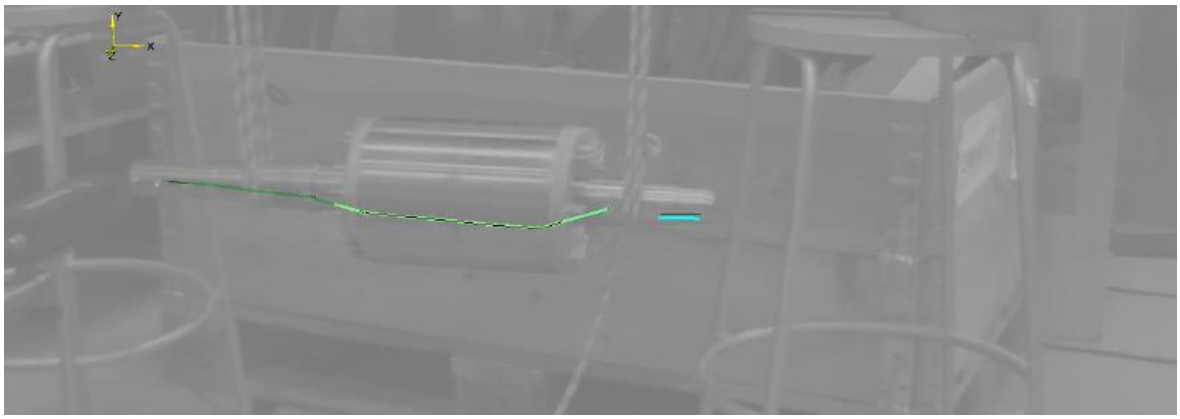

**Figure II.5.** The second bending mode in the *y*-axis at 1446.9 Hz

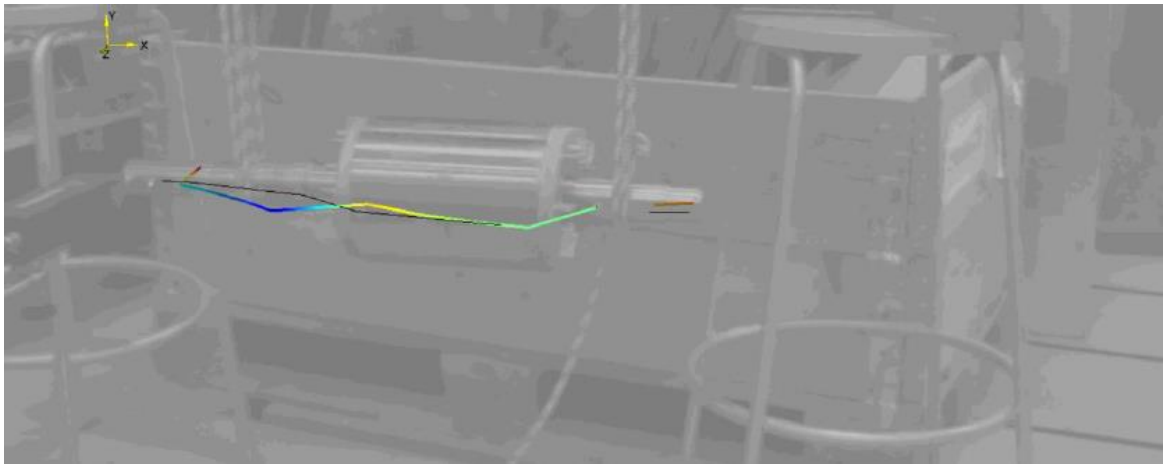

**Figure II.6.** The third bending mode in the *y*-axis at 2085.2 Hz.

APPENDIX III: Mode shapes and natural frequencies in the respective axis obtained from the eigenvalue analysis of the FE model without modal damping.

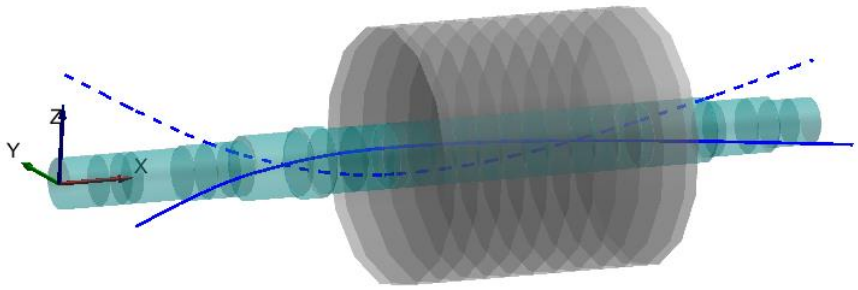


**Figure III.1.** First bending mode in the *y*-axis (solid blue line) and *z*-axis (dotted blue line) at 595 Hz.

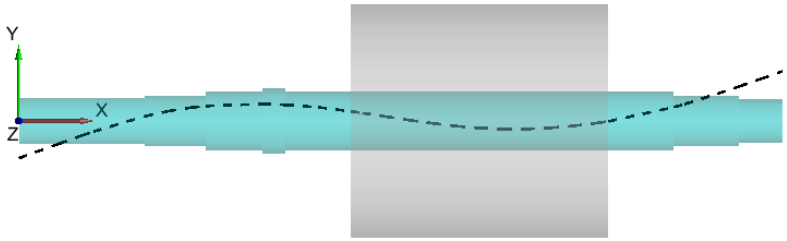


**Figure III.2.** The second bending mode in the *y*-axis (dotted black line) at 1328 Hz. The second bending mode in *z*-axis is like that as in *y*-axis at same frequency.

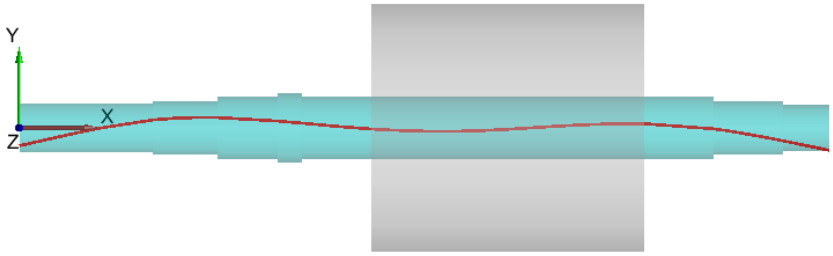


**Figure III.3.** The third bending mode in the *y*-axis (solid red line) at 2140 Hz. The third bending mode in *z*-axis is like that as in *y*-axis at same frequency.